半導体ナノクリスタルの永続的ホールバーニングの研究

（研究課題番号　08454075）

平成８年度～平成９年度科学研究費補助金（基盤研究（B））
研究成果報告書

平成10年3月

研究代表者　舛本泰章
（筑波大学 物理学系教授）

半導体ナノクリスタルの
永続的ホールバーニングの研究

(研究課題番号　08454075)

平成８年度～平成９年度科学研究費補助金(基盤研究(Ｂ))

研 究 成 果 報 告 書

平 成 10 年 3 月

研究代表者　舛 本 泰 章

(筑波大学物理学系教授)

平成８年度～平成９年度科学研究費補助金（基盤研究（Ｂ））

半導体ナノクリスタルの永続的ホールバーニングの研究

（研究課題番号　08454075）

研究組織

研究代表者　舛本泰章　（筑波大学物理学系教授）

研究経費

平成８年度　　６，３００千円
平成９年度　　１，４００千円
計　　７，７００千円

半導体ナノクリスタルの永続的ホールバーニングの研究

筑波大学物理学系教授　舛本泰章

１．研究の背景と目的

物理,化学、電子工学の広い分野でナノメートルサイズの半導体微結晶（ナノクリスタル）が盛んに研究されている。ナノメートルサイズになると電子・正孔や励起子が狭い空間に閉じ込められ、運動エネルギーが量子化され、電子・正孔間に働くクーロンエネルギーが大きく増大する。この量子現象および、全原子数の数％～数十％に達する原子が構成する表面に起因する現象が半導体ナノクリスタル（量子点）の本質である。

本研究に先だって、1994年、半導体ナノクリスタル（量子点）の不均一拡がりを持った吸収スペクトル中に、低温で永続的にスペクトルホールが開く現象（永続的ホールバーニング）という新しい光機能性が見出された[1, 2]。ホールの寿命が、光励起キャリアの寿命によって決まるならば、直接許容遷移型の半導体結晶においては、寿命はナノ秒程度となる。しかし、半導体ナノクリスタル（量子点）で発見された、永続的ホールバーニング現象とは作られたホールが数時間も永く保たれる現象である。これは、励起状態からの緩和が始状態とは別の基底状態へ起こり、この基底状態が低温においては永続的に保たれることで一般的に説明される。

半導体ナノクリスタル（量子点）の永続的ホールバーニング現象は、それ自体、新奇な現象としてその機構や新しい材料の探索が研究の対象となる他、光多重メモリへの応用、更には、単光子による光スイッチの可能性を示し、応用や波及する新現象まで含めて総合的に研究する価値がある。ナノクリスタル（量子点）の永続的ホールバーニング現象とは、ナノクリスタル（量子点）の界面に１電子がトラップするだけで、１電子励起のエネルギーが大きく変化する現象である。より一般的に、10^{3}～10^{6}個程度の少数の原子から構成されるナノクリスタル（量子点）中に励起される電子・正孔や励起子の数の離散性がエネルギー・スペクトル上に顕に現われれば、単光子によるナノクリスタル（量子点）のエネルギー制御、光スイッチが実現できるからである。

２．研究経過と成果及び考察

２－１　半導体ナノクリスタル(量子点)の永続的ホールバーニング現象

半導体ナノクリスタル（量子点）の不均一拡がりを持った吸収スペクトル中に、低温で永続的にホールが開く現象（永続的ホールバーニング）の発見[1, 2]に続き、この現象の普遍性の検討、メカニズムの研究、および応用の研究を行った。現在までにCdS, CdSe, CdSSe, CdTe, CuCl, CuBr, CuIのナノクリスタル(量子点)が埋め込まれたガラス、結晶、ポリマーにおいて、広く永続的ホールバーニング現象が発見された[1, 2, 5, 8, 10, 12, 13, 16, 18]。これにより現象の普遍性は十分に実証された。この現象の機構、本質を明らかにするため、試料の温度を変えて、波長可変狭帯域レーザーによる

サイト選択励起により、スペクトル領域で精密な測定を行い、ナノクリスタル（量子点）の光イオン化が原因であることをほぼ明らかにした[10, 12]。また、電子，正孔、励起子やフォノンの量子閉じ込めエネルギーのナノクリスタルサイズや外場に対する依存性に関する精密分光への応用を実証し[6]、光多重メモリーへの応用の可能性を指摘した[2, 9, 31]。

半導体ナノクリスタル(量子点)の永続的ホールバーニング現象は、ゲストとホスト両者に依存しており、この意味で多様であり、ホールバーニング、ホールフィリングの機構も唯一ではないかもしれない。しかし、今までに得られた実験結果を説明するためには、光イオン化機構が最も可能性の高いものと考えている。光励起された中に生成された励起子はナノクリスタル表面に局在化し、電子（正孔）が表面にトラップされる。正孔（電子）はガラス中のトラップ準位へ、ナノクリスタルとガラスが構成するポテンシャル障壁をトンネル過程により透過して捕獲される。このナノクリスタル（量子点）の光イオン化過程により、ナノクリスタル（量子点）のエネルギーは光励起前のエネルギーと異なる事となり、スペクトルホールが開く事となる[16]。時間分解分光によっても、励起子局在と電子・正孔への分解への振る舞いは明らかにされた[20]。

２－２　ルミネセンスホールバーニングと量子サイズ効果を受けたイオン化励起子

更に、ルミネセンスホールバーニングと量子サイズ効果を受けたイオン化励起子の存在が明らかになった[16, 22]。吸収スペクトル中にホールが形成されるとき、同時に発光スペクトルにホールが形成されることが予想される。この現象はルミネセンスホールバーニングと呼ぶことができる。ルミネセンスホールバーニングは吸収スペクトルのホールバーニングとは異なる新たな知見を与える。吸収スペクトルは、基底状態と励起状態との結合状態密度の大きさを反映する。一方、発光スペクトルは、 基底状態と励起状態の結合状態密度の大きさだけでなく、励起準位の緩和様式も反映し、ルミネセンスホールバーニングによって、よく光る励起状態を感度よく観測することができる。

NaCl 結晶中の CuCl 半導体ナノクリスタル（量子点）においてルミネセンスホールバーニングの測定を行なった結果、発光スペクトルの励起位置に鋭いホールと低エネルギー側にいくつかの構造を確認することができた。励起波長依存性からこれらの構造の中に、量子サイズ効果を受けた束縛励起子、イオン化励起子、およびイオン化励起子分子の構造があると同定した。イオン化励起子は２個の電子と１個の正孔によって、構成され、イオン化励起子分子は１個の電子と２個の正孔から構成される。これらの発光が観測されるということは、ナノクリスタル（量子点）がイオン化していることを示す。これらの発光帯の発光強度が積算励起強度の増加に従って増加することや、温度に対する依存性が、永続的ホールバーニングの温度依存性と類似することから、ナノクリスタル（量子点）のイオン化が永続的ホールバーニング現象において、重要な役割を担っている証拠になった。また量子点中のイオン化励起子の存在は、１個の量子点に１個の電子または正孔を注入するだけで、励起子のエネルギーを変えうること、すなわち量子点の光学遷移エネルギーを変えうる事を意味しており、単光子により量子点のエネルギー制御の可能性を示したものである。

２－３　永続的ホールバーニングの形成効率

永続的ホールバーニングを光多重メモリーに応用するとき、高いホールの形成効率を持つ材料が求められる。ガラスや結晶中に分子やイオンを分散させた試料についてのホールの形成効率は、１つの光子を吸収することによって、生じるホールの大きさを１つの分子やイオンの吸収で規格化した値を量子効率として評価される。同様に，半導体ナノクリスタル（量子点）のホールの形成効率の量子効率としては、１つの光子の吸収によって、生じるホールの大きさを１つの量子点の吸収で規格化した値を用いるべきである。CuCl ナノクリスタル(量子点)のホールの形成効率について測定の結果、ガラス中の CuCl ナノクリスタル（量子点）において最大 0.097 という大きな値を得た。この結果は、これまで報告されている量子効率としては最大である[27]。

光メモリーへの応用では、情報は、スペクトルホールとして記録される。読み出される信号の大きさは、記録されたスペクトルホールの大きさに比例する。すなわち、記録に用いる光の強さが同じならば、記録され読み出される信号の大きさは、量子効率と１個あたりの分子、イオンあるいは、半導体ナノクリスタル（量子点）の光吸収の断面積に比例する。10^{3}～10^{6}個の原子で構成される１個の半導体ナノクリスタル（量子点）の吸収断面積は１個の分子やイオンの吸収断面積より桁違いに大きい。この事実は、半導体ナノクリスタル（量子点）が有望な光多重メモリー材料であることを示している。

２－４　半導体ナノクリスタル（量子点）の永続的ホールバーニング現象の精密分光への応用

半導体ナノクリスタル（量子点）の永続的ホールバーニング現象の精密分光への応用も進展した[6, 21, 24, 28, 33, 34]。粒径分布のため不均一に広がった半導体ナノクリスタル（量子点）の吸収スペクトルを選択的（波長選択＝粒径選択）に励起することによって、選択励起した粒径だけをマーキングしスペクトルホールを作り、半導体ナノクリスタル（量子点）の電子エネルギーの粒径依存性を調べる詳細な研究が進みはじめた。その一例はナノクリスタル（量子点）中に閉じ込められた音響型フォノンの量子サイズ効果の観測であり[6]、量子化された励起状態の観測である。特に、CuCl ナノクリスタル（量子点）の立方体形状の量子箱に閉じ込められた高次量子数状態の観測は、その成功例である[28, 33]。

NaCl マトリックス中の CuCl ナノクリスタル（量子点）は立方体形状の量子箱として説明される振動構造を Z_3 励起子吸収スペクトル中に示すことがある。低温において、スペクトル幅の狭いレーザ光で Z_3 励起子吸収帯内を励起すると、シャープな永続的な励起子吸収の減少（永続的ホールバーニング）が観測される他、量子箱に閉じ込められた量子数 n_x、n_y、n_z の Z_3 励起子準位 $(n_x, n_y, n_z) = (2, 1, 1)$, $(2, 2, 1)$, $(3, 1, 1)$ または $(2, 2, 2)$ で光吸収をおこし、$(1, 1, 1)$ の状態に緩和した励起子が永続的ホールバーニングになる様子が観測された。量子箱に閉じ込められた高次量子数の状態がはじめて観測された例である。

２－５　半導体ナノクリスタル（量子点）中の多励起子状態（二励起子状態、三励起子状態）の観測

CuCl ナノクリスタル（量子点）に関する励起子共鳴励起下におけるサイズ選択ピコ秒ポンプ・プローブ測定から、量子点中の２励起子状態に起因する顕著な誘導吸収を発見した[29,36]。この２励起子状態は３次元的な量子閉じ込めの起こる量子点に特有の状態であり、量子点の光学非線形性に重要な寄与があると考えられている。

励起エネルギーの高エネルギー側に誘導吸収として現れる量子点中の励起子分子の励起状態＝弱く束縛された２励起子状態の存在は、量子点では１つの励起子がある時に、量子点中にさらに２つめの励起子を作るためにはより大きなエネルギーが必要になる事を示している。２励起子以上の励起子が閉じ込められた状態のエネルギーはどのようになるかという事についても興味が持たれるが、３励起子状態も同様に誘導吸収スペクトルに見出された。強励起下での吸収スペクトル変化、および２つのエネルギーの異なる励起パルスを用いた２段階の選択励起の方法による実験結果から、３励起子状態のエネルギーの粒径依存性が明らかになった。

２－６　量子ドットにおける励起子-フォノン相互作用

低温でのバルク半導体中の励起子の均一幅は、ゼロから連続的なエネルギー分布をもつ音響型フォノンとの相互作用により支配されており、温度に比例して広がり、$\Gamma = \Gamma_0 + AT$ と表わされることがよく知られているが、音響型フォノンが量子化されると、この通則が成り立たないのではないかと予想される。量子ドットでは音響型フォノンも量子化され、フォノンのエネルギーはゼロから連続的に分布したスペクトルから、とびとびのエネルギーを持つ様になる。これにより量子ドット中の量子化された電子や励起子の準位の温度に依存した均一幅は、温度に対しバルクとは異なった振る舞いを示す。この問題は最近の単一量子ドットの分光研究で 0.1meV をきるような極めて線幅の狭い発光スペクトルが観測されるようになって、顕在化してきた。

永続的ホールバーニングにより、CuCl 量子ドット中の量子化された励起子準位の均一幅を温度の関数として研究し、量子化された励起子と量子化された音響型フォノンとの相互作用を研究した。低温で、CuCl 量子ドットの励起子吸収帯中に微弱光で共鳴ホールを注意深く掘ると、その半値幅は極めて狭く 0.14meV であり、量子ドット中に閉じ込められた音響型フォノンが、サイドバンドホールとして十分分離して観測される。温度を上げて測ると、共鳴ホールに比べ、その閉じ込められた音響型フォノンによるサイドバンドホールは大きくなり、ついには、お互いに融合し、分離不能なバンドとなり、更に幅が広がっていく。共鳴ホールの半値幅の温度依存性は、励起子の線幅の温度依存性がバルク半導体で観測される温度リニアの依存性（$\Gamma = \Gamma_0 + AT$）ではなく、量子化されたフォノンがボーズ分布を反映して活性化され、励起子の均一幅に寄与できる様になり、均一幅が広がり始める。この様な特異な量子化された励起子と量子化されたフォノンの相互作用は量子ドットのサイズや温度の関数として永続的ホールバーニング分光によりスペクトル領域で明らかになった[35]。

３．今後の展望

情報化時代を迎え超高密度光メモリーは不可欠なものとなっている。更に単光子で制

御できる光スイッチの必要性もでてくるであろう。今後、半導体ナノクリスタル（量子点）の永続的ホールバーニング現象の研究とその応用の研究は、ホスト、ゲストのバラエティ、現象のバラエティが豊富で、大きな広がりが予想される。物理、応用物理だけでなく　広く材料科学まで含めた包括的研究が必要と思われる。また、単光子による半導体ナノクリスタル（量子点）のエネルギー制御の実現から、単光子量子点デバイスへの道も開けてくると思われる。

研究発表

(1)学会誌等

半導体ナノクリスタルの永続的ホールバーニングの研究論文
(*印はこの研究成果報告書に収録)

1) Y. Masumoto, L.G. Zimin, K. Naoe, S. Okamoto and T. Arai:
"Persistent Spectral Hole Burning in Semiconductor Microcrystals"
Mater. Sci. Eng. B 27, L5 (1994).

2) K. Naoe, L.G. Zimin, and Y. Masumoto:
"Persistent Spectral Hole Burning in Semiconductor Nanocrystals"
Phys. Rev. B 50, 18200 (1994).

3) Y. Masumoto:
"Persistent Spectral Hole-Burning of Semiconductor Nanocrystals"
Solid State Physics (Kotai Buturi) 29, 691 (1994)(in Japanese).

4) Y. Masumoto:
"Persistent Spectral Hole-Burning Phenomenon of Semiconductor Nanocrystals"
Proc. 22nd Int. Conf. Physics of Semiconductors, vol. 3, p.2015 (Vancouver, Canada, August 15-19, 1994).

5) Y. Masumoto, L.G. Zimin, K. Naoe, S. Okamoto, T. Kawazoe and T. Yamamoto:
"Observation of Persistent Spectral Hole-Burning in Semiconductor Nanocrystals"
J. Lumin. 64, 213 (1995); Proc. Spectral Hole-Burning and Related Spectroscopies: Science and Applications 4th Topical Meeting.

6) S. Okamoto and Y. Masumoto:
"Observation of Confined Acoustic Phonons in Semiconductor Nanocrystals by Means of the Persistent Spectral Hole-Burning Spectroscopy"
J. Lumin. 64, 253 (1995); Proc. Spectral Hole-Burning and Related Spectroscopies: Science and Applications 4th Topical Meeting.

7) Y. Masumoto:
"Persistent Spectral Hole-Burning in Semiconductor Quantum Dots"
Surf. Rev. Lett. 3, 143 (1996); Proc. 7th Int. Symp. Small Particles and Inorganic Clusters (Kobe, 1994). //INVITED PAPER//

8) Y. Masumoto:
"Persistent Spectral Hole Burning Phenomenon of Semiconductor Nanocrystals: Observation, Mechanism and Application"
Jap. J. Appl. Phys. 34, Suppl. 34-1, 8 (1995); Proc. Int. Conf. Optical Properties of Nanostructures (Sendai, 1994). //INVITED PAPER//.

9) S. Okamoto and Y. Masumoto:

"Persistent Spectral Hole-Burning in CuCl Nanocrystals: Demonstration of Optical Data Storage"
Jap. J. Appl. Phys. 34, Suppl. 34-1, 128 (1995); Proc. Int. Conf. Optical Properties of Nanostructures (Sendai, 1994).

10)*Y. Masumoto, S. Okamoto, T. Yamamoto and T. Kawazoe:
"Persistent Spectral Hole-Burning Phenomenon of Semiconductor Quantum Dots"
phys. status solidi 188, 209 (1995); Proc. 4th Int. Work. on Nonlinerar Optics and Excitation Kinetics in Semiconductors (Berlin, 1994). //INVITED PAPER//

11)Y.Masumoto:
"Semiconductor Nanocrystals: Lasing and Persistent Spectral Hole-Burning"
Inst. Elec. Inf. Commun. Eng. 77, 1125 (1994)(in Japanese).
Superlattices and Microstructures, 15, 33 (1994).

12)*Y. Masumoto, T. Kawazoe and T. Yamamoto:
"Observation of Persistent Spectral Hole Burning in CuBr Quantum Dots"
Phys. Rev. B 52, 4688 (1995).

13)*Y. Masumoto, K. Kawabata and T. Kawazoe:
"Quantum Size Effect and Persistent Hole Burning of CuI Nanocrystals"
Phys. Rev. B 52, 7834 (1995).

14)Y. Masumoto:
"Persistent Hole-Burning Spectroscoy in Semiconductor Quantum Dots"
Technical Digest of Quantum Electronics and Laser Science Conference (QELS'95, Baltimore) 16, p.96 (1995).//INVITED PAPER//

15)S. Okamoto and Y. Masumoto:
"Persistent Hole-Burning Spectroscopy of CuCl Microcrystallites: Host-Matrix-Dependence on the Hole-Burning Effects"
Technical Digest of the Pacific Rim Conference on Lasers and Electro-Optics (CLEO/ Pacific Rim '95, Makuhari Messe), p.260 (1995).

16)*Y. Masumoto and T. Kawazoe:
"Luminescence Hole Burning in Semiconductor Quantum Dots"
J. Lumin. 66 & 67, 142 (1996); Proc. 10th Intern. Conf. on Dynamical Processes in Excited States of Solids (Cairns, Australia, August 31, 1995).

17)Y. Masumoto:
"Persistent Spectral Hole Burning in Quantum Dots"
Prog. Crystal Growth and Charact. 33, 65 (1996); Proc. 5th ISSP Intern. Symp. Frontiers in Laser Physics and Spectroscopy (Tokyo, Nov., 1995). //INVITED PAPER//

18)*J. Qi and Y. Masumoto:
"Spectral Hole Burning in CdS Nanocrystals Embedded in Polyvinyl Alcohol"
Solid State Commun. 99, 467 (1996).

19)L.G. Zimin and Y. Masumoto:
"Semiconducting Nanocrystals in an Insulating Matrix: New Nonlinear Phenomena and a New Region of Application"
Opt. Technol. 62, 797 (1995). [Opticheski Zhurnal 62, 55 (1995)].
20)*T. Okuno, H. Miyajima, A. Satake and Y. Masumoto:
"Exciton Localization and Decomposition Dynamics in Cuprous-Halide Nanocrystals"
Phys. Rev. B 54, 16952 (1996).
21)Y. Masumoto, K. Sonobe and N. Sakakura:
"Persistent Hole Burning Spectroscopy of Semiconductor Quantum Dots"
Proc. 23rd Int. Conf. Physics of Semiconductors, vol.2, p.1481 (Berlin, Germany, July 21-26, 1996).
22)*T. Kawazoe and Y. Masumoto:
"Luminescence Hole Burning and Quantum Size Effect of Charged Excitons in CuCl Quantum Dots"
Phys. Rev. Lett. 77, 4942 (1996).
23)T. Kawazoe and Y. Masumoto:
"Observation of Luminescence Hole-Burning in CuCl Quantum Dots"
J. Lumin. 72-74, 862 (1997); Proc. Int. Conf. on Luminescence and Optical Spectroscopy of Condensed Matter (Aug. 1996, Prague).
24)Y. Masumoto, K. Sonobe and N. Sakakura:
"Application of Persistent Hole Burning to Site-Selective Spectroscopy of Semiconductor Quantum Dots"
J. Lumin. 72-74, 294 (1997); Proc. Int. Conf. on Luminescence and Optical Spectroscopy of Condensed Matter (Aug. 1996, Prague).
25)T. Okuno, A. Satake and Y. Masumoto:
"Reconsideration of Relaxation Processes of Excitons in CuCl Nanocrystals"
J. Lumin. 72-74, 383 (1997); Proc. Int. Conf. on Luminescence and Optical Spectroscopy of Condensed Matter (Aug. 1996, Prague).
26)*Y. Masumoto:
"Persistent Hole Burning in Semiconductor Nanocrystals"
J. Lumin. 70, 386 (1996).
27)T. Kawazoe and Y. Masumoto:
"Highly Efficient Persistent Hole Burning in Cuprous Halide Quantum Dots"
To be published in Jap. J. Appl. Phys.
28)*N. Sakakura and Y. Masumoto:
"Observation of Excited State Excitons in CuCl Quantum Cubes"
Jap. J. Appl. Phys. 36, 4212 (1997); Proc. Int. Symp. on Formation, Physics and Device Application of Quantum Dot Structures (Sapporo, 1996).
29)*M. Ikezawa and Y. Masumoto:

"Observation of Excited Biexciton States in CuCl Quantum Dots: Control of the Quantum Dot Energy by a Photon"
Jap. J. Appl. Phys. 36, 4191 (1997); Proc. Int. Symp. on Formation, Physics and Device Application of Quantum Dot Structures (Sapporo, 1996),.

30)*S. Okamoto and Y. Masumoto:
"Correlation between the Cu^{+}-Ion Instability and Persistent Spectral Hole-Burning Phenomena of CuCl Nanocrystals"
Phys. Rev. B 56, 15729 (1997).

31)S. Okamoto and Y. Masumoto:
"Demonstration of Frequency-Domain Optical Data Strorage of CuCl Semiconductor Nanocrystal Systems"
Jap. J. Appl. Phys. 35, 512 (1996).

32)S. Okamoto and Y. Masumoto:
"Persistent Spectral Hole-Burning of CuCl Quantum Dots"
Mater. Res. Soc. Symp. Proc. 405, 301 (1996).

33)*N. Sakakura and Y. Masumoto:
"Persistent spectral-hole-burning spectroscopy of CuCl quantum cubes"
Phys. Rev. B 56, 4051 (1997).

34)*Y. Masumoto and K. Sonobe:
"Size-dependent energy levels of CdTe quantum dots"
Phys. Rev. B 56, 9734 (1997).

35)Y. Masumoto, T. Kawazoe and N. Matsuura:
"Exciton-confined phonon interaction in quantum dots"
To be published in J. Lumin.

36)*M. Ikezawa, Y. Masumoto, T. Takagahara and S. Nair:
"Biexciton and triexciton states in quantum dots in the weak confinement regime"
Phys. Rev. Lett. 79, 3522 (1997).

その他の論文

37)L. Zimin, S.V. Nair and Y. Masumoto:
"LO phonon renormalization in optically excited CuCl nanocrystals"
To be published in Phys. Rev. Lett.

38)Y. Masumoto:
"Semiconductor Quantum Dots Behave Like Molecules"
Proc. Int. Symp. Similarities and Differences between Atomic-Nuclei and Microclusters: Unified Developments for Cluster Sciences, AIP Conference Proceeding 416 (Tsukuba, 1997)p.45. //INVITED PAPER//

39)M. Ikezawa and Y. Masumoto:
"A Stochastic Treatment of the Dynamics of Excitons and Excitonic Molecules in CuCl Nanocrystals"
Phys. Rev. B 53, 13694 (1996).
40)M. Ikezawa and Y. Masumoto:
"Observation of the Stochastic Exciton Dynamics in CuCl Quantum Dots"
Prog. Crystal Growth and Charact. 33, 175 (1996); Proc. 5th ISSP Intern. Symp. Frontiers in Laser Physics and Spectroscopy (Tokyo, Nov., 1995).
41)T. Mishina and Y. Masumoto:
"Nonlinear Coherent Propagation of Femtosecond Optical Pulses in Semiconductors"
Prog. Crystal Growth and Charact. 33, 113 (1996); Proc. 5th ISSP Intern. Symp. Frontiers in Laser Physics and Spectroscopy (Tokyo, Nov., 1995).
42)Y. Iwazaki, T. Mishina, Y. Masumoto and M. Nakayama:
"Coherent Zone-Folded Phonons in GaAs/AlAs Superlattices Measured by Femtosecond Pump-Probe Spectroscopy"
Proc. 23rd Int. Conf. Physics of Semiconductors, vol.1, p.701 (Berlin, Germany, July 21-26, 1996).
43)B.-R. Hyun, T. Mishina, Y. Masumoto and M. Nakayama:
"Time-Resolved Reflection Spectroscopy in Multiple Quantum Wells at Brewster-Angle Incidence"
Proc. 23rd Int. Conf. Physics of Semiconductors, vol.1, p.761 (Berlin, Germany, July 21-26, 1996).
44)S. Okamoto, Y. Kanemitsu and Y. Masumoto:
"Quantum Confinement Effects on Photoluminescence from Silicon Single Quantum Wells"
Proc. 23rd Int. Conf. Physics of Semiconductors, vol.3, p.1863 (Berlin, Germany, July 21-26, 1996).
45)S. Yamaguchi, Y. Kawakami, Sz. Fujita and Sg. Fujita, Y. Yamada, T. Mishina and Y. Masumoto:
"Recombination Dynamics of Localized Excitons in CdSe/ZnSe/ZnS_xSe_{1-x} Single-Quantum-Well Structures"
Phys. Rev. B 54, 2629 (1996).
46)N. Peyghambarian, E. Hanamura, S. W. Koch, Y. Masumoto and E. M. Wright:
"Optical Characterization and Applications of Semiconductor Quantum Dots"
in "Nanomaterials; Synthesis, Properties and Applications", ed. by A. S. Edelstein and R. C. Cammarata, chapt.16, p.395-p.436 (Institute of Physics Publishing, 1996).
47)H.-W. Ren, K. Nishi, S. Sugou, M. Sugisaki and Y. Masumoto:
"Control of InAs Self-Assembled Islands on GaAs Vicinal Surfaces by Annealing

in Gas-Source Molecular Beam Epitaxy"
Jap. J. Appl. Phys. 36, 4118 (1997); Proc. Int. Symp. on Formation, Physics and Device Application of Quantum Dot Structures (Sapporo, 1996).

48)T. Matsumoto, Y. Masumoto, S. Nakashima, H. Mimura and N. Koshida:
"Photoluminescence from Deuterium Terminated Porous Silicon"
Extended Abstracts of the 1996 Int. Conf. on Solid State Devices and Materials (Yokohama, 1996) p.709.

49)Y. Yamada, T. Mishina, Y. Masumoto, Y. Kawakami, J. Suda, Sz. Fujita, Sg. Fujita, and T. Taguchi:
"Dynamics of Dense Excitonic Systems in ZnSe-Based Single Quantum Wells"
Crys. Growth 159, 814 (1996).

50)Y. Kawakami, M. Funato, Sz. Fujita, Sg. Fujita, Y. Yamada, T. Mishina, and Y. Masumoto:
"Effects of High Excitation on Localized Excitons in Cubic ZnCdS Lattice Matched to GaAs"
Crys. Growth 159, 830 (1996).

51)A.V. Baranov, Y. Masumoto, K. Inoue, A.V. Fedorov and A.A. Onushchenko:
"Size-Selective Two-Photon Spectroscopy of CuCl Spherical Quantum Dots"
Phys. Rev. B 55, 15675 (1997).

52)A.V. Baranov, S. Yamauchi and Y. Masumoto:
"Exciton-LO-phonon interaction in CuCl spherical quantum dots studied by resonant hyper-Raman spectroscopy"
Phys. Rev. B 56, 10332 (1997).

53)T. Mishina, Y. Iwazaki, Y. Masumoto and M. Nakayama:
"Coherent dynamics of zone-folded acoustic phonon in GaAs/AlAs superlattices"
To be published in J. Lumin.

54)T. Matsumoto, Y. Masumoto, S. Nakashima, H. Mimura and N. Koshida:
"Coupling effect of surface vibration and quantum confinement carriers in porous silicon"
Appl. Surf. Science 113, 140 (1997).

55)T. Matsumoto, Y. Masumoto, T. Nakagawa, M. Hashimoto, K. Ueno and N. Koshida:
"Electroluminescence from Deuterium Terminated Porous Silicon"
Jap. J. Appl. Phys. 36, L1089 (1997).

56)B.-R. Hyun, T. Mishina, Y. Masumoto and M. Nakayama:
"Coherent reflected-pulses of exciton-polaritons in multiple quantum wells at Brewster's angle incidence"
Phys. Rev. B 56, 12780 (1997)(Rapid Communications).

57)Y. Masumoto and M. Ikezawa:
"Electron-hole plasma and its pulsation luminescence in CuBr"

Solid State Commun. 105, 151 (1998).

58)S. Kuroda, Y. Terai, K. Takita, T. Okuno and Y. Masumoto:
"Self-Organized Quantum Dots of Zinc-Blende MnTe Grown by Molecular Beam Epitaxy"
Proc. 8th Int. Conf. II-VI Compounds (Grenoble, 1997).

59)T. Okuno, H.-W. Ren, M. Sugisaki, K. Nishi, S. Sugou and Y. Masumoto:
"Time-resolved luminescence of InP quantum dots in $Ga_{0.5}InP_{0.5}$ matrix: Carrier injection from the matrix"
Phys. Rev. B. 57, 1386 (1998).

60)T. Okuno, H.-W. Ren, M. Sugisaki, K. Nishi, S. Sugou and Y. Masumoto:
"Time-resolved luminescence study of InP quantum dots in GaInP matrix"
Proc. Int. Workshop Nano-Physics and Electronics '97.

61)M. Sugisaki, H. W. Ren, S. Sugou, K. Nishi and Y. Masumoto:
"Sharp Photoluminescence Lines of InAs Quantum Dot Embedded in GaAs Mesa"
Proc. Int. Workshop Nano-Physics and Electronics '97.

62)A. Satake, Y. Masumoto, T. Miyajima, T. Asatsuma, F. Nakamura and M. Ikeda:
"Localized exciton and its stimulated emission in surface mode from single-layer $In_xGa_{1-x}N$"
Phys. Rev. B 57, 2041 (1998)(Rapid Communications).

63)T. Mishina, Y. Iwazaki Y. Masumoto and M. Nakayama:
"Real Time-Sapce Dynamics of Zone-Folded Phonons in GaAs/AlAs Superlattices"
Submitted to Solid State Commun.

64)A. Satake and Y. Masumoto:
"Localized Exciton and Its Stimulated Emission in InGaN Multiple Quantum Wells"
Proc. Second Int. Conf. Nitride Semiconductors (Tokushima, 1997), J. Crys. Growth, special issue.

(2)口頭発表

主な招待講演

1) Y. Masumoto: "Control of the quantum dot energy by a photon", Intern. Symp. of Quantum Structures for Photonic Applications (Sendai, March, 1997). //INVITED PAPER//
2) 舛本泰章："量子点・ナノクリスタルの新しい物理と応用"（シンポジュウム講演） 第43回応用物理学会春季講演会（1996年3月）

3) 舛本泰章：“量子点研究により、わかったこと、わからないこと”（シンポジュウム講演）日本物理学会（1996 年 4 月）
4) 舛本泰章：“単光子による量子ドットのエネルギー制御”応用物理学会（1997 年 10 月）

その他の口頭発表

1) 川添忠、舛本泰章：“CuCl ナノクリスタルにおけるルミネッセンス・ホールバーニング”日本物理学会（1996 年 4 月）
2) 坂倉成、川添忠、舛本泰章：“CuCl 量子箱の永続的ホールバーニング分光”日本物理学会（1996 年 4 月）
3) 佐竹昭泰、奥野剛史、舛本泰章：“CuCl ナノクリスタル中の励起子の緩和過程”日本物理学会（1996 年 4 月）
4) 奥野剛史、佐竹昭泰、舛本泰章：“CuCl ナノクリスタルにおける励起子発光のストークスシフトと発光寿命”日本物理学会（1996 年 4 月）
5) 池沢道男、舛本泰章：“CuCl ナノクリスタル中の励起子・励起子分子のダイナミクスⅡ”日本物理学会（1996 年 4 月）
6) 奥野剛史、佐竹昭泰、舛本泰章:“ハロゲン化銅ナノクリスタルにおける励起子の緩和過程”物性研短期研究会「ナノ構造の光物性の新局面」（1996 年 6 月）
7) 園部孝二、舛本泰章：“CdTe ナノクリスタルの励起状態の研究”日本物理学会(1996 年 9 月)
8) 伊藤敦史、坂倉成、三品具文、舛本泰章：“NaCl 中の CuCl ナノクリスタルの２光子共鳴散乱”日本物理学会(1996 年 9 月)
9) 坂倉成、川添忠、舛本泰章：“CuCl 量子箱の永続的ホールバーニング分光Ⅱ”日本物理学会(1996 年 9 月)
10) 川添忠、舛本泰章：“銅ハライドナノクリスタルにおける永続的ホールの形成効率測定”日本物理学会(1996 年 9 月)
11) 池沢道男、舛本泰章：“CuCl ナノクリスタル中の励起子・励起子分子のダイナミクスⅢ”日本物理学会(1996 年 9 月)
12) 奥野剛史、佐竹昭泰、辻原康弘、舛本泰章：“ハロゲン化銅ナノクリスタルにおける励起子発光の緩和過程”日本物理学会(1996 年 9 月)
13) 川添忠、舛本泰章：“CuBr ナノクリスタルの“量子サイズ効果”” 日本物理学会(1996 年 9 月)
14) 戚継発、奥野剛史、舛本泰章：“CdS:Mn ナノクリスタルにおける発光分光研究”日本物理学会（1996 年 10 月）
15) Jifa Qi, Tsuyoshi Okuno and Yasuaki Masumoto:“Optical Properties of CdS:Mn nanocrystal in Polyvinyl Alcohol”, 2nd Asia Symposium on Condensed Matter Photophysics, Nara, Japan, (1996).
16) Jifa Qi, Tsuyoshi Okuno and Yasuaki Masumoto:“Mn^{2+} luminescence in CdS:Mn quantum

dots", 2nd Symposium on the Physics and Application of Spin-Related Phenomena in Semiconductors, Sendai, Japan, (Jan 26-27, 1997).

17) 戚継発、奥野剛史、舛本泰章：“CdS:Mn ナノクリスタルの Mn 発光”（招待講演）電気化学学会(97)年会蛍光体シンポジウム（1997 年 3 月）

18) 戚継発、奥野剛史、舛本泰章：“CdS:Mn ナノクリスタルのおける発光分光研究Ⅱ”日本物理学会（1997 年 3 月）

19) 奥野剛史、任紅文、杉崎満、西研一、菅生繁男、舛本泰章:“InP 量子点の発光の時間分解 -マトリックスからのキャリア流入-”応用物理学会（1997 年 3 月）

20) 川添忠、舛本泰章：“CuCl 量子点における永続的ホールの狭い線幅とその温度依存性”日本物理学会（1997 年 3 月）

21) 坂倉成、舛本泰章：“CuCl 量子ドットにおけるサテライトホールの線幅”日本物理学会（1997 年 3 月）

22) 伊藤敦史、A. V. Baranov、三品具文、舛本泰章、井上久遠：“CuCl 量子点の２光子選択励起分光：量子点中に縦波励起子は存在するのだろうか？”日本物理学会(1997 年 3 月）

23) 池沢道男、舛本泰章 ：“CuCl 量子点における多励起子状態”日本物理学会（1997 年 3 月）

24) 園部孝二、舛本泰章：“CdTe ナノクリスタルの励起状態の研究Ⅱ”日本物理学会（1997 年 3 月）

25) Lev Zimin、兼松泰男、櫛田孝司、舛本泰章:“Electron-phonon interaction in CuCl nanocrystals doped into glass as investigated by persistent spectral hole burning”日本物理学会（1997 年 3 月）

26) 寺井慶和、黒田眞司、滝田宏樹、奥野剛史、舛本泰章：“MBE 法における MnTe 自己形成量子ドットの作製とその光物性”日本物理学会（1997 年 10 月）

27) 玄柄律、三品具文、舛本泰章、Kim Dae Sik、Lim Yong Sik：“GaAs/AlGaAs AQWS 中の励起子におけるフェムト秒ポンプープローブ分光測定”日本物理学会（1997 年 10 月）

28) 新田一樹、三品具文、舛本泰章：“グラファイトにおけるフェムト秒ポンプ・プローブ分光”日本物理学会（1997 年 10 月）

29) 山内掌吾、A. V. Baranov、舛本泰章： “CuCl 量子点の共鳴２光子分光”日本物理学会（1997 年 10 月）池沢道男、勝田泰生、舛本泰章：“Glass 中の CuCl 量子点における励起子分子状態”日本物理学会（1997 年 10 月）

30) 池沢道男、三品具文、舛本泰章：“NaCl 中の CuCl 量子点におけるフォトンエコー”日本物理学会（1997 年 10 月）

31) L. Zimin, S. Nair, Y. Masumoto:“Phonon-assisted absorption in CuCl nanocrystals”日本物理学会（1997 年 10 月）

32) 杉崎満、任紅文、徳永英司、松本貴祐、田中正規、西研一、菅生繁雄、奥野剛史、舛本泰章：“InP 量子点における光学異方性”日本物理学会（1997 年 10 月）

33) 徳永英司、V. G. Davydov、杉崎満、S. V. Nair、任紅文、西研一、菅生繁雄、舛本泰章：“InP 量子点の２波長ポンププローブ分光”日本物理学会（1997 年 10 月）

34) Yasuaki Masumoto, Valentin Davydov: “Energy transfer observation in Ⅲ－Ⅴ self-assembled quantum dots”日本物理学会（1997 年 10 月）
35) 徳永英司、松本貴祐、杉崎満、田中正規、松浦直紀、セルバクマール・ナイア、舛本泰章：“CuCl 励起子分子の励起子逆系列発光”日本物理学会（1997 年 10 月）
36) 三品具文、舛本泰章：“半導体超格子におけるコヒーレントフォノン”日本物理学会（1997 年 10 月）
37) 松本貴祐、近藤道雄、舛本泰章：“ポーラスシリコンにおける発光強度と中性欠陥密度の負の相関”応用物理学会（1997 年 10 月）
38) 松本貴祐、舛本泰章、中川隆史、越田信義：“重水素終端したポーラスシリコンの電気的・光学的性質”応用物理学会（1997 年 10 月）
39) 佐竹昭泰、舛本泰章、宮嶋孝夫、朝妻庸紀、中村文彦、池田昌夫：“高密度励起下における InGaN の励起子誘導発光”応用物理学会（1997 年 10 月）
40) 任紅文、杉崎満、菅生繁雄、西研一、舛本泰章：“InAs/GaAs 自己形成単一量子点の PL 発光”応用物理学会（1997 年 10 月）
41) 奥野剛史、任紅文、杉崎満、西研一、菅生繁雄、舛本泰章：“GaInP マトリックス中 InP 量子点の発光の時間分解”応用物理学会（1997 年 10 月）
42) 田中正規、戚継発、徳永英司、松本貴祐、杉崎満、舛本泰章：“ポリマー中 ZnS:Mn ナノ結晶の光学特性”応用物理学会（1997 年 10 月）

以降は、研究発表論文リストの＊印の論文です。
一部（下記6件）は、著作権者（出版社、学会等）の許諾を得ていないため、筑波大学では電子化・公開しておりません。
なお、電子ジャーナルとして出版社から公開されており、契約している場合は全文を読むことができますので、下記のリンク先をご覧ください。

論文 10）　http://dx.doi.org/10.1002/pssb.2221880118

論文 16）　http://dx.doi.org/10.1016/0022-2313(95)00126-3

論文 18）　http://dx.doi.org/10.1016/0038-1098(96)00310-9

論文 26）　http://dx.doi.org/10.1016/0022-2313(96)00073-7

論文 28）　http://dx.doi.org/10.1143/JJAP.36.4212

論文 29）　http://dx.doi.org/10.1143/JJAP.36.4191

Observation of persistent spectral hole burning in CuBr quantum dots

Yasuaki Masumoto, Tadashi Kawazoe, and Tetsuya Yamamoto
Institute of Physics and Center for TARA (Tsukuba Advanced Research Alliance), University of Tsukuba, Tsukuba, Ibaraki 305, Japan
(Received 16 May 1995)

Persistent spectral hole-burning phenomenon in CuBr quantum dots embedded in glass was observed. The spectral hole and the sideband holes were made together with the redshift of the absorption spectrum in proportion to the logarithm of the laser fluence and were preserved for more than 8 h at 2 K. They were erasable by the temperature rise or by the light exposure. Electron trapping at the surface of the dots and hole tunneling into traps in the glass host is the most probable origin of the persistent spectral hole-burning phenomenon in CuBr quantum dots.

Nanometer-size semiconductor crystals, abbreviated to semiconductor nanocrystals, are known as zero-dimensional quantum dots.[1-3] Their optical properties have been characterized by the quantum confinement effect, and the lowest excited states show blueshifts depending on their size. Quantum dots are sharply different from quantum wells and quantum wires in the point that quantum dots are made of as small as 10^3-10^6 atoms. A considerable fraction of atoms face the surface or the interface of quantum dots in the surrounding materials. Therefore, it is quite natural to consider that the structure and the electronic states of quantum dots should not be treated by themselves, but should be treated together with the real surfaces or interfaces and the surrounding materials.

However, this natural consideration has been treated lightly. Semiconductor quantum dots have been generally treated as spherical- or cubic-shaped dots isolated from surrounding materials for the calculation of the fundamental and nonlinear optical properties.[2,3] Afterwards, interaction between dots and surrounding materials was taken into account as the effects of traps, surface states, etc., for the interpretation of experimental results which cannot be explained by the theoretical treatment of the idealized quantum dots. The interaction is considered to induce the change of the dynamical or nonlinear optical properties of quantum dots, but is not considered to induce the fundamental absorption spectra of the quantum dots. As a proof of this statement, the generally accepted model of inhomogeneous broadening treats the size distribution of dots as the unique origin of inhomogeneity.

Let us consider molecular or ionic guests embedded in glass, crystal, or polymer hosts which are much smaller than the quantum dot system. We can naturally understand that guests consisting of small numbers of atoms are greatly influenced by the surrounding hosts, and that the energy levels of the guest-host system are inhomogeneously broadened. Persistent spectral hole-burning (PSHB) phenomenon has been observed in a number of these materials.[4] The PSHB phenomenon requires the existence of more than one energetically inequivalent ground state of the total system consisting of guest and matrix. Moreover, the relaxation among the ground states must be slower than the decay rate of any excited state. This condition causes the persistency of the hole.

When spectrally narrow light excites the ensemble of semiconductor quantum dots having inhomogeneously broadened absorption bands, a spectral hole is formed at the position of the excitation photon energy in the absorption band. So far, spectral hole burning observed in quantum dots has been believed to be transient. Nevertheless, CdSe and CuCl quantum dots embedded in glasses and crystals show the PSHB phenomena.[5,6] Similarly, we may be able to find other kinds of quantum dots which show the PSHB phenomenon. The observation of the phenomenon requires additional inhomogeneous broadening for quantum dots coming from the various ground-state configurations of the dot-matrix system. In this sense, the concept for the inhomogeneous broadening of quantum dots should be drastically changed. In this paper, we present an experimental observation of the PSHB of CuBr quantum dots embedded in glass, and consider the mechanism of the phenomenon.

The samples studied are CuBr nanocrystals in potassium aluminoborosilicate glass.[7] The mean size of the nanocrystals was measured by small-angle x-ray scattering and was 3.6 nm in radius. The sample was directly immersed in superfluid helium or mounted on the cold finger of the temperature variable cryostat. A spectrally narrow dye laser with DPS dye pumped by a Q-switched Nd^{3+}:YAG (yttrium aluminum garnet) laser was used as a pump source, and a halogen lamp was used as a probe source. The spectral width of the dye laser was 0.014 meV. The transmittance spectrum was measured by using an optical multichannel analyzer in conjunction with a 25-cm monochromator. For the hole-filling experiment, another halogen lamp was used with a set of interference filters.

Figure 1(a) shows the inhomogeneously broadened absorption spectrum of the sample. The average radius of the CuBr nanocrystals was 3.6 nm. The spectrum has a pronounced peak at 3.073 eV which is higher than the $Z_{1,2}$ exciton energy of bulk CuBr by 109 meV. The blueshift is consistent with the previous data of CuBr quantum dots which were interpreted by the donorlike exciton model.[8]

After the center of the $Z_{1,2}$ exciton absorption band of the sample was excited by 9000 shots of dye laser pulses

with an energy density of 5 $\mu J/cm^2$, the absorption spectrum was changed, as is displayed in Fig. 1(b). The absorption spectral change $-\Delta\alpha d$ is defined as the difference in the absorbance of the sample from that of the virgin sample. This spectral change is long preserved. The upper spectrum in Fig. 1(b) shows the spectral change at 2 min after the laser exposure was stopped. The spectral change was found to decrease in proportion to the logarithm of time between 2 and 100 min, and does not decrease substantially at 50 min. At 2 K, we observed that the spectral hole was preserved for more than 8 h after the excitation. The persistent spectral change is the sharp peak of a main spectral hole marked by ● and satellite holes marked by ■ which are superimposed on the broad wavy structure (○). The wavy structure is well approximated by the first derivative of the absorption spectrum. This means the occurrence of a small redshift of the absorption spectrum. If the derivative of the absorption spectrum is subtracted from the observed spectral change, satellite holes are on the induced absorption structure at the higher-energy side of the main hole. We consider the induced absorption structure comes from a photoproduct.

With the change of the pump photon energy, energy positions of the main hole and the satellite holes change. The energy separation between the main hole and the satellite holes (1, 1′, 2′) does not change with the change of the pump photon energy, and is equal to the optical phonon energy or twice the size of it, so that the satellite holes 1, 1′, and 2′ are optical-phonon sidebands. The energy separation between the main hole and the satellite holes 2 and 3 changes with the change of the pump photon energy, and their change is interpreted by the energy separation between size-quantized levels of anisotropic multicomponent $Z_{1,2}$ excitons. This observation suggests that PSHB spectroscopy can be applicable to precise optical measurement of size-dependent quantum dots by laser marking.

The hole depth and the amplitude of the wavy structure increase in proportion to logarithm of the laser fluence, as is shown in Fig. 2. The logarithmic dependence holds for more than four decades of the fluence. The logarithmic hole growth has been observed in molecules in organic glasses and color centers in crystals, and is explained by a model which assumes the broad distribution of the burning rate.[9] This model is based on tunneling through the potential barrier with distributed barrier height and thickness. The model assumes that the burning rate is proportional to $\exp(-\lambda)$ and that the tunneling parameter λ is rather uniformly distributed. Similarly, the hole burning in CuBr quantum dots is considered to take place via tunneling through a potential barrier with a broadly distributed barrier height and thickness.

The hole structures and the wavy structure are erasable by the temperature rise. Figure 3 shows the absorption change of the sample after the temperature cycle between T_b and T. First, the absorption spectrum of the virgin sample was taken at the burning temperature T_b. The sample was exposed by 9000 shots of dye laser pulses with an energy density of 5 $\mu J/cm^2$ at T_b. The temperature of the sample was raised to T and maintained for 5 min. After that, it was cooled down to T_b. Then the absorption spectrum was measured and the difference spectrum was obtained. Even if we prolong the annealing time up to 60 min, the difference spectrum changes little. With the increase of annealing temperature, the hole depth and the amplitude of the wavy structure is reduced similarly. At the lower part of Fig. 3, both of them are plotted as a function of temperature.

The thermal hole filling is explained by the thermally activated barrier crossing mechanism.[10] The rate of this

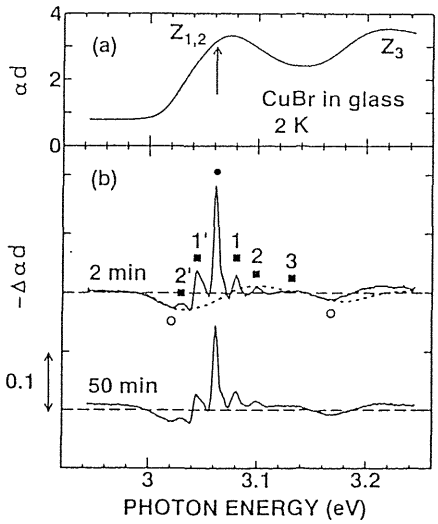

FIG. 1. (a) Absorption spectrum of a virgin sample, CuBr nanocrystals (the average radius is 3.6 nm) embedded in glass. (b) The absorption spectral change of the sample after the spectrally narrow laser exposure (9000 shots of dye laser pulses with the pump photon energy of 3.061 eV, and an excitation energy density of 5 $\mu J/cm^2$). Long-dashed lines show the zero base, and the short-dashed line shows the derivative of the absorption spectrum (a).

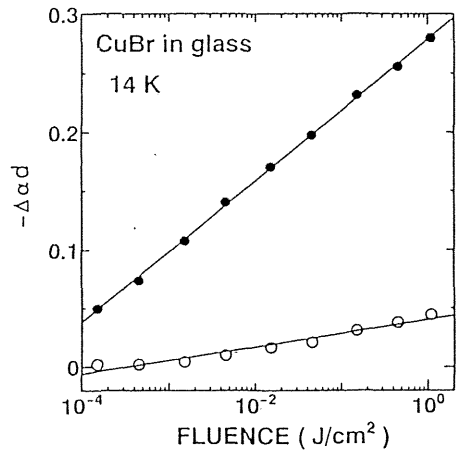

FIG. 2. Solid circles show the hole depth as a function of the laser fluence. Open circles show the maximum amplitude of the wavy structure. Both data are taken by changing the exposure time with the excitation energy density of 5 $\mu J/cm^2$.

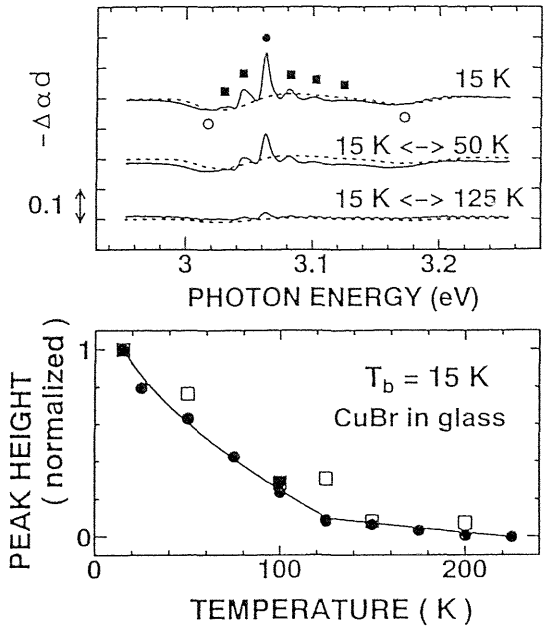

FIG. 3. The upper figure shows the persistent spectral change remaining after the temperature cycle. The hole was burned at 15 K. The lower figure shows the normalized hole depth (solid circles) and the normalized amplitude of the wavy structure (open squares) as a function of the annealing temperature. The solid line is the fit of the hole depth by the expressions shown in the text.

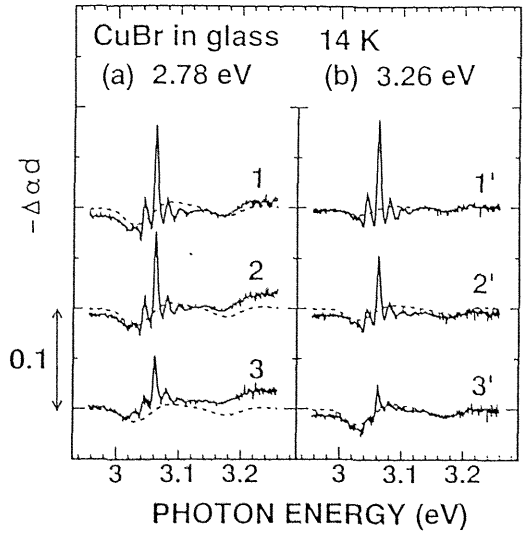

FIG. 4. Light-induced hole-filling experiments for case (a), in which the erase light energy, 2.78 eV, is below the absorption edge of the CuBr quantum dots, and for case (b), in which the erase light energy, 3.26 eV, is above the absorption edge. The spectral width of the erase light is 0.07 eV. Exposure times for spectra 1(1'), 2(2'), and 3(3') are 0, 120, and 3000 s, respectively. Dashed lines show the derivative of the absorption spectrum.

mechanism is represented by $\nu=\nu_0\exp(-V/kT)$, where ν_0 is the frequency factor whose order is given by $kT/h\approx 10^{11}-10^{13}\ \mathrm{s}^{-1}$, and V the potential barrier. During the holding time t at the annealing temperature T, the hole is filled if the condition $\nu t>1$ holds. Therefore the hole is filled if $V<kT\ln(\nu_0 t)$. From the rather uniform distribution of the tunneling parameter, we assume that the distribution of the potential barrier $P(V)$ is represented by $P(V)\propto 1/\sqrt{V}$ with a maximum barrier height $V_{\max}$.[10] The normalized hole depth observed after the temperature cycle between T_b and T can be calculated by

$$\int_{kT\ln(\nu_0 t)}^{\infty} P(V)dV \Big/ \int_{kT_b\ln(\nu_0 t)}^{\infty} P(V)dV \ .$$

This expression gives the functional form of $(1-\sqrt{kT\ln(\nu_0 t)/V_{\max}})/(1-\sqrt{kT_b\ln(\nu_0 t)/V_{\max}})$ for $kT\ln(\nu_0 t)<V_{\max}$. The experimental results shown in Fig. 3 are well fitted by this expression, if we consider two distributions of potential barriers. In fact, fitting by the expression $0.7\ (1-0.089\sqrt{T})/(1-0.089\sqrt{T_b})$ for $T<125$ K, plus $0.3\ (1-0.067\sqrt{T})/(1-0.067\sqrt{T_b})$ for $T<225$ K, gives a good result. The obtained maximum barrier heights for two distributions are 0.36 and 0.65 eV.

The hole structures are also erasable by the broad-band light exposure. The light-induced hole-filling spectrum is shown in Fig. 4. Hole filling takes place even when the transparent region of the CuBr absorption spectrum is excited, as is shown in Fig. 4(a). As low as 1.2 eV, broad-band infrared light erased the hole. The hole-filling efficiency depends on the photon energy, and decreases monotonously with the decrease in the photon energy. The erased spectrum almost returns to the spectrum of the virgin sample, when the erase light is below the absorption edge of the CuBr quantum dots. On the other hand, when the absorption band of CuBr dots is excited by the broad-band light, it causes hole filling more efficiently than the below-absorption-edge light, but the persistent wavy structure coming from the redshift of the absorption spectrum is more enhanced, as is seen in Fig. 4(b).

The observation of the PSHB phenomenon, hole persistency, and thermal-annealing and light-induced hole filling, is confirmed in this way in CuBr quantum dots embedded in glass. The following is the most probable scenario of the observed PSHB phenomena. Photoexcited exciton in a CuBr dot is localized somehow, and an electron is trapped at the surface of the dot. A hole escapes from the dot, tunnels through the potential barrier in glass, and is trapped at the H_1^+ center in the glass host.[11] The potential barrier height between CuBr quantum dots and traps in glass is considered to be broadly distributed, and the maximum heights 0.36 and 0.65 eV are reasonably less than the difference in the energy gaps of CuBr and glass.[12] An exciton bound to an ionized donor or an ionized acceptor is a well-known problem in analogy with the problem of H_2^+. In the case that the mass ratio of electron to hole, m_e^*/m_h^*, is less than 0.4, the exciton is bound to an ionized donor but is not bound to an ionized acceptor.[13] From the values of $m_e^*=0.28m_0$ and $m_h^*=1.4m_0$,[14] $m_e^*/m_h^*=0.2$ holds, so that the exciton is not bound to an electron trapped at the surface of dots. In this case, Coulomb interaction in the dots causes the blueshift of the exciton energy, which results in hole burning and induced absorption at the high-energy side. This explains the observed main hole

and the associated induced absorption at the higher-energy side. Spatially separated electrons and holes apply the local electric field to CuBr dots and cause the quantum-confined Stark effect. The effect gives the redshift of the exciton structure. Not only photoexcited dots but also nonphotoexcited dots feel the electric field because of the long-range character of the Coulomb field. The ensemble of dots shows the quantum-confined Stark shift. Therefore, the redshift of the inhomogeneously broadened absorption spectrum is observed.

The spectral hole and the redshift of the absorption spectrum behave similarly in Figs. 2, 3, and 4(a). Now we can clearly understand these observations on the photoionization model. The only difference is observed in Fig. 4(b). When the erase light energy is below the absorption edge of CuBr dots, trapped holes are excited and recombine with electrons localized at the interface of dots. This process erases both the burned hole structures and the wavy structures coming from the redshift of the absorption spectrum, because the photoionized dots return to deionized dots. On the other hand, the broad erase light above the absorption edge of CuBr dots may deionize the burned dots but ionize many unburned dots. The former process fills the burned hole and reduces the redshift. However, the latter process fills the burned hole, gives the photoproduct which fills the hole burned previously, and increases the redshift, because the trapped carrier density increases.

Photoionized dots and trapped holes are stable enough to give the PSHB at low temperature. There are many spatial arrangements for electrons and holes in both dots and glass. A variety of the spatial arrangements induce the additional inhomogeneous broadening of the absorption spectra of CuBr dots. The presence of the inhomogeneous broadening coming from the carrier distribution satisfies the basic requirement of the PSHB.

There are several reports about long-lived spectral change[15–17] and the Stark effect[18] in semiconductor quantum dots. The observed spectral change is the broadening of the inhomogeneously broadened absorption spectra, similar to the redshift of them observed in this paper, and is not the hole burning. Although the spectral changes were due to the broadening of the absorption spectra, they were explained by the trapped-carrier-induced quantum-confined Stark effect on the basis of their similarity to the Stark effect data[15,17] or the simulated result.[16] In CuBr quantum dots, on the other hand, we observed the small redshift of the $Z_{1,2}$ exciton absorption spectrum. We feel there remains an unresolved question about the spectral change of quantum dots induced by the Stark effect. Further study is necessary to resolve the question.

[1]A. I. Ekimov, Al.L. Efros, and A. A. Onushchenko, Solid State Commun. 56, 921 (1985).

[2]A. D. Yoffe, Adv. Phys. 42, 173 (1993), and references therein.

[3]For example, L. Bányai and S. W. Koch, *Semiconductor Quantum Dots* (World Scientific, Singapore, 1993).

[4]*Persistent Spectral Hole-Burning: Science and Applications,* edited by W. E. Moerner (Springer, Berlin, 1988).

[5]Y. Masumoto, L. G. Zimin, K. Naoe, S. Okamoto, and T. Arai, Mater. Sci. Eng. B 27, L5 (1994).

[6]K. Naoe, L. G. Zimin, and Y. Masumoto, Phys. Rev. B 50, 18 200 (1994).

[7]The composition of the sample is as follows: SiO_2: 64; B_2O_3: 32; Al_2O_3: 1.8; K_2O: 0.6; Sb_2O_3: 0.6; CuBr: 0.6; and P_2O_5: 0.4, in units of mol %.

[8]A. I. Ekimov, Al. L. Efros, M. G. Ivanov, A. A. Onushchenko, and S. K. Shumilov, Solid State Commun. 69, 565 (1989).

[9]R. Jankowiak, R. Richert, and H. Bässler, J. Phys. Chem. 89, 4569 (1985).

[10]W. Köhler, J. Meiler, and J. Friedrich, Phys. Rev. B 35, 4031 (1987).

[11]J. H. Mackey, H. L. Smith, and A. Halperin, J. Phys. Chem. Solids 27, 1759 (1966).

[12]The optical gap of the glass was measured to be 4.7 eV with the absorption tail down to 4.0 eV. The energy difference between the absorption tail of glass and the absorption edge of CuBr is 1.0 eV.

[13]D.C. Reynolds and T. C. Collins, *Excitons, Their Properties and Uses* (Academic, New York, 1981), p. 166; see also P. J. Dean and D. C. Herbert, in *Excitons,* edited by K. Cho (Springer, Berlin, 1979), p. 70.

[14]C. I. Yu, T. Goto, and M. Ueta, J. Phys. Soc. Jpn. 34, 693 (1973).

[15]V. Esch, B. Fluegel, G. Khitrova, H. M. Gibbs, Xu Jiajin, K. Kang, S. W. Koch, L. C. Liu, S. H. Risbud, and N. Peyghambarian, Phys. Rev. B 42, 7450 (1990).

[16]K. Kang, A. D. Kepner, Y. Z. Hu, S. W. Koch, N. Peyghambarian, C.-Y. Li, T. Takada, Y. Kao, and J. D. Mackenzie, Appl. Phys. Lett. 64, 1487 (1994).

[17]D. J. Norris, A. Sacra, C. B. Murray, and M. G. Bawendi, Phys. Rev. Lett. 72, 2612 (1994).

[18]For example, F. Hache, D. Ricard, and C. Flytzanis, Appl. Phys. Lett. 55, 1504 (1989).

Quantum size effect and persistent hole burning of CuI nanocrystals

Yasuaki Masumoto, Kanae Kawabata,* and Tadashi Kawazoe
Institute of Physics and Center for TARA (Tsukuba Advanced Research Alliance), University of Tsukuba, Tsukuba, Ibaraki 305, Japan
(Received 26 April 1995)

A quantum size effect of nanometer-size CuI microcrystallites (nanocrystals) embedded in glass was investigated and was found to follow the strong-confinement model. Persistent spectral hole burning and thermally annealing hole filling phenomena were observed in samples (CuI nanocrystals in glass). Unusual luminescence behavior (luminescence elongation followed by the increase of light exposure) was also observed. These observed phenomena are explained by the photoionization model of nanocrystals.

Quantum size effects of nanometer-size semiconductor microcrystallites (nanocrystals) have been extensively investigated recently. They are classified into two categories, a strong-confinement regime where electrons and holes are individually quantum confined, and a weak-confinement regime where excitons are quantum confined, depending on the size ratio of R/a_B, where R is the radius of nanocrystals, and a_B the exciton Bohr radius of the bulk crystal.[1-3] Ideally, the strong confinement corresponds to the case of $R/a_B \ll 1$, and the weak confinement to the case of $R/a_B \gg 1$. Strong- and weak-confinement regimes are shown to be two limiting cases of a unified theory for the quantum size effect of nanocrystals given by Kayanuma and quantitative criteria for the boundary between the two regimes are clarified by the theory.[4] The criteria are $R/a_B \geq 4$ for the regime of exciton confinement, $R/a_B \leq 2$ for the regime of individual electron hole confinement, and $2 \leq R/a_B \leq 4$ for the intermediate regime.

CuCl nanocrystals, whose radius is larger than a few nanometers, are the typical materials of the weak confinement,[1,5] because a_B is as small as 0.68 nm. In fact, the experimental blueshift of the exciton structure is well explained by the exciton confinement model, when R ranges from 1.5 to 10 nm. Exciton Bohr radii of CuI is 1.5 nm,[5] which is larger than the Bohr radius of CuCl. If R/a_B is smaller than 4 corresponding to $R \leq 6$ nm, Kayanuma's criteria tell us that CuI nanocrystals do not follow the weak-confinement model.[6] However, the quantum size effect of the CuI nanocrystals has been *a priori* classified into the weak-confinement regime on the experimental data of a sample with unknown size distribution.[5] In another publication,[7] the quantum size effect of the CuI nanocrystals also has been classified into the weak-confinement regime on the experimental data of a few samples with a highly dispersive radius distribution of nanocrystals peaked at 1.6 and 2 nm. The question about the *a priori* assumption and the discrepancy between experiments and theory should be solved by the systematic experimental study of the quantum size effect of CuI nanocrystals.

Another aim of this study is to clarify whether the phenomenon of persistent spectral hole burning (PSHB) occurs in CuI nanocrystals or not. PSHB has been observed in several kinds of semiconductor nanocrystals, such as CdSe, CdSSe, CuCl, and CuBr, embedded in glass or crystals.[8-11] Generality of these phenomena in semiconductor nanocrystals should be tested more by changing the materials. If we can find features related to the PSHB phenomena, they will serve as another hint for the clarification of the phenomena.

Samples studied in this work are nanometer-size CuI nanocrystals embedded in sodium-aluminoborosilicate glass. The size of the nanocrystals was changed by heat treatment and was measured by small-angle x-ray scattering. The small-angle x-ray scattering measurement was done by using a 0.15-nm x-ray, monochromator output of the electron synchrotron orbital radiation, and a position-sensitive proportional counter. For the low-temperature optical measurement, samples were directly

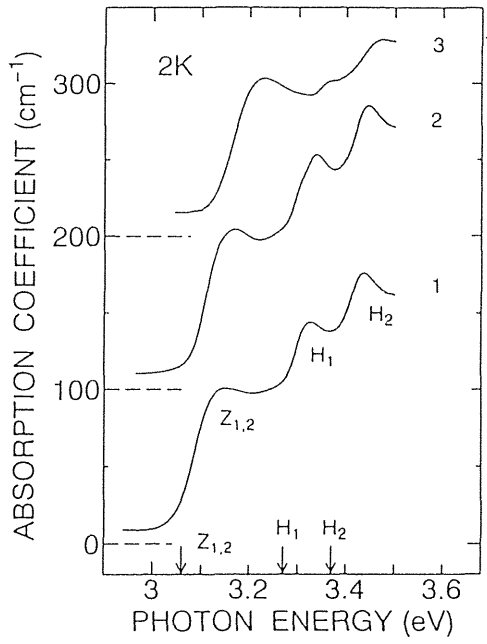

FIG. 1. Absorption spectra of CuI nanocrystals embedded in glass at 2 K. Average radii of nanocrystals 1, 2, and 3 are 4.8, 3.5, and 2.9 nm, respectively. Arrowed positions are $Z_{1,2}$, H_1, and H_2 exciton energies in bulk CuI crystals.

immersed in superfluid He held in a double Pyrex Dewar or were mounted on a cold finger of a closed-cycle-type helium cryostat. The optical absorption measurement was done by using a halogen lamp. The hole burning was done by using a narrow-band dye laser (Lumonics; HD-500) pumped by a Q-switched Nd^{3+}:YAG (yttrium-aluminum garnet) laser (Spectra Physics; GCR-3). The spectral linewidth of the dye laser was 0.014 meV and the pulse duration was 5 ns. A halogen lamp was used for the optical absorption measurement of the sample before and after the narrow-band dye laser irradiation. The absorption spectral change $-\Delta\alpha d$ is defined as the difference in the absorbance of the laser irradiated sample from that of the virgin sample. The luminescence measurement was done by using the third harmonics of the Nd^{3+}:YAG laser.

Absorption spectra of samples show the $Z_{1,2}$ exciton structure whose energy increases with the decrease of the size, as shown in Fig. 1. Besides the $Z_{1,2}$ exciton structure, the H_1 and H_2 exciton structures observed in hexagonal layered CuI (Ref. 12) appear in the nanocrystals of large size but are obscured in smaller size nanocrystals.[7]

Blueshift of the $Z_{1,2}$ exciton structure is plotted in Fig. 3 as a function of the average radius of nanocrystals. The average radius of nanocrystals, R, is estimated from the Guinier plot of the small-angle x-ray scattering data of Fig. 2.[13] The plot shows straight lines, which denote the monodispersive size distribution. The average radius ranges from 2.3 to 5.1 nm. The blueshift calculated on the simplest strong-confinement model is shown by a solid line in Fig. 3. It is expressed by $\Delta E=\hbar^2\pi^2/2\mu R^2$, where $\mu=(1/m_e^*+1/m_h^*)^{-1}$ is the reduced mass.

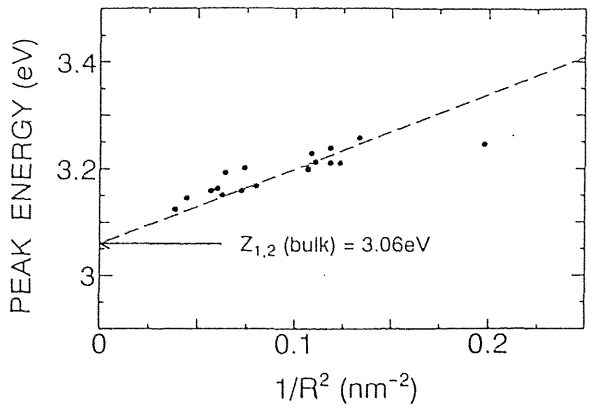

FIG. 3. Peak energy of the $Z_{1,2}$ exciton structure as a function of $1/R^2$, where R is the average radius of nanocrystals. The dashed line shows the calculated blueshift on the strong-confinement model.

Values of $m_e^*=0.33m_0$, $m_h^*=1.40m_0$, and $\mu=0.27m_0$ are adopted for the calculation.[14] The strong-confinement model satisfactorily explains the experimental blueshift. Size-dependent blueshift is much larger than that expected from the weak-confinement model, because exciton translational mass, $1.73m_0$, is 6.4 times larger than the reduced mass. On the basis of the agreement between experimental data and the strong-confinement model, we concluded that the weak-confinement model does not hold, but the strong-confinement model holds for CuI nanocrystals whose ra-

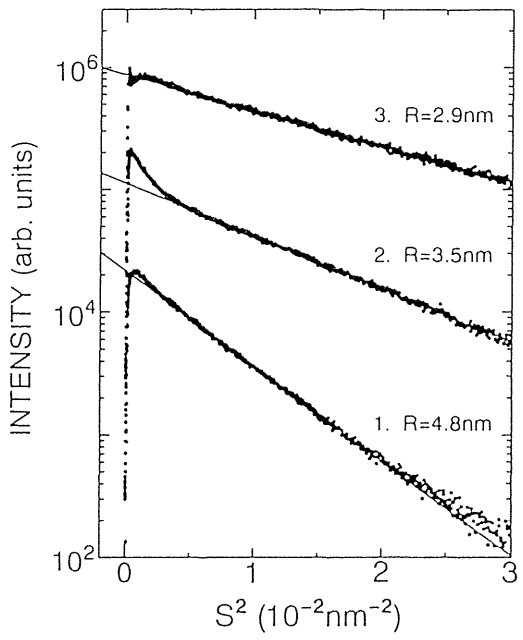

FIG. 2. Guinier plot of the small-angle x-ray scattering intensity. S^2 is defined by $\sin^2\theta/\lambda^2$, where θ is the scattering angle and $\lambda=0.15$ nm is the wavelength of the x ray. Samples 1, 2, and 3, respectively show the absorption spectra 1, 2, and 3 in Fig. 1.

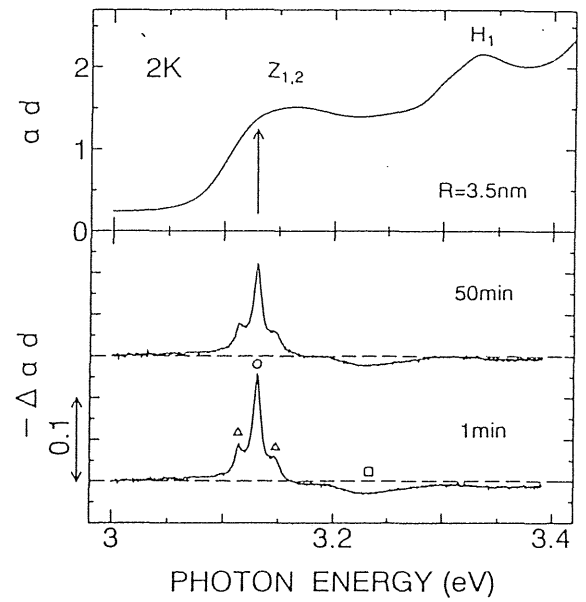

FIG. 4. Top: Absorption spectrum of a virgin sample, CuI nanocrystals embedded in glass. Average radius of nanocrystals is 3.5 nm. Bottom: The absorption spectral change of the sample after the spectrally narrow laser exposure. The sample was excited by 1800 shots of dye laser pulses with the photon energy of 3.130 eV, and an excitation energy density of 80 $\mu J/cm^2$. Long dashed lines show the zero base.

dius ranges from $1.5a_B$ to $3.4a_B$.

Persistent spectral hole burning phenomena were observed in CuI nanocrystals, in the same way as CuCl, CuBr, and CdSe nanocrystals.[8-11] Figure 4 shows the absorption spectrum and the absorption spectral change $-\Delta\alpha d$. The absorption spectral change consists of a spectral hole (open circle), phonon sideband holes (open triangle), and an induced absorption structure (open square). Energy separation between the main hole and the phonon sideband hole agrees with the transverse optical phonon energy of CuI, 16.5 meV.[15] The absorption spectral change is conserved for more than 2 h at 2 K.

The hole depth was found to increase almost in proportion to the logarithm of the laser fluence. Similar logarithmic growth was observed for CuCl and CuBr nanocrystals.[11] The logarithmic hole growth indicates the broad distribution of the burning rate. The broad distribution is explained by the presence of the tunneling process through the potential barrier with broadly distributed barrier height and thickness.[16] Thermally annealing hole filling is also observed. The experimental procedure is the same as described previously.[11] With the increase of annealing temperature, the depth of the hole made at 13.5 K decreases and disappears at about 200 K. The temperature dependence was found to be well fitted by the functional form of

$$\frac{1-\sqrt{kT\ln(\nu_0 t)/V_{\max}}}{1-\sqrt{kT_b\ln(\nu_0 t)/V_{\max}}}$$

for $kT\ln(\nu_0 t) < V_{\max}$, if a fitting parameter $\sqrt{k\ln(\nu_0 t)/V_{\max}}$ is set to be 0.07 $K^{-1/2}$. Here $\ln(\nu_0 t)$ is the logarithm of the product of the frequency factor and the annealing time, which is given by 32–35, and $V_{\max}$ is the maximum barrier height. This functional form is derived on the model for the thermally activated barrier crossing process across the distributed potential height.[17] The maximum barrier height estimated on this model is 0.6 eV.

Photoionization of the site selectively excited nanocrystals and carrier tunneling into traps in the host materials are considered to be the mechanisms for the PSHB phenomenon of CuCl and CuBr nanocrystals.[11] The same scenario is considered to hold for CuI nanocrystals, because characteristic features of hole burning and hole filling observed in CuI nanocrytals are the same as observed in CuCl and CuBr nanocrystals.

The presence of carrier trapping is supported by the following unusual phenomena of luminescence. The luminescence spectrum of CuI nanocrystals shows a Stokes shift from the absorption peak of the $Z_{1,2}$ exciton. The low-energy tail of the luminescence spectrum is below the $Z_{1,2}$ free-exciton energy, 3.06 eV, of bulk CuI. These results suggest the luminescence comes from the localized or bound exciton. With the increase of the in-

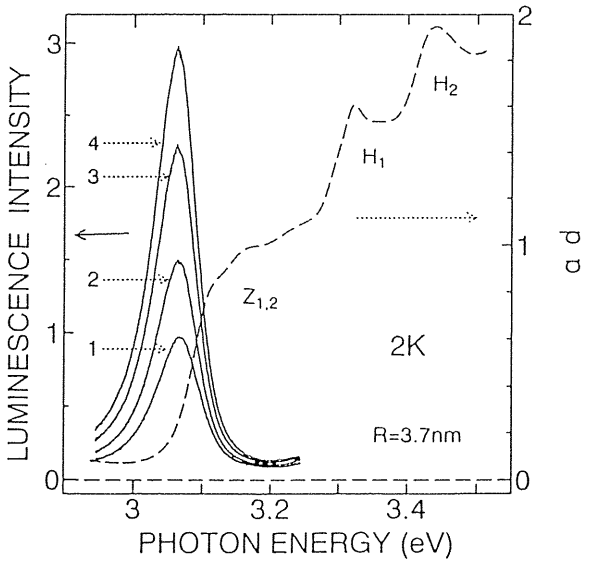

FIG. 5. Luminescence spectra of CuI nanocrystals embedded in glass at 2 K. The absorption spectrum of the sample is shown by a dashed line. The average radius of nanocrystals is 3.7 nm. Excitation laser pulses with the photon energy of 3.49 eV and the excitation density of 5 mJ/cm^2 hit the sample. Spectra 1, 2, 3, and 4 correspond to accumulated luminescence signals of the sample excited by 3000 shots of laser pulses obtained after 0, 4500, 16 500, and 31 500 shots of the laser exposure, respectively.

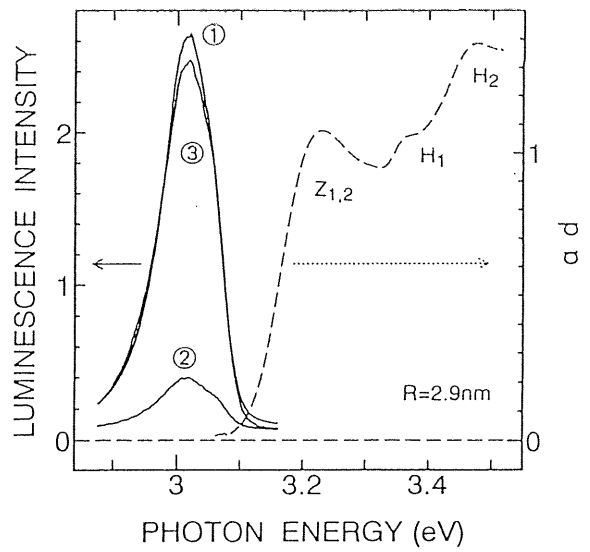

FIG. 6. Thermal cycling effect of the luminescence of CuI nanocrystals embedded in glass. The absorption spectrum of the sample at 2 K is shown by the dashed line. The average radius of nanocrystals is 2.9 nm. Spectrum 1 was taken at 20 K under the excitation density of 50 μJ/cm^2 at 3.49 eV, after the sample had been exposed by integrated excitation density of 600 mJ/cm^2. Then the sample temperature was elevated to 77 K and cooled down to 20 K again. Spectrum 2 was taken just after the temperature cycle at 20 K under the excitation density of 50 μJ/cm^2 at 3.49 eV. After that, the sample was exposed by the integrated excitation density of 600 mJ/cm^2 at 3.49 eV. Spectrum 3 was taken after the 600-mJ/cm^2 exposure at 20 K under the excitation density of 50 μJ/cm^2 at 3.49 eV.

tegrated intensity of laser exposure, the luminescence intensity increases, as is shown in Fig. 5. However, the luminescence intensity is quenched after the annealing cycle, as is shown in Fig. 6. These characteristic phenomena of luminescence are explained, if the carrier trapping at the capture centers in the host glass is saturated with the increase of the laser fluence and if trapped carriers are released with the rise in temperature. We speculate localized or bound excitons formed from free excitons in nanocrystals are radiatively annihilated or nonradiatively decay through ionization, tunneling, and capture by traps in the host glass. The number of traps that are easily accessible by tunneling from nanocrystals are finite and traps seized by carriers become ineffective. This is the reason that the carrier trapping at the capture centers is saturated. A rise in temperature causes the thermal activation of the trapped carriers at the capture centers. Activated carriers are radiatively or nonradiatively annihilated. As a result, traps in the host become effective again. In this way, the above-mentioned unusual phenomena of luminescence are explained by the same scenario as is used to explain the PSHB phenomena.

In summary, the quantum size effect of nanometer-size CuI microcrystallites (nanocrystals) was investigated. Size-dependent blueshift of the $Z_{1,2}$ exciton structure was well explained by the strong-confinement model. Persistent spectral hole burning and thermally annealing hole-filling phenomena were observed. The characteristics of the observed phenomena are the same as observed in CuCl and CuBr nanocrystals. Photoionization of nanocrystals and carrier tunneling into traps in the host glass are considered to be the mechanism for the PSHB phenomena. Unusual luminescence behavior (luminescence elongation with the increase of the light exposure) was observed. This observation is consistent with the photoionization model of nanocrystals.

Small-angle x-ray scattering experiments were done at the Photon Factory (PF) of the National Laboratory for High Energy Physics by the approval of the PF Advisory Committee (Proposals 92-117). The authors wish to thank Professor Y. Amemiya in PF for his guidance to the small-angle x-ray scattering experiments. This work was supported in part by TARA (Tsukuba Advanced Research Alliance) project in University of Tsukuba.

---

*Present address: R&D Laboratories for Photographic Materials, KONICA Corp., Hino, Tokyo 191, Japan.

[1]A. I. Ekimov, Al. L. Efros, and A.A. Onushchenko, Solid State Commun. 56, 921 (1985).

[2]L. Brus, IEEE J. Quantum Electron. QE-22, 1909 (1986).

[3]A. D. Yoffe, Adv. Phys. 42, 173 (1993).

[4]Y. Kayanuma, Phys. Rev. B 38, 9797 (1988).

[5]T. Itoh, Y. Iwabuchi, and T. Kirihara, Phys. Status Solidi B 146, 531 (1988).

[6]As for CuBr, exciton Bohr radius is 1.25 nm. The weak confinement model does not hold for CuBr nanocrystals, but a donorlike exciton model explains the experimental data of them, when R/a_B ranges from 1 to 3. Because of rather large hole mass, hole localization at the center of nanocrystals takes place. See A. I. Ekimov, Al. L. Efros, M. G. Ivanov, A. A. Onushchenko, and S. K. Shumilov, Solid State Commun. 69, 565 (1989).

[7]O. Gogolin, Yu. Berosashvili, G. Mschvelidze, E. Tsitsishvili, S. Oktjabrski, H. Giessen, A. Uhrig, and C. Klingshirn, Semicond. Sci. Technol. 6, 401 (1991).

[8]Y. Masumoto, L. G. Zimin, K. Naoe, S. Okamoto, and T. Arai, Mater. Sci. Eng. B 27, L5 (1994).

[9]K. Naoe, L. G. Zimin, and Y. Masumoto, Phys. Rev. B 50, 18 200 (1994).

[10]Y. Masumoto, Jpn. J. Appl. Phys. 34, Suppl. 34-1, 8 (1995).

[11]Y. Masumoto, S. Okamoto, T. Yamamoto, and T. Kawazoe, Phys. Status Solidi B 188, 209 (1995).

[12]M. Cardona, Phys. Rev. 129, 69 (1963).

[13]A. Guinier and G. Fournet, *Small-Angle Scattering of X-Rays* (Wiley, New York, 1955).

[14]C. I. Yu, T. Goto, and M. Ueta, J. Phys. Soc. Jpn. 34, 693 (1973).

[15]*Physics of II-VI and I-VII Compounds, Semimagnetic Semiconductors*, edited by O. Madelung, Landolt-Börnstein, New Series, Group III, Vol. 17, Pt. b (Springer-Verlag, Berlin, 1982).

[16]R. Jankowiak, R. Richert, and H. Bässler, J. Phys. Chem. 89, 4569 (1985).

[17]W. Köhler, J. Meiler, and J. Friedrich, Phys. Rev. B 35, 4031 (1987).

Exciton localization and decomposition dynamics in cuprous halide nanocrystals

Tsuyoshi Okuno, Hiroshi Miyajima, Akihiro Satake, and Yasuaki Masumoto
Institute of Physics and Center for TARA (Tsukuba Advanced Research Alliance), University of Tsukuba, Tsukuba, Ibaraki 305, Japan
(Received 10 July 1996)

We report temporal changes of luminescence and absorption (differential transmission) of excitons in nanometer-size semiconductor crystals (nanocrystals) of CuCl embedded in NaCl or in glass, and CuBr nanocrystals embedded in glass. In CuCl nanocrystals in NaCl, an exciton relaxes nonradiatively to some localized state. In CuCl and CuBr nanocrystals in glass, the temporal changes of the differential transmission have a longer decay component in addition to the fast decay component which agrees with the luminescence decay. This result suggests exciton decomposition and the existence of an electron or a hole remainder in the nanocrystals. The decay time of the longer decay component increases by the accumulation of photoexcitation. This phenomenon indicates persistent trapping of carriers in the glass matrix, which is concerned with persistent spectral hole burning in nanocrystals. [S0163-1829(96)11449-1]

I. INTRODUCTION

In this decade, semiconductor nanometer-size microcrystallites (nanocrystals) have attracted much attention even since the quantum size effect was observed in them.[1–4] One of the interests in nanocrystals is motivated by theoretical studies of the enhancement of the oscillator strength and the third-order susceptibility for confined excitonic systems.[5,6] A super-radiant decay, in the sense that a coherently superposed polarization is involved, was reported in Wannier excitons in CuCl nanocrystals.[7,8]

In the studies mentioned above the optical properties of I-VII nanocrystals were characterized only by the quantum confinement, and little attention seemed to be paid to the effect of the surface or the interface of nanocrystals embedded in crystals or glasses. In II-VI nanocrystals which show large Stokes-shifted exciton luminescence, the importance of surface states was recognized and studied.[9] In another paper on II-VI nanocrystals, photoionization of nanocrystals is discussed.[10] In addition, nanocrystalline systems including I-VII nanocrystals widely reveal persistent spectral hole burning, and this phenomenon suggests electron or hole trapping at the surface or in the matrix (photoionization of nanocrystals).[11–13] Therefore, it is possible that the relaxation of excitons in I-VII nanocrystals is affected by the surface or matrix states. In other words, carrier transfer to the surface or the matrix may affect the relaxation mechanism of excitons.

As for the systems in which charge transfer takes place in real space, type-II quantum wells are known. In type-II (Al,Ga)As/AlAs quantum wells, the real-space Γ-X transfer of electrons determines the lifetime of luminescence of Γ-Γ heavy-hole excitons, since the lowest conduction-band state is in the X minima of the AlAs layers. In these systems, the luminescence lifetime of Γ-Γ excitons is reported to be in an order of 100 fs $\sim$ 10 ps;[14,15] this time corresponds to the transfer-time of photoexcited electrons from the Γ state in well layers to the X state in AlAs layers. However, temporal changes of induced absorption show not only the similar fast decay (100 fs–10 ps) but also much slower tail.[15,16] This slower component mainly reflects annihilation of holes remaining in the Γ valence state in well layers.

In order to investigate carrier dynamics in intrinsic semiconductors, time-resolved measurements of luminescence as well as induced absorption are useful. Exciton luminescence is proportional to the number of pairs of electrons and holes, while the sum of electron number and hole number is reflected in induced absorption. Since numbers of electrons and holes are equal to each other in ordinary cases of intrinsic semiconductors, temporal change of the luminescence intensity and that of the induced absorption intensity agree with each other. Nevertheless, in such cases as type-II quantum wells where electrons and holes are decomposed into different layers, temporal changes of luminescence and induced absorption can be different from each other. Measurements of both experiments and comparison of them are useful and important to discuss carrier dynamics.

In this paper, we report the experimental study of temporal changes of luminescence and differential transmission of Wannier excitons in CuCl nanocrystals embedded in NaCl crystals, and CuCl or CuBr nanocrystals embedded in glasses. From these results, we clarify an important role of "localized" or trap states on the relaxation mechanisms of excitons. Then, we discuss the relation between the relaxation mechanism and persistent hole-burning phenomena.

II. EXPERIMENTAL PROCEDURE

The samples under investigation are CuCl nanocrystals embedded in NaCl crystals,[17,18] CuCl nanocrystals embedded in glass, and CuBr nanocrystals embedded in glass (potassium aluminoborosilicate glass was used for the glass matrix). These nanocrystals were grown by heat treatment. The mean sizes of the nanocrystals were measured by small-angle x-ray scattering and were 2.5 nm for CuCl nanocrystals in NaCl, 3.5 nm for CuCl nanocrystals in glass, and 3.6 nm for CuBr nanocrystals in glass. The samples were directly immersed in superfluid helium at 2 K in an optical cryostat. In order to measure absorption spectra, a halogen lamp was used. As an exciting source for measurement of luminescence, frequency-doubled 100-fs pulses from a mode-locked Ti:sapphire laser were used. The excitation photon energy was 3.37 eV. Temporal changes of luminescence were mea-

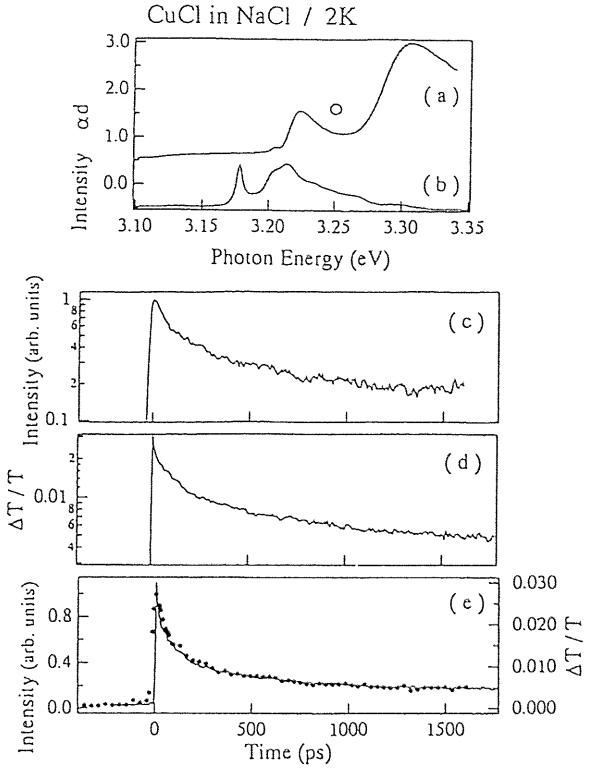

FIG. 1. (a) Absorption spectrum of CuCl nanocrystals embedded in NaCl crystal measured at 2 K. (b) Luminescence spectrum with an excitation photon energy of 3.37 eV. (c) Temporal change of luminescence at 3.25 eV shown on a log scale. The excitation density is 0.1 μJ/cm^2. (d) Temporal change of differential transmission at 3.25 eV shown on a log scale. The excitation density is 20 μJ/cm^2. (e) Temporal changes of luminescence (circles) and differential transmission (line) shown on a linear scale.

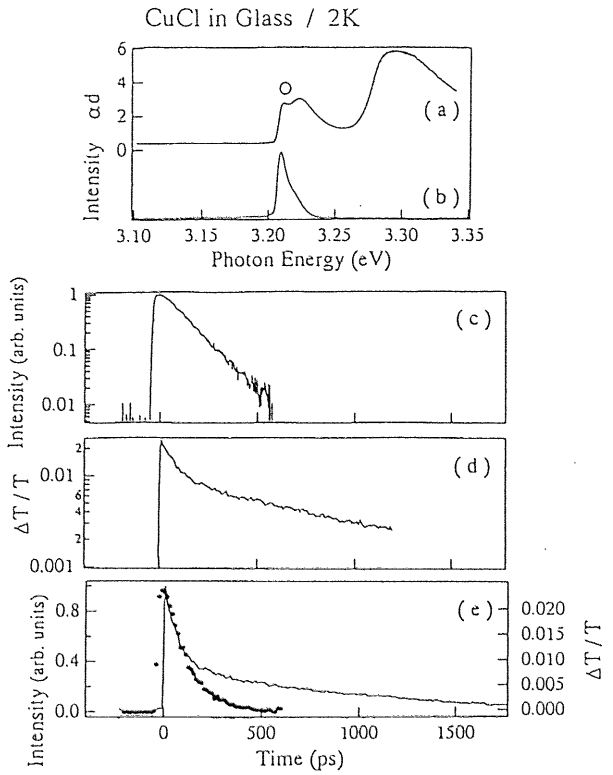

FIG. 2. (a) Absorption spectrum of CuCl nanocrystals embedded in glass measured at 2 K. (b) Luminescence spectrum with an excitation photon energy of 3.37 eV. (c) Temporal change of luminescence at 3.21 eV shown on a log scale. The excitation density is 0.004 μJ/cm^2. (d) Temporal change of differential transmission at 3.21 eV shown on a log scale. The excitation density is 0.4 μJ/cm^2. (e) Temporal changes of luminescence (circles) and differential transmission (line) shown on a linear scale.

sured by using a synchroscan streak camera. Time resolution of this measurement was about 15 ps. In order to obtain temporal changes of differential transmission by pump-probe measurements, frequency-doubled pulses with a repetition rate of 250 kHz from a regenerative amplifier of the Ti:sapphire laser were used. A laser beam was split into two; one is used as a pump beam, and the other with the intensity of $\sim 1/10$ of the pump beam was used as a probe beam. Time resolution of this pump-probe measurement was about 300 fs.

III. RESULTS AND DISCUSSION

A. Comparison of temporal changes between luminescence and differential transmission

Figure 1(a) shows the absorption spectrum of CuCl nanocrystals embedded in NaCl obtained at 2 K. The Z_3 and $Z_{1,2}$ exciton peaks are located around 3.22 eV and 3.30 eV, respectively. Figure 1(b) shows the luminescence spectrum. This luminescence can be roughly separated into two parts; one peak is located at 3.175 eV and the other broader luminescence band with several structures is around 3.21 eV. The peak at 3.175 eV is attributed to an exciton bound to a neutral acceptor I_1,[19] and we do not discuss this peak in this paper. The other luminescence band around 3.21 eV corresponds to the Z_3 exciton. When we compare the luminescence peak with the absorption peak of the Z_3 exciton, we find that this luminescence shows Stokes shift of ~ 12 meV. Thus the dominant luminescence is thought to come from some "localized" state.[20] In order to avoid the contribution of the "localized" state to the luminescence and to discuss the dynamics of "free" Z_3 exciton, we made experiments of time-resolved luminescence and pump-probe measurements at 3.25 eV denoted by the circle in Fig. 1(a).

Figure 1(c) shows the semilogarithmic plot of the temporal change of the luminescence observed at 3.25 eV; the excitation density was 0.1 μJ/cm^2. We find that this luminescence decay cannot be fitted by single-exponential decay but by two exponential decay; two decay time constants are approximately 100 ps and 2 ns. Figure 1(d) shows the temporal change of differential transmission at 3.25 eV plotted on a log scale under the excitation density of 20 μJ/cm^2. This profile also shows two-exponential decay with decay time constants of ~ 100 ps and ~ 2 ns, and is quite similar to the luminescence-decay profile in Fig. 1(c). In Fig. 1(e), both of the temporal changes in Figs. 1(c) and 1(d) are plotted on a linear scale; circles are the results of the luminescence and the line is of the differential transmission. We find that both data are in good agreement. Slight difference of rise times around 0 ps between two data comes from the difference of the time resolution between the two experiments.

Figure 2 shows results for CuCl nanocrystals in glass.

Figure 2(a) shows the absorption spectrum and Fig. 2(b) shows the luminescence spectrum. We find that the luminescence band is overlapped with the absorption band of the Z_3 exciton. Disagreement between the luminescence peak and the absorption peak may come from smaller luminescent efficiency of smaller nanocrystals with larger absorption photon energy. Figure 2(c) shows the temporal change of the luminescence observed at the luminescence-peak energy of 3.21 eV denoted by the circle in Fig. 2(a); the excitation density was 0.004 μJ/cm^2. We find that this luminescence decay is well fitted by the single-exponential decay; the decay time constant is approximately 100 ps.

Figure 2(d) shows the temporal change of differential transmission at 3.21 eV under the excitation density of 0.4 μJ/cm^2. Although the temporal changes of luminescence and differential transmission of CuCl nanocrystals in NaCl in Fig. 1(e) are quite similar to each other, the profiles of CuCl nanocrystals in glass in Figs. 2(c) and 2(d) are different. Even if we use the same excitation density in both experiments, this disagreement remains. The profile of differential transmission in Fig. 2(d) cannot be fitted by single-exponential decay, but by two-exponential decay; the fast decay time constant is ~100 ps, which agrees with the decay time constant of luminescence in Fig. 2(c), and the slow decay time constant is ~1 ns. In Fig. 2(e), both of the temporal changes in Figs. 2(c) and 2(d) are plotted together. From 0 ps to 100 ps two data agree well with each other. Then the luminescence (circles) decays in a single-exponential profile, while the differential transmission (line) has a longer decay component.

The results of CuBr nanocrystals in glass shown in Fig. 3 are similar to the results of CuCl nanocrystals in glass. Figure 3(a) shows the absorption spectrum, and the $Z_{1,2}$ absorption band is located around 3.07 eV. Figure 3(b) shows the luminescence spectrum. The luminescence band is at the lower-energy tail of the absorption band.

Figure 3(c) shows the temporal change of the luminescence observed at the luminescence-peak energy of 3.02 eV denoted by the circle in Fig. 3(a); the excitation density was 0.1 μJ/cm^2. We find that this luminescence decay is well fitted by single-exponential decay with the decay time constant of ~20 ps. Figure 3(d) shows the temporal change of differential transmission at 3.02 eV under the excitation density of 4 μJ/cm^2. This profile is different from that in Fig. 3(c), and is fitted by two-exponential decay; the decay time constants are ~20 ps and ~70 ps. In Fig. 3(e), both of the temporal changes in Figs. 3(c) and 3(d) are plotted. From 0 ps to 10 ps two data agree well with each other. Then the luminescence (circles) decays in a single-exponential profile, while the differential transmission (line) has a longer decay component.

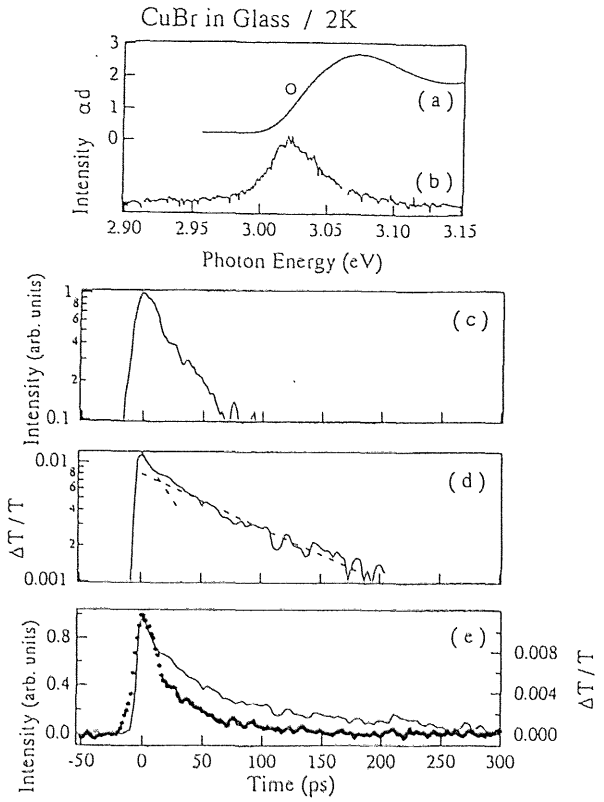

FIG. 3. (a) Absorption spectrum of CuBr nanocrystals embedded in glass measured at 2 K. (b) Luminescence spectrum with the excitation photon energy of 3.37 eV. (c) Temporal change of luminescence at 3.02 eV shown on a log scale. The excitation density is 0.1 μJ/cm^2. (d) Temporal change of differential transmission at 3.02 eV shown on a log scale. The excitation density is 4 μJ/cm^2. (e) Temporal changes of luminescence (circles) and differential transmission (line) shown on a linear scale.

B. Relaxation mechanism of excitons

In CuCl nanocrystals in NaCl, the Z_3 exciton relaxes in the decay time constants of ~100 ps and ~2 ns. As will be discussed in the forthcoming paper, luminescence rise is observed at the lower energy (~3.20 eV) region of the "localized" state; the rise time agrees with the fast decay time (in this case, ~100 ps) in the high-energy region of the "free" Z_3 exciton. Therefore, the fast decay component of ~100 ps is thought to be nonradiative relaxation time from the "free" Z_3 exciton to the "localized" state (the detailed experimental results and discussion will be shown in the subsequent paper). The appearance of the longer decay component means that some nanocrystals have no "localized" state to which "free" Z_3 excitons will relax. We assume that this time constant of ~2 ns corresponds to the radiative recombination time of the exciton. The exciton relaxation dynamics in CuCl nanocrystals in NaCl mentioned above is depicted in Fig. 4(a).

In CuCl (CuBr) nanocrystals in glass, the temporal change of luminescence does not agree with that of differential transmission. This result can be understood by nonradiative decomposition of excitons as is depicted in Fig. 4(b). In some nanocrystals, a photoexcited exciton is decomposed nonradiatively into an electron and a hole. They may be trapped into defects or surfaces. We assume that an electron or a hole remains in the nanocrystal and that an electron-hole pair recombine nonradiatively in the time constant of ~1 ns in CuCl nanocrystals in glass (~70 ps in CuBr nanocrystals in glass). Then these nanocrystals contribute to the longer decay time constant of ~1 ns (~70 ps) of the differential transmission, but not to luminescence. In other nanocrystals, excitons relax radiatively or nonradiatively in the decay time constant of ~100 ps (~20 ps), which is reflected in the fast

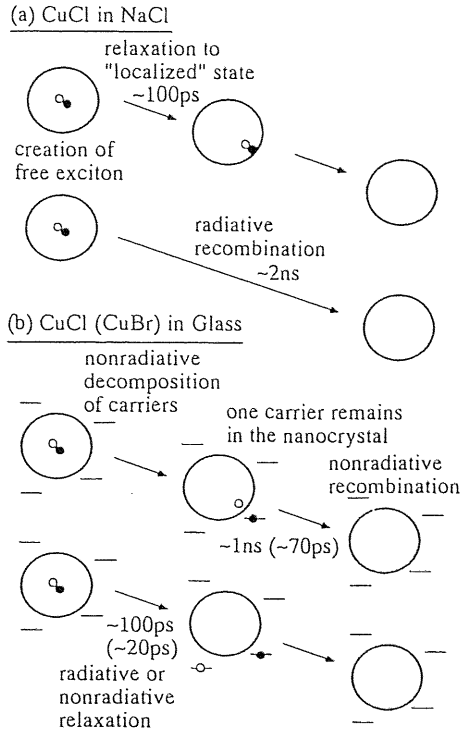

FIG. 4. Schematic drawing of relaxation mechanisms of excitons in CuCl nanocrystals embedded in NaCl crystal, and in CuCl (or CuBr) nanocrystals embedded in glass.

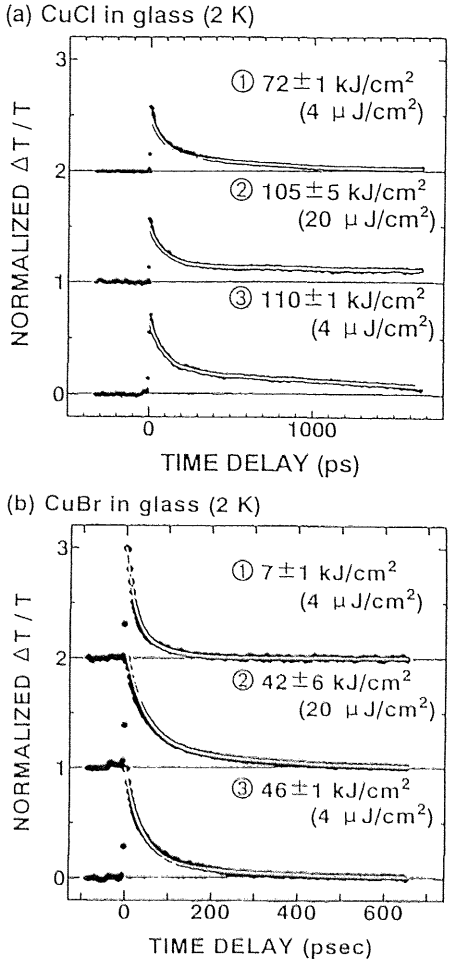

FIG. 5. Photoaccumulation effects on the temporal changes of differential transmission in (a) CuCl or (b) CuBr nanocrystals embedded in glass. Three temporal changes drawn by symbols are measured successively from the top to the bottom. The accumulated excitation densities (and the pump-beam densities in the parentheses) are shown in the figure. The excitation photon energy was (a) 3.22 eV or (b) 3.09 eV. Lines are results of fitting by the two-exponential decay of $I_0\,[a\exp(-t/\tau_a)+b\exp(-t/\tau_b)]$.

decay component of differential transmission and in the single-exponential decay of luminescence. In this way, we can explain the disagreement between the temporal changes of the luminescence and the differential transmission.

In our previous paper, we reported persistent spectral hole burning in CuBr nanocrystals in glass.[13] This phenomenon was ascribed to electron trapping at the surface of the nanocrystals and hole tunneling into traps in the glass host. Following this consideration, the fast decay time constant of ~100 ps (~20 ps) corresponds to the trapping time of electrons and the tunneling time of holes. The long decay time constant of ~1 ns (~70 ps) corresponds to the nonradiative recombination time between the electron at the surface and the hole at the traps in the glass. At this time, some of these carriers remain without recombination, and induce persistent spectral hole burning.

In CuCl nanocrystals in NaCl, the temporal changes of luminescence and differential transmission agree with each other, and thus we need not assume decomposition of excitons. Considering that the band gap of NaCl is 8.6 eV (Ref. 21) and the optical gap of the glass is 4.7 eV, barrier height for the carriers in CuCl nanocrystals in NaCl is higher than that in the glass matrix. This is thought to be the reason why decomposition of excitons scarcely takes place in CuCl nanocrystals in NaCl. However, some excitons in CuCl nanocrystals in NaCl may be decomposed and electrons or holes may be trapped at the surface or in the matrix, which induces persistent spectral hole burning in CuCl nanocrystals in NaCl. The hole-burning quantum efficiency of CuCl nanocrystals in NaCl is smaller than that of CuCl nanocrystals in glass,[22] and this observation is consistent with the different decomposition probability between excitons in the nanocrystals in glass and those in the nanocrystals in NaCl.

C. Photoaccumulation effect on the transmission time trace

In the temporal changes of differential transmission in CuCl or CuBr nanocrystals in glass, we noticed the photoaccumulation effect. Figure 5 shows the results of (a) CuCl and (b) CuBr nanocrystals in glass. In both the samples, three time traces drawn by symbols were obtained successively from the top to the bottom. For CuCl nanocrystals in glass, the accumulated excitation densities and the pump-beam energy densities in the parentheses were shown in Fig. 5(a), and the excitation photon energy was 3.22 eV. For CuBr nanocrystals in glass, the accumulated excitation densities and the pump-beam densities were shown in Fig. 5(b), and the excitation photon-energy was 3.09 eV. The results shown in Figs. 2(d) and 3(d) correspond to the top traces in Fig. 5 obtained at the smallest accumulated intensities. All the temporal changes in Fig. 5 can be fitted by two-

exponential decay, given by $I_0[a\exp(-t/\tau_a)+b\exp(-t/\tau_b)]$. The used parameters for the fitting in Fig. 5(a) are (1) $I_0=1$, $a=0.64$, $\tau_a=71$ ps, $b=0.35$, $\tau_b=0.67$ ns, (2) $I_0=1.2$, $a=0.75$, $\tau_a=71$ ps, $b=0.25$, $\tau_b=6.2$ ns, and (3) $I_0=0.48$, $a=0.70$, $\tau_a=74$ ps, $b=0.30$, $\tau_b=2$ ns. Here, I_0 in (1) was set to be unity, and I_0 in (2) and (3) represents the relative intensity. In the same manner, the used parameters in Fig. 5(b) are (1) $I_0=1$, $a=0.71$, $\tau_a=22$ ps, $b=0.29$, $\tau_b=67$ ps, (2) $I_0=29$, $a=0.86$, $\tau_a=43$ ps, $b=0.24$, $\tau_b=250$ ps, and (3) $I_0=0.52$, $a=0.85$, $\tau_a=38$ ps, $b=0.15$, $\tau_b=280$ ps.

When we compare the trace (1) with the trace (3), we can find that the fast decay time constant is about the same but the longer decay time constant increases. These traces (1) and (3) were obtained by the same pump density but a different accumulated density. If we compare the time integral of trace (1) with that of trace (3), we find that the integral was scarcely changed. We can say that the photoaccumulation effect means the increase of the long decay time constant which was ascribed to the nonradiative recombination time discussed in the previous section.

The increase of the long decay time constant can be explained by the following scenario concerned with persistent spectral hole burning. A photoexcited exciton is decomposed, and then the electron is captured at the surface and the hole is at the trap in the glass. At the small accumulated densities, the hole is captured by a trap near the photoexcited nanocrystal. At this time, an exciton is easily decomposed in a nanocrystal when a trap is located near the nanocrystal. In this case, the electron and the hole recombine quickly (~ 1 ns for CuCl nanocrystals in glass, or ~ 70 ps for CuBr nanocrystals in glass), and the small portion of the pairs are left without recombination. These pairs induce persistent spectral hole burning. With the increase of the accumulated density of photoexcitation, traps near nanocrystals capture holes and become inactive. Then a hole coming from the decomposed exciton is captured in traps distant from the nanocrystals. The recombination time of a far separated electron-hole pair becomes longer. In this way, we can explain the increase of the long decay time constant in the transmission time trace. As for the relationship between this photoaccumulation effect and persistent spectral hole-burning phenomena, we note that a persistent hole is found in an absorption spectrum after the measurement of Fig. 5.

In contrast with the differential transmission, no photoaccumulation effect was observed on luminescence. The reason may be that separated electron-hole pairs do not luminesce. Temporal changes of luminescence show single-exponential profiles without a longer decay component coming from separated pairs. Hence only electron-hole pairs without separation (excitons) are thought to contribute to luminescence. When a photoexcited exciton is decomposed, the electron-hole pair recombines nonradiatively (without luminescence) or is left without recombination. Thus some of the separated pairs without recombination induce photoaccumulation effect on the differential transmission but not on luminescence.

We did not observe the photoaccumulation effect on the transmission time trace in CuCl nanocrystals in NaCl so far. In this system, the long decay time constant (~ 2 ns) was not ascribed to the recombination time of a separated and trapped electron-hole pair but to the radiative recombination time of the exciton. Thus the long decay component has no relation to the persistent spectral hole burning and the photoaccumulation effect. Further experimental study is necessary to clarify the exciton dynamics causing hole-burning phenomena in CuCl nanocrystals in NaCl, because we did not find any photoaccumulation effect on the exciton dynamics.

IV. CONCLUSION

We measured temporal changes of luminescence and absorption of excitons in CuCl nanocrystals embedded in NaCl or glass, and CuBr nanocrystals embedded in glass. Both of the temporal changes for CuCl nanocrystals in NaCl agree well with each other, and show two-exponential decay. Two decay time constants of ~ 100 ps and ~ 2 ns correspond to relaxation to the "localized" state and radiative recombination, respectively. In CuCl and CuBr nanocrystals in glass, the temporal changes of the differential transmission show two-exponential decay, and are different from the single-exponential luminescence decay; the decay time constant of the luminescence agrees with the fast decay time constant in the differential transmission. This disagreement between two decay profiles shows nonradiative decomposition of excitons and existence of an electron or a hole remainder in the nanocrystals. In addition, in the temporal changes of the differential transmission in CuCl or CuBr nanocrystals in glass, the decay time constant of the longer decay component increases with the increase of accumulated excitation density. This result shows persistent trapping of carriers, which is thought to be the origin of persistent spectral hole-burning phenomena in nanocrystals.

ACKNOWLEDGMENTS

Small-angle x-ray-scattering experiments were done at the Photon Factory (PF) of the National Laboratory for High Energy Physics by the approval of the PF Advisory Committee (Proposals Nos. 92–117). The authors wish to thank Professor Y. Amemiya in PF for his guidance to the small-angle x-ray-scattering experiments. The authors would like to express appreciation for Dr. Y. Yamada's collaboration at the early stage of this study.

[1] A. I. Ekimov, A. L. Efros, and A. A. Onushchenko, Solid State Commun. **56**, 921 (1985).
[2] L. E. Brus, J. Chem. Phys. **80**, 4403 (1984).
[3] A. D. Yoffe, Adv. Phys. **42**, 173 (1993).
[4] L. Bányai and S. W. Koch, *Semiconductor Quantum Dot* (World Scientific, Singapore, 1993).
[5] E. Hanamura, Phys. Rev. B **38**, 1228 (1988).
[6] Y. Kayanuma, Phys. Rev. B **38**, 9797 (1988).

[7] A. Nakamura, H. Yamada, and T. Tokizaki, Phys. Rev. B **40**, 8585 (1989).
[8] T. Itoh, M. Furumiya, T. Ikehara, and C. Gourdon, Solid State Commun. **73**, 271 (1990).
[9] M. G. Bawendi, W. L. Wilson, L. Rothberg, P. J. Carroll, T. M. Jedju, M. L. Steigerwald, and L. E. Brus, Phys. Rev. Lett. **65**, 1623 (1990).
[10] D. I. Chepic, Al. L. Efros, A. I. Ekimov, M. G. Ivanov, V. A. Kharchenko, I. A. Kudriavtsev, and T. V. Yazeva, J. Lumin. **47**, 113 (1990).
[11] Y. Masumoto, L. G. Zimin, K. Naoe, S. Okamoto, and T. Arai, Mater. Sci. Eng. B **27**, L5 (1994).
[12] K. Naoe, L. G. Zimin, and Y. Masumoto, Phys. Rev. B **50**, 18 200 (1994).
[13] Yasuaki Masumoto, Tadashi Kawazoe, and Tetsuya Yamamoto, Phys. Rev. B **52**, 4688 (1995).
[14] G. Peter, E. Göbel, W. W. Ruhle, J. Nagle, and K. Ploog, Superlatt. Microstruct. **5**, 197 (1989).
[15] J. Feldmann, J. Nunnenkamp, G. Peter, E. Göbel, J. Kuhl, K. Ploog, P. Dawson, and C. T. Foxon, Phys. Rev. B **42**, 5809 (1990).
[16] Y. Masumoto, T. Mishina, F. Sasaki, and M. Adachi, Phys. Rev. B **40**, 8581 (1989).
[17] T. Itoh, Y. Iwabuchi, and M. Kataoka, Phys. Status Solidi B **145**, 567 (1988).
[18] T. Itoh, Y. Iwabuchi, and T. Kirihara, Phys. Status Solidi B **146**, 531 (1988).
[19] M. Ueta, H. Kanzaki, K. Kobayashi, Y. Toyozawa, and E. Hanamura, *Excitonic Processes in Solids* (Springer, Berlin, 1986), Chap. 3.
[20] S. Yano, T. Goto, S. Iwai, K. Edamatsu, and T. Itoh, Jpn. J. Appl. Phys. **34**, Suppl. 34-1, 140 (1995).
[21] J. F. Eby, K. J. Teegarden, and D. B. Dutton, Phys. Rev. **116**, 1099 (1959).
[22] T. Kawazoe and Y. Masumoto (unpublished).

Luminescence Hole Burning and Quantum Size Effect of Charged Excitons in CuCl Quantum Dots

Tadashi Kawazoe and Yasuaki Masumoto

Institute of Physics and Center for TARA (Tsukuba Advanced Research Alliance), University of Tsukuba, Tsukuba, Ibaraki 305, Japan

(Received 12 August 1996)

Luminescence hole-burning phenomena were observed in CuCl quantum dots embedded in a NaCl crystal. As a result of the selective excitation of the Z_3 exciton band of CuCl quantum dots, a resonantly burned hole and moreover its sidebands appear in the luminescence spectrum. The Stokes shift of the sidebands increases with the increase in the burning photon energy, and its dependence is explained by the quantum size effect of the negatively charged exciton X^- and the positively charged exciton X_2^+. New exciton complexes, X^- and X_2^+, confined in quantum dots were first observed by the luminescence hole burning. [S0031-9007(96)01828-5]

PACS numbers: 73.20.Dx, 71.35.–y, 78.40.Ha, 78.55.Fv

The quantum confinement effect for electrons, holes, and excitons in semiconductor quantum dots (QDs) has been studied extensively [1]. Many experimental results are systematically explained by a ratio of QD radius to the exciton Bohr radius [2]. In this sense, understanding of the quantum size effect for electrons, holes, and excitons is in the matured stage. However, the effect for bound exciton complexes in semiconductor QDs have not been investigated so far. It was pointed out that exciton complexes in semiconductor QDs play an important role in interesting and applicable phenomena, such as persistent spectral hole burning (PSHB) [3–6]. Therefore, the study of exciton complexes in semiconductor QDs is valuable to clarify their quantum size effect and the mechanism of the PSHB.

Excitons are bound to impurities or structural defects. In a bulk CuCl crystal, bound excitons are observed as the I_1 and I_2 luminescence lines [7]. In addition, the existence of positively (X_2^+) and negatively (X^-) charged excitons were predicted by Lampert [8], and its existence in CuCl was suggested by Stébé *et al.* [9]. A negatively charged exciton is a complex composed of two electrons and a hole, analogous to H^-. A positively charged exciton is a complex composed of an electron and two holes, analogous to H_2^+. They have been experimentally confirmed in CdTe and GaAs quantum wells recently [10,11]. Stébé and Ainane pointed out that the binding energy of the charged exciton is enhanced in a quantum well [12]. However, the charged exciton has never been observed in QDs. In this paper, we report the observation of the charged exciton in CuCl QDs and discuss their quantum size effect. The study is initiated by the observation of the luminescence hole burning (LHB) in CuCl QDs.

The formation of a spectral hole in luminescence, so-called luminescence hole burning, was first reported in a dye by Gorokhovski *et al.* in 1974 and 1976 [13,14]. In spite of a long history of the phenomenon, it has been studied compared with the absorption hole burning. The LHB can give us additional information which the absorption hole burning cannot. An absorption spectrum simply reflects the joint density of initial and final states of the transition. On the other hand, a luminescence spectrum reflects the relaxation mode of the luminescent excited states as well as the joint density of states. Therefore, in the LHB, the lowest-energy luminescent excited states, such as bound excitons and the charged excitons, are sensitively observed. The absorption hole spectrum corresponds to the absorption spectrum of the QDs excited selectively. In the same way, the luminescence hole spectrum is recognized as the luminescence spectrum of the QDs excited selectively. The fluorescence line narrowing (FLN) affords us similar information as the LHB does. However, it is sometimes difficult to obtain the spectrum near the excitation photon energy because of the scattering of the excitation light. In the LHB experiment, on the other hand, it is comparatively easy to observe the accurate hole spectrum even just at the burning energy, as is mentioned later. Moreover, in case of the semiconductor QDs, the FLN signal is reduced, because the absorption of the selectively excited QDs is reduced with very large burning efficiency [15]. In these senses, the LHB experiment is superior to the FLN experiment.

First, the peculiar characteristics of the luminescence in CuCl QDs are explained in connection with the LHB. Figure 1 shows absorption, luminescence, and absorption change spectra of the Z_3 exciton band in CuCl QDs embedded in a NaCl crystal at 2 K. The luminescence was measured under the band-to-band excitation at 3.49 eV. The absorption spectra and the luminescence spectra inhomogeneously broadened partly because of the size distribution of QDs. The oscillatory fine structures come from a stepwise growth of the CuCl quantum cubes in a NaCl crystal [16]. Below 30 K, the luminescence peak shows the large Stokes shift in CuCl QDs in a NaCl crystal. It may be explained by the recombination of bound excitons [17]. However, an attentive investigation of the luminescence was necessary for the definitive identification of the luminescence origin, because the luminescence spectrum changes with the increase of the accumulated light ex-

 0031-9007/96/77(24)/4942(4)$10.00

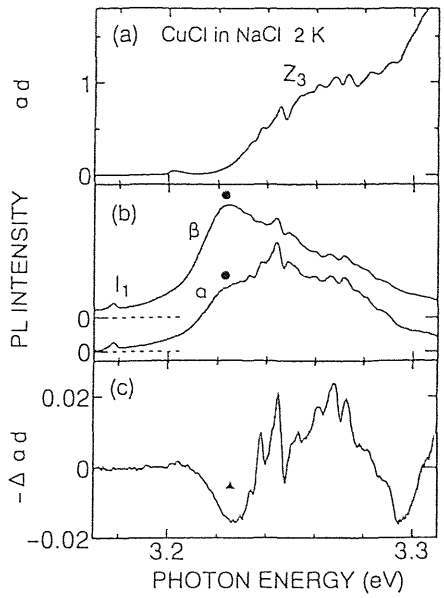

FIG. 1. (a) Z_3-exciton absorption, (b) luminescence, and (c) absorption change spectra of CuCl quantum dots in a NaCl crystal at 2 K.

posure. The luminescence spectral change is shown in Fig. 1(b). The luminescence signals that were accumulated during the sample was excited by 9000 shots of 3.49 eV pulses with the energy density of 0.1 $\mu J/cm^2$. The spectra α and β correspond to luminescence after the sample was exposed to accumulated energy density of 0 and 9.9 mJ/cm^2 of the 3.49 eV pulses, respectively. At low accumulated energy density, the luminescence peak almost agrees with the absorption peak. Therefore, the luminescence spectrum α is considered to come from the recombination of free excitons confined in the dots. With the increase of the accumulated energy density, the luminescence at the lower-energy tail marked by a solid circle grows. It is quenched after the thermal annealing cycle. The phenomena are similar to thermally annealing hole filling [3–6], and the thermal quenching of the luminescence elongation caused by the light exposure [6].

Figure 1(c) shows the absorption spectral change after the luminescence changes from α to β. The minute structures in the differential absorption spectrum corresponds to those in the absorption spectrum one by one, and the induced absorption marked by ▲ appears. The absorption change takes place together with the luminescence change. The energy position of the induced absorption band ▲ corresponds to that of the induced luminescence band ●. Both the spectral changes are persistent. We consider that the induced luminescence band comes from the charged exciton and is formed by the photoionization of QDs.

A scenario for the photoionization of QDs is the same as described for the mechanism of the PSHB phenomena [4–6]. First, an exciton is created by the light absorption. Second, the exciton is localized at the surface of the QD. Next, the exciton is dissociated and an electron or a hole tunnels through the potential barrier in the host and is trapped at a bound center in the host. Another carrier remains in the QD, and the dot is ionized. According to previous works [10,11], a prerequisite for the observation of a negatively charged exciton is that sufficiently high density of electrons should exist for the observation and that the electron density must not be so high as to screen the Coulomb interaction working inside the exciton. For example, in n-doped ($\sim 10^{16}$ cm^{-3}) GaAs quantum wells and CdTe quantum wells, the negatively charged excitons were observed together with excitons. When the charged exciton is observed, the exciton structure decreases and the charged exciton structure increases in the optical spectrum with increasing the electron density. At higher electron density, exciton and charged exciton structures decrease and are replaced by broad, structureless absorption and emission peaks showing a Fermi-edge singularity. Supposing that an electron is trapped in a QD whose radius is 5 nm, the electron density becomes 2×10^{18} cm^{-3}. The electron density is much higher than that in the previous reports of the charged excitons in GaAs and CdTe. In a CuCl crystal, an exciton Bohr radius is much smaller than the radius in GaAs or CdTe crystals. Therefore, the Coulomb screening hardly takes place in CuCl. We consider that the density is not unreasonable for the observation of the charged exciton in a CuCl crystal.

The LHB experiment gives us detailed information for the induced luminescence band. The experimental result definitely shows that the induced luminescence band comes from the recombination of charged excitons confined in QDs. The laser system used in the LHB experiment was a Q-switched Nd^{3+} : YAG laser and a dye laser pumped by it. The excitation photon energy of the dye laser was tuned to the Z_3 exciton band of CuCl QDs. The spectral linewidth of the dye laser was 0.014 meV, which was much narrower than the instrumental resolution of the experiment. The third harmonics of the Nd^{3+} : YAG laser (3.49 eV) was used as a band-to-band excitation light source for the measurement of the luminescence at 2 K. The laser pulse width was 5 ns, and the repetition rate was 30 Hz. For the observation of the LHB, the sample was excited alternatively by 3.49 eV and dye laser pulses, and a synchronized chopper selectively collects luminescence generated by the 3.49 eV excitation. When the dye laser pulse excited the sample, the chopper shut the path between the sample and the monochromator. At 33 ms after the dye laser pumped the sample, the 3.49 eV pulse excited the sample for the measurement of luminescence and the chopper opened the path. The luminescence lifetime of the sample, measured experimentally, was 4 ns at 2 K. The alternative excitation method is suitable for the observation of luminescence of the sample exposed to the dye laser, because the 3.49 eV excitation causes the hole filling. The luminescence produced by the 3.49 eV excitation is observed in this way.

Figure 2(a) shows the absorption spectrum of CuCl QDs embedded in a NaCl host crystal at 2 K. The Z_3 exciton

absorption peak shows a blueshift of 20 meV from its energy of a CuCl bulk crystal. The blueshift is explained by the exciton confinement model [1,2]. An average radius of the CuCl QDs estimated on the exciton confinement model is 3.0 nm. Figure 2(b) shows the luminescence spectra of the sample. The sample was exposed to the preexcitation of the 3.49 eV pulses with the accumulated fluence density of 10 mJ/cm^2. The luminescence signals were accumulated while the sample was excited by 900 shots of the 3.49 eV pulses with the energy density of 0.5 μJ/cm^2. The luminescence change caused by the 3.49 eV pulses for the luminescence observation was avoided by the preexcitation, because the luminescence change comes to an end after the excitation by the 3.49 eV pulses reaches the accumulated energy density of 10 mJ/cm^2. A dashed line shows the luminescence spectrum before the sample is exposed to the dye laser pulses. The luminescence peak is located at 3.206 eV, which is lower than the absorption peak of the Z_3 exciton, 3.223 eV. This Stokes shift of the luminescence was caused by the light preexposure. A solid line shows the luminescence spectrum, after the 3.220 eV narrow-band dye laser pulses exposed the sample with the energy density of 10 μJ/cm^2. The burning energy position is indicated by an arrow in Fig. 2(a). The luminescence shows a sharp hole (X) at the burning energy in the spectrum. Much larger satellite holes A, B, and • are observed at the lower-energy side of the burning laser energy. At the high energy side, the luminescence intensity increases. Figure 2(c) shows the absorption spectral change $-\Delta\alpha d$ after the LHB experiment. The luminescence-hole spectrum gives us information which the absorption-hole spectrum does not.

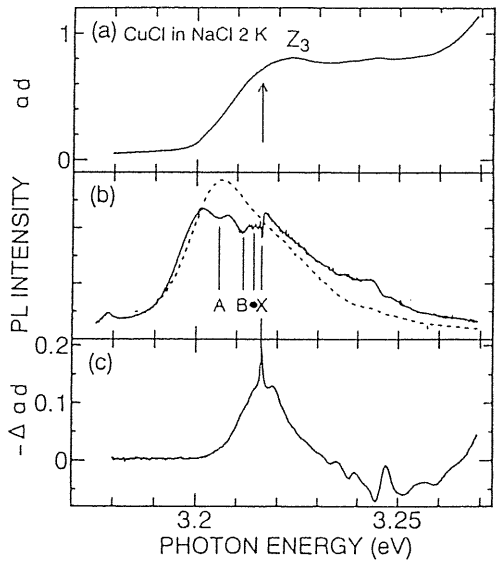

FIG. 2. (a) Absorption spectrum of CuCl quantum dots embedded in a NaCl crystal at 2 K. An arrow shows the burning energy of the dye laser. (b) Luminescence spectra before and after the sample is exposed at 3.220 eV with the excitation density of 10 μJ/cm^2. Luminescence spectra was taken under the excitation at 3.49 eV with the excitation density of 0.5 μJ/cm^2. (c) Absorption spectral change of the sample exposed to the narrow-band dye laser at 3.220 eV.

Figure 3 shows the luminescence-decrease spectra. The luminescence-decrease spectrum is defined by the luminescence spectrum of the sample exposed to the dye laser pulses minus that of the sample which is not exposed to the dye laser pulses. Arrows in the figure indicate the burning energies. Every spectrum has a sharp hole X at the burning energy, and much larger satellite holes, A, A', B, and •. With the increase in the burning energy, satellite hole structures are shifted toward the higher-energy side, and their separation increases. As the burning photon energy increases, the depth of the sharp resonant hole becomes smaller and a new structure (A') grows up. The luminescence hole reflects the luminescence of selectively burned QDs. The peak positions of the structures A, B, and A' depend on the excitation photon energy.

Figure 4 shows the Stokes shift of the luminescence-hole structures as a function of the burning photon energy. Here the Stokes shift means the energy differences between the burning laser and the luminescence-hole structures. The peak X comes from the luminescence of the resonantly excited Z_3 free exciton confined in QDs, because the energy position of the peak (X) coincides with the burning energy. The solid lines labeled by C and D correspond to a confined transverse acoustic phonon energy and a confined longitudinal acoustic phonon energy, respectively [18]. They explain the Stokes shift of the peaks labeled by • in Fig. 3, whose energy is lower than the burning energy by a few meV. Therefore, the luminescence-decrease peaks • are ascribed to the luminescence of the Z_3 exciton accompanied by the emission of acoustic phonons. The peaks in the luminescence-decrease spectrum, A', A, and B, show large Stokes shifts, and depend strongly on the burning photon energy. The positions of the A' structure seem to approach the energy position of I_1 bound exciton in bulk CuCl, as the burn-

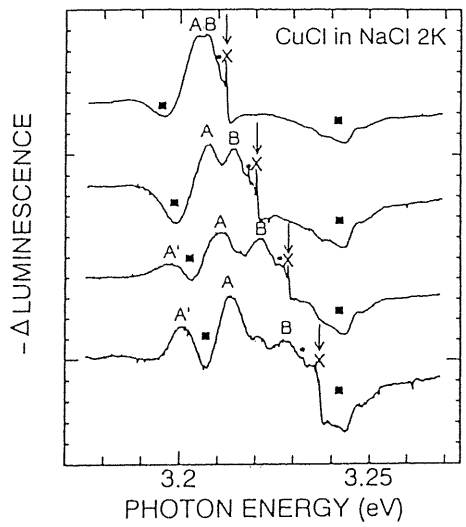

FIG. 3. Photoluminescence decrease at 2 K. Arrows indicate the burning energy.

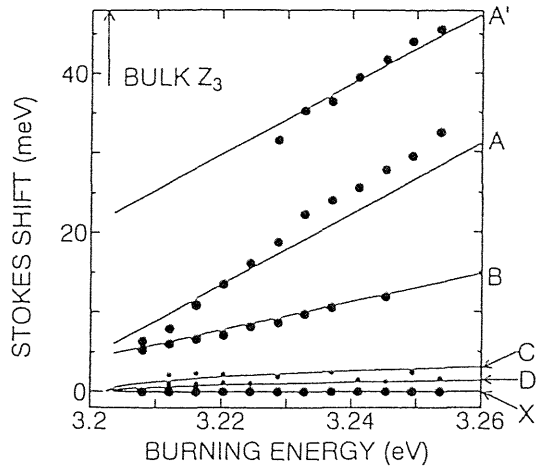

FIG. 4. The burning-energy dependence of the luminescence hole spectra. The burning energy is the photon energy of the dye laser. The Stokes shift is the energy difference between the burning laser and the hole structures.

ing energy approaches the Z_3-exciton energy in the bulk crystal [7]. Therefore, (A') structure is assigned to the I_1 bound exciton. On the other hand, structures, A and B, are ascribed to the charged exciton luminescence as is verified in the following.

We consider the quantum confinement of the translational motion of the charged exciton. The translational masses of negatively and positively charged excitons, M^- and M_2^+, are given by $M^- = 2m_e^* + m_h^*$ and $M_2^+ = m_e^* + 2m_h^*$, where $m_e^* = 0.5m_0$ and $m_h^* = 1.8m_0$ are effective masses of an electron and a hole in a CuCl crystal, respectively [7]. The energy shifts due to the quantum confinement effect are represented by $\Delta E^- = \hbar^2\pi^2/2M^-R^2$, for the negatively charged exciton, and $\Delta E^+ = \hbar^2\pi^2/2M_2^+R^2$, for the positively charged exciton, where R is the effective radius of the QD defined by radius of the QD minus half of the exciton Bohr radius [19]. Then, the energy separations, $-\Delta E_s^-$ and $-\Delta E_s^+$, between the quantum confined free exciton and the quantum confined charged exciton is given by

$$-\Delta E_s^- = \hbar^2\pi^2/2MR^2 - \hbar^2\pi^2/2M^-R^2 + E_{\text{bind}}^-$$
$$= 0.18 \times (E_{\text{free}} - 3.2025) + E_{\text{bind}}^-(eV), \quad (1)$$

and

$$-\Delta E_s^- = \hbar^2\pi^2/2MR^2 - \hbar^2\pi^2/2M_2^+R^2 + E_{\text{bind}}^+$$
$$= 0.44 \times (E_{\text{free}} - 3.2025) + E_{\text{bind}}^+(\text{eV}), \quad (2)$$

where E_{bind}^- and E_{bind}^+ are the binding energy of the charged exciton in bulk CuCl, and E_{free} is the energy of the free exciton confined in QDs given by $E_{\text{free}} = E_{\text{bulk}} + \hbar^2\pi^2/2MR^2$, where E_{bulk} and M are the exciton resonant energy and the exciton translational mass of a bulk CuCl [1]. In Eqs. (1) and (2), the value of 3.2025 eV is the Z_3 free exciton energy in bulk CuCl [7].

Solid lines A and B in Fig. 4 show the calculated results of (1) and (2) with $E_{\text{bind}}^- = 4.7$ meV and $E_{\text{bind}}^+ = 5.6$ meV, respectively. The binding energy of X^- and X_2^+ in bulk CuCl were set to be 4.7 and 5.6 meV, respectively, based on the calculation by Stébé *et al.* [9]. The solid lines A and B agree with the experimental points. Therefore, we consider the structures A and B, in Figs. 2 and 3, come from the recombination of the positively charged exciton and negatively charged exciton, respectively.

As is seen in Fig. 4, the burning energy dependence of the A' series coming from the I_1 bound exciton structure, resembles that of A series. The I_1 line denoted also by A^0X comes from the recombination of the exciton bound to a neutral acceptor. Therefore, A^0X can be regarded as an excitonic molecule whose constituent electron is pinned and can be considered as the complex X_2^+ going around the pinned electron. In this sense, the I_1 bound exciton resembles the X_2^+ charged exciton. Similarly to the positively charged exciton X_2^+, the translational motion of the I_1 bound exciton is confined in the QDs. Therefore, the burning energy dependence of the A' series resembles that of the A series. The solid line A is calculated by Eq. (2), where $E_{\text{bind}}^+ = 22$ meV is the binding energy of the I_1 bound exciton [7].

In summary, the luminescence spectral change induced by the accumulated light exposure and the LHB phenomena were observed in CuCl QDs in NaCl crystal. The luminescence spectral change was understood by the photoionization of the QDs and the creation of the charged exciton states. This conjecture was verified by the study of the LHB. The Stokes shift of the luminescence sideband holes can be explained by the quantum confinement of the charged excitons. This is the first observation of the charged excitons in QDs.

[1] A. I. Ekimov *et al.*, Solid State Commun. **56**, 921 (1985); see also A. D. Yoffe, Adv. Phys. **42**, 173 (1993).
[2] Y. Kayanuma, Phys. Rev. B **38**, 9797 (1988).
[3] K. Naoe *et al.*, Phys. Rev. B **50**, 18 200 (1994).
[4] Y. Masumoto *et al.*, Phys. Status Solidi B **188**, 209 (1995).
[5] Y. Masumoto *et al.*, Phys. Rev. B **52**, 4688 (1995).
[6] Y. Masumoto *et al.*, Phys. Rev. B **52**, 7834 (1995).
[7] M. Ueta *et al.*, *Excitonic Processes in Solids* (Springer, Berlin, 1989).
[8] M. A. Lampert, Phys. Rev. Lett. **1**, 450 (1958).
[9] B. Stébé and C. Comte, Phys. Rev. B **15**, 3967 (1977).
[10] K. Kheng *et al.*, Phys. Rev. Lett. **71**, 1752 (1993).
[11] G. Finkelstein *et al.*, Phys. Rev. Lett. **74**, 976 (1995).
[12] S. Stébé and A. Ainane, Superlattices Microstruct. **5**, 545 (1989).
[13] A. A. Gorokhovski *et al.*, JETP Lett. **20**, 216 (1974).
[14] A. A. Gorokhovski and L. A. Rebane, Opt. Commun. **20**, 144 (1976).
[15] The quantum efficiency of the hole burning for CuCl quantum dots in NaCl was found to be 0.015 at 2K.
[16] T. Itoh *et al.*, J. Lumin. **60&61**, 396 (1994).
[17] S. Yano *et al.*, Jpn. J. Appl. Phys. **34**, 140 (1994).
[18] S. Okamoto and Y. Masumoto, J. Lumin. **64**, 253 (1995).
[19] T. Itoh *et al.*, Phys. Status Solidi B **145**, 567 (1988).

Correlation between Cu^+-ion instability and persistent spectral hole-burning phenomena of CuCl nanocrystals

Shinji Okamoto* and Yasuaki Masumoto
Institute of Physics and Center for TARA (Tsukuba Advanced Research Alliance), University of Tsukuba, Tsukuba, Ibaraki 305, Japan
(Received 10 February 1997; revised manuscript received 11 August 1997)

We have studied persistent spectral hole-burning (PSHB) phenomena of CuCl nanocrystals embedded in a NaCl crystal. We found correlations between the PSHB phenomena and the photoluminescence spectral changes of excitons in CuCl nanocrystals and of Cu^+ dimers in a NaCl crystal. The spectral changes can be triggered by photoinduced Cu^+-ion displacements in CuCl nanocrystals and in a NaCl crystal. [S0163-1829(97)03048-8]

Semiconductor nanocrystals have attracted considerable attention not only because of their unique properties but also because of applicability to nonlinear optical devices.[1,2] For the investigation of the size-dependent properties of nanocrystals, it is ideal to fabricate a well-defined single-sized nanocrystal. However, nanocrystal size is difficult to control in many preparation methods, so that the samples have size distribution and then the absorption bands are inhomogeneously broadened.

Hole-burning spectroscopy is a powerful tool to extract individual and intrinsic information, i.e., information of certain-sized nanocrystals, from the inhomogeneously broadened absorption band. The hole-burning phenomena in the nanocrystal systems were considered to be caused by the absorption saturation of photoexcited carriers, so that the hole spectra had been expected to disappear within a few nanoseconds.

Recently, there have been many reports on persistent spectral hole-burning (PSHB), long-lived hole-burning, or photoinduced absorption-spectral change phenomena of various semiconductor nanocrystals.[3] The spectral holes persist for more than a few microseconds or even several hours. Understanding of the mechanism of the PSHB phenomena is indispensable for the understanding of nanocrystals but still poor: The PSHB phenomena were considered to be caused by carrier trapping or photochemical reactions. However, further study is necessary for the understanding of the mechanism.

Ab initio calculations predict that structural instabilities occur in zinc-blende cuprous halides, CuCl, CuBr, and CuI and cause Cu^+-ion related defects at low temperatures.[4,5] Such instabilities are expected to induce anomalous phenomena by light irradiation, e.g., persistent photoconductivity in Si-doped GaAs ("*DX* centers").[6] However, there is no experimentally strong evidence of the instabilities in CuCl, and whether the instabilities occur or not is now under discussion.[7]

In this paper, we have investigated a typical sample that exhibits the PSHB phenomena, CuCl nanocrystals embedded in a NaCl crystal, by using the laser-induced spectral-change and temperature-cycle experiments. The experimental results show that the PSHB phenomena can be explained by the two-level-system (TLS) model, in a way analogous to dye molecule-glass systems. The results also indicate that there are two types of TLS's in the samples. We also found correlations between the PSHB phenomena and photoluminescence (PL) spectral-changes of excitons in CuCl nanocrystals and Cu^+ dimers in NaCl crystals: The absorption and PL spectra are simultaneously modified with an increase of the laser irradiation, and recover at the same cycling temperatures. The spectral-changes can be triggered by Cu^+-ion displacement in CuCl nanocrystals and NaCl crystals. The *ab initio* calculations of the potential barrier heights for the Cu^+-ion displacements support this interpretation.

Samples investigated here were CuCl nanocrystals embedded in NaCl crystals. The samples were prepared in the same fashion as is described in Ref. 8. The mean radii of the nanocrystals were determined by small-angle x-ray scattering (SAXS) experiments. The samples were immersed in superfluid helium or mounted on the cold finger of a temperature-variable cryostat. A Q-switched Nd^{3+}:YAG (yttrium aluminum garnet) laser, a narrow-linewidth dye laser, and a halogen lamp were used in the experiments. For the band-to-band excitation, the third harmonics of the output of the Q-switched Nd^{3+}:YAG laser was used as a pump source. For site-selective excitation, the dye laser with Exalite 384 dye pumped by the third harmonics of the output of the Q-switched Nd^{3+}:YAG laser was used as a pump source. The spectral linewidth of the dye laser was 0.014 meV. The pulse width and repetition of the lasers were 5 ns and 30 Hz, respectively. The halogen lamp was used as a probe source. Transmittance spectra of the samples were measured by using a diode-array-type optical multichannel analyzer in conjunction with a 25-cm monochromator or a charge-coupled-device in conjunction with a 93-cm monochromator. Absorption-change spectra are defined as the difference of the absorption spectra taken before and after the sample is exposed to the laser light.

Figure 1(a) shows absorption spectra of CuCl nanocrystals embedded in a NaCl crystal at 2 K. The dash-dotted line in Fig. 1(a) represents the spectrum before the dye laser irradiation. The mean radius of the nanocrystals is 3.5 nm, estimated from SAXS experiments. The Z_3-exciton absorption band is inhomogeneously broadened, and shows the blueshift from its position in bulk CuCl. The mean radius estimated from the blueshift (15 meV) on the exciton quan-

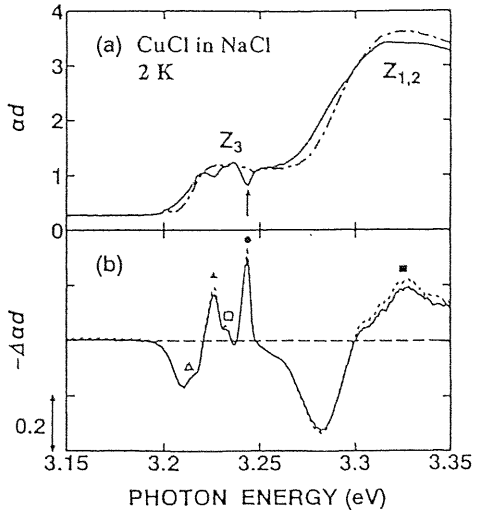

FIG. 1. Persistent spectral holes of CuCl nanocrystals embedded in a NaCl crystal at 2 K. (a) Absorption spectra before (dash-dotted line) and after (solid line) the laser exposure; (b) absorption-spectral change measured at 2 min (dotted line) and 20 min (solid line) after the burning laser is stopped. The main hole (●) and satellite holes (▲, △, ■, and □) are clearly observed. The mean radius of the nanocrystals is 3.5 nm. The burning photon energy, the energy density, the pulse duration, the pulse repetition, and the excitation period are 3.245 eV, 33 μJ/cm^2, 5 ns, 30 Hz, and 3 min, respectively.

tum confinement model[9] is 3.3 nm, almost consistent with the SAXS results. The absorption spectrum is changed after the dye laser exposure, as indicated by a solid line in Fig. 1(a). Figure 1(b) shows the absorption-spectral change of the sample. The hole spectra were recorded at 2 min (dotted line) and at 20 min (solid line) after the laser exposure was stopped. The spectral holes are preserved for more than 20 min, much longer than the exciton lifetime.[3] Further, we confirmed the persistency of the holes for several hours. The hole spectrum is more complicated than that of CuCl nanocrystals embedded in glass:[3] The main spectral holes are superposed on the large wavy structures coming from the redshiftlike spectral change of the absorption band. Satellite holes are also clearly observed: The solid circle (●) in Fig. 1(b) indicates the main hole; the open triangle (△) the LO-phonon sideband; the solid triangle (▲) the TO-phonon sideband; the open square (□) the sideband of the TA-phonon at the Brillouin-zone edge; the solid square (■) the sideband related to the $Z_{1,2}$ excitons.

We found that the hole depth and the wavy structure coming from the redshiftlike spectral changes grow nearly in proportion to the logarithm of the laser exposure time, similar to CuBr and CuI nanocrystals embedded in glass[3,10] and dye-doped organic glass.[11] The logarithmic hole growth is due to a broad distribution of the hole-burning rate. The PSHB phenomena can be explained by tunneling from one site to another through the potential barrier with distributed barrier height and width, which is called a double-well potential model or TLS model.[12]

The hole structures are erasable by the temperature rise. Figure 2 shows (a) absorption spectrum, (b) hole spectra after various temperature cycles, and (c) the hole area plotted as a function of the cycling temperature. This experimental sequence is as follows: At first, the spectral holes are burned

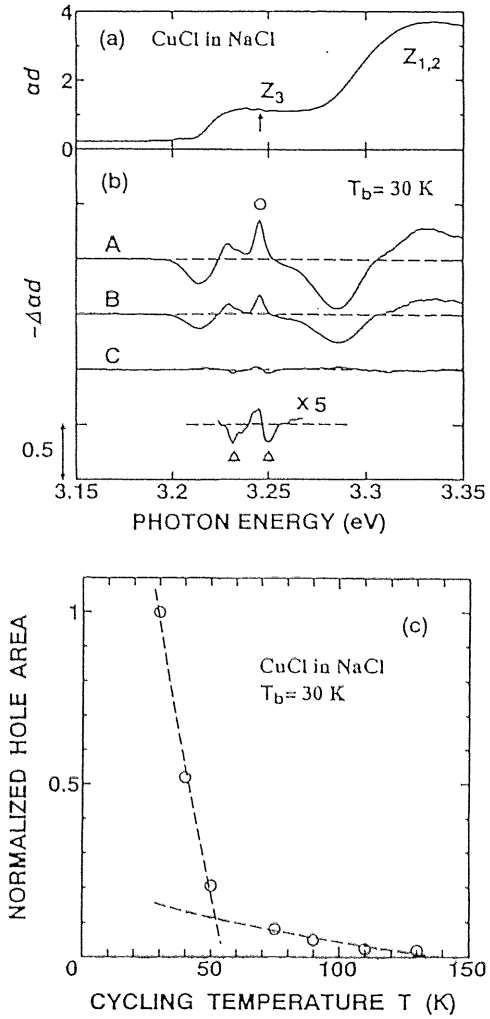

FIG. 2. Spectral holes of thermally annealed CuCl nanocrystals embedded in a NaCl crystal after the intense laser exposure as a function of the cycling temperatures. (a) Absorption spectrum; (b) absorption-spectral change recorded after the various temperature cycles: (A) 30, (B) 45, and (C) 75 K. Open circle (○) and triangles (△) represent the main hole and antiholes, respectively. (c) Normalized hole area of CuCl nanocrystals as a function of the cycling temperature T. After hole-burning at T_b and cycling through the elevated temperature T, the hole is measured at T_b again. The dashed lines represent the calculated results on the model described in Ref. 13 and are fit by the following expressions; $0.15(1-0.016\sqrt{T})/(1-0.016\sqrt{30})$ [$T>50$ K] and $0.15(1-0.016\sqrt{T})/(1-0.016\sqrt{30})+0.85(1-0.084\sqrt{T})/(1-0.084\sqrt{30})$ [$T<50$ K]. The mean radius of the nanocrystals is 3.5 nm. The hole-burning temperature T_b is 30 K. The temperature-cycling measurements were done after the 1-min laser exposure at the pump photon energies of 3.245 eV with the energy density of 40 μJ/cm^2.

at certain temperature T_b, and the hole spectrum is measured; after cycling through the elevated temperature (cycling temperature) T, the hole spectrum is measured again at T_b. The experimental cycling-temperature dependence of hole filling is well expressed by the thermal activation model across distributed barrier height.[13] The rate of this model is expressed by $\nu=\nu_0\exp(-V/kT)$, where ν_0 is the frequency factor which is the order of 10^{11} s^{-1} and V the potential barrier height. During the holding time t at the temperature T, the hole is filled if the condition $\nu t>1$ holds. Therefore,

the hole is filled, if $V<kT\ \ln(\nu_0 t)$. Moreover, we assume that the distribution of the potential barrier height $P(V)$ is expressed by $P(V)\propto 1/\sqrt{V}$ with a maximum barrier height $V_{0\,\max}$.[13] The annealing temperature-dependent hole area have been fitted by the functional form of $[1-\sqrt{kT\ \ln(\nu_0 t)/V_{0\,\max}}]/[1-\sqrt{kT_b \ln(\nu_0 t)/V_{0\,\max}}]$ for $kT\ \ln(\nu_0 t)<V_{0\,\max}$ in the case of dye molecules in organic glass.[13] Here, $\ln(\nu_0 t)$ is the logarithm of the product of the attempt frequency (ν_0) and the holding time (t), and is given by 32–35. We tried to fit the expression to the experimental results and estimated the maximum barrier height $V_{0\,\max}$ between the TLS. Two components are necessary to account for the data. The maximum barrier height is 140–160 meV for $T<50$ K and 400–420 meV for $T>50$ K. The absorption-change spectra abruptly varied after the temperature cycles above 50 K, as displayed in Fig. 2(b): After the temperature cycles above 50 K, the large wavy structures coming from redshiftlike spectral changes almost disappear, and antiholes, induced absorption adjacent to the spectral hole [Δ in Fig. 2(b)], appear. Antiholes are important signs that the PSHB phenomena are photophysical,[12] e.g., local-environmental changes around the nanocrystals. After the temperature cycles above 150 K, the spectral hole almost disappears. These observations prove the coexistence of two kinds of TLS's in the sample. The cycling temperature dependence is almost independent of the energy positions of the burned holes.

We found correlations between the absorption spectral changes showing PSHB phenomena and PL spectral-changes of excitons and Cu^+ dimers. Figures 3(a), 3(b), and 3(c) show absorption, absorption-change spectra, and PL spectra after the laser irradiation with the 3.492-eV excitation energy, respectively, at 2 K. The excitation source was the third harmonics of the output of the Q-switched Nd^{3+}:YAG laser. This experimental sequence is as follows: At first, absorption spectrum before the laser exposure is measured. Next, the band-to-band excitation of the sample is started and, during the first 10 s of exposure, PL spectrum is measured. After the sample is exposed for a certain time (300 or 3000 s, in this experiment), the laser exposure is stopped, and then the absorption spectrum is measured. After that, the PL spectrum is measured again. The PL-data accumulated time is 10 s.

In this case, the absorption-change spectra show the wavy structures coming from redshiftlike spectral change and the bleaching of the Z_3-exciton absorption band but do not show spectral holes. This is because the band-to-band transition occurs under the pump photon energy. Laser irradiation induces not only absorption-spectral changes but also PL-spectral changes:[14] At first, PL peak energy was at the Z_3-exciton absorption peak energy (●). With an increase of the laser irradiation time, another PL peak (×) grew and the absorption spectrum was modified. Moreover, we found that the peak of the PL spectra (×) in the well-irradiated sample is at almost the same energy position as the lowest-energy peak of the absorption-change (○). Using the nanocrystal samples with various mean radius, we determined the relations between the Z_3-exciton absorption peak energy (●), the lowest-energy peak of the absorption-change (○), and the peak energy of the PL spectra (×). The results are plotted in Fig. 3(d). With the decrease of the Z_3-exciton absorption

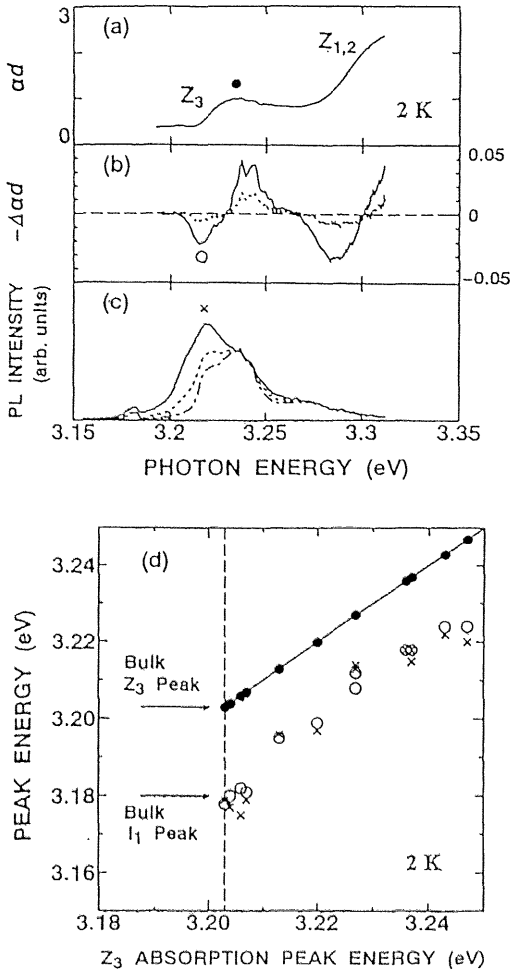

FIG. 3. Laser-exposure time dependence of absorption- and photoluminescence (PL) spectra of CuCl nanocrystals embedded in a NaCl crystal under the 3.492-eV laser excitation with the 30-Hz pulse repetition and the 0.85-μJ/cm^2 energy density at 2 K. (a) Absorption spectrum; (b) absorption-change spectra measured at 300 s (dotted line) and 3000 s (solid line) after the laser exposure; (c) PL spectra measured at 0 s (dash-dotted line), 300 s (dotted line), and 3000 s (solid line) after the laser exposure is started. The PL-data accumulated time is 10 s. (d) Peak energies of Z_3-exciton absorption spectra (●) vs those of well-exposed absorption-change spectra (○) and of well-exposed PL spectra (×). Horizontal axis also represents the peak energies of Z_3-exciton absorption spectra.

peak energy (●), i.e., the increase of the mean radius of the nanocrystals, the lowest-energy peak of the absorption-change (○), and the peak energy of the PL spectra (×) approach to the energy position of the I_1 center of bulk CuCl crystal: I_1 center is attributed to excitons bound to neutral acceptors made of Cu^+ vacancies in CuCl.[15] They probably contain the charged exciton components as shown in Ref. 14. This result suggests that the observed peaks (○ and ×) are correlated with I_1 centers, namely, Cu^+-ion vacancies in CuCl nanocrystals and resultant charge instability of the nanocrystals.

Moreover, we found that the PL spectra as well as the absorption-change spectra change with an increase of cycling temperatures: After the temperature cycles above 50 K, the absorption spectral changes, i.e., wavy structures coming from redshiftlike absorption change, almost disappear. This observation is consistent with the abrupt spectral change ob-

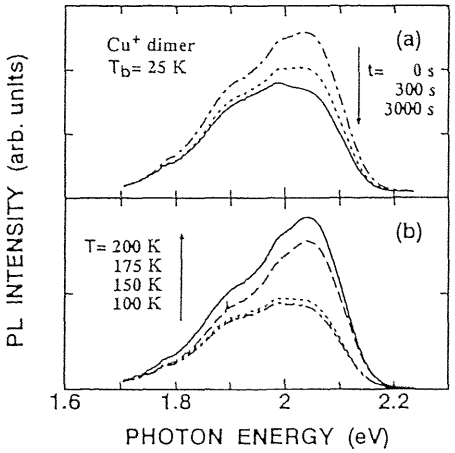

FIG. 4. Photoluminescence (PL) spectral-change of Cu^+ dimers at $T_b = 25$ K under the 3.492-eV and 30-Hz excitation. (a) PL spectra measured at 0 s (dash-dotted line), 300 s (dotted line), and 3000 s (solid line) after the laser exposure with the 8.5-μJ/cm^2 energy density is started. The PL-data accumulated time is 10 s. (b) PL spectra after the various temperature cycles: 100 K (dash-dotted line), 150.K (dotted line), 175 K (dashed line), and 200 K (solid line) under the laser irradiation with the 420-nJ/cm^2 energy density. The temperature-cycling measurements were done after the 1-min laser exposure with the 850-μJ/cm^2 energy density.

served at 50 K, as shown in Fig 2(b). Simultaneously, the PL spectra returned to the spectra observed before the intense laser irradiation. This can be explained by considering that I_1 centers, namely, Cu^+-ion vacancies, and resultant charge instability were reduced by thermal activation.

PL spectral changes triggered by Cu^+-ion displacements are observed not only in CuCl nanocrystals but also in a NaCl crystal. Figure 4 shows PL spectra at around 2.1 eV in CuCl nanocrystals embedded in a NaCl crystal. The sample was the same as used in Figs. 1–3. The PL band in Fig. 4 is ascribed to Cu^+ dimers in a NaCl crystal since the PL lifetime (50 μs), the bandwidth (0.2 eV), and the peak position (2.1 eV) are consistent with those of Cu^+ dimers at low temperatures reported in Refs. 16–18. It is reasonable to expect that CuCl nanocrystals are surrounded by Cu^+ dimers since the nanocrystals are formed by aggregation of Cu^+ ions.[9,16] At 25 K, the PL ascribed to Cu^+ dimers decreases its intensity with the increase of the laser irradiation time, as shown in Fig. 4(a). Moreover, after the PL spectra of the dimers are sufficiently changed by the intense laser irradiation, the PL intensity increases with the increase of the cycling temperature and quickly recovers when the cycling temperature exceeds 150 K, as shown in Fig. 4(b). These observations can be explained by photodissolution of Cu^+ dimers and thermal aggregation of Cu^+ monomers. The phenomena are considered to occur via the ion-exchange between Na^+ and Cu^+ ions, similar to Cu^+ ions in Cu^+-doped Na^+-β''-alumina.[17]

The cycling-temperature dependence of recovery of the PL and absorption spectra are correlated with the return movement of Cu^+ ions in CuCl nanocrystals and in a NaCl crystal to the previous sites after the temperature cycles above 50 and 150 K, respectively. The cycling-temperature dependence of the PL spectral change due to the movement of Cu^+ ions coincides with that of the PSHB phenomena.

Here, it should be noted that the potential barrier heights obtained from the temperature-cycling experiments in the PSHB phenomena are almost consistent with those for Cu^+-ion displacements in CuCl and NaCl crystals obtained from *ab initio* calculations: from the temperature-cycling experiments, potential barrier heights were estimated to be 140–160 and 400–420 meV; from *ab initio* calculations, potential barrier heights are estimated to be 120 (Ref. 4) and 180 meV (Ref. 5) for Cu^+-ion displacements between on- and off-center sites in bulk CuCl, and to 160–870 meV for a formation of a Cu^+ site in NaCl crystals via Na^+-Cu^+ ion exchange.[19] Thus, barrier heights of 140–160 meV obtained from the temperature-cycling experiments corresponds to those for Cu^+-ion displacement in CuCl nanocrystals, and the barrier heights of 400–420 meV to those for Cu^+-ion displacement in NaCl crystals.

Observed facts suggest the strong correlation between the Cu^+ displacements and the PSHB phenomena. Although we cannot explain the persistent spectral-change quantitatively, we speculate a possible PSHB mechanism as follows. Laser irradiation on the samples induces two types of Cu^+ displacements: one occurs in CuCl nanocrystals and the other in a NaCl crystal. These processes result in photocreation of I_1 centers in CuCl nanocrystals and photodissolution of Cu^+ dimers in a NaCl crystal. The photocreation of I_1 centers and resultant charge instability forms new absorption band at the lower-energy side of the Z_3-exciton absorption band, and then reduces the Z_3-exciton absorption band. At the same time, the Cu^+-ion displacement can affect the $Z_{1,2}$ excitons. The Cu^+-ion displacement forms a new absorption band at the lower-energy side of the $Z_{1,2}$-exciton absorption band, and then reduces the $Z_{1,2}$-exciton absorption band, like the I_1 center. This is a possible origin of the large wavy structure coming from the redshiftlike absorption change and some of spectral hole. On the other hand, the photodissolution of Cu^+ dimers to Cu^+ monomers around nanocrystals induces local-environmental changes, e.g., the change of the number of carriers trapped in matrix defects, or/and local-distortional change caused by the Cu^+-Na^+ exchange around the nanocrystals. The environmental changes probably perturb the excitons in nanocrystals. This is a possible origin of antiholes and some of spectral hole. Thus, the absorption changes due to the Cu^+ displacements inside and outside of the nanocrystals simultaneously occur under the laser exposure. When the cycling temperature is below 50 K, most of Cu^+ ions in CuCl nanocrystals and a NaCl crystal will not return to the sites before the intense laser irradiation. When the cycling temperature is above 50 K, most of Cu^+ ions in CuCl nanocrystals return to the previous sites, and then I_1 centers and charged exciton bands disappear: wavy structures and some of the spectral hole disappears. On the other hand, Cu^+ ions in a NaCl crystal do not return because the potential barrier is higher. As a result, only the spectral change attributed to the Cu^+-displacements in a NaCl crystal remains, and then the abrupt spectral changes, i.e., antiholes are observed [spectrum C in Fig. 2(b)]. The spectral change vanishes after the temperature cycles above 150 K.

In conclusion, we have reported on the PSHB phenomena of CuCl nanocrystals embedded in a NaCl crystal. The experimental results show that the PSHB phenomena can be explained by two types of TLS's. The PSHB and PL

spectral-change phenomena can be triggered by photoinduced Cu^+-ion displacements in CuCl nanocrystals and a NaCl crystal.

Small-angle x-ray scattering experiments were done by the approval of the Photon Factory (PF) Advisory Committee (Proposals 90-222 and 92-117). We wish to acknowledge Professor Y. Amemiya at PF for his gentle guidance to the experiments. This work was done under the TARA (Tsukuba Advanced Research Alliance) project at the University of Tsukuba. S.O. is grateful to the JSPS Research Associate Program ("Research for the Future" Program from the Japan Society for the Promotion of Science, No. JSPS-RFTF96R12501).

*Present address: Faculty of Engineering, Tokyo Engineering University, 1404-1 Katakura, Hachiohji, Tokyo 192, Japan. Also at Department of Electrical and Electronic Engineering, Faculty of Engineering, Tottori University, Koyama, Tottori 680, Japan.

[1] A. I. Ekimov, Al. L. Efros, and A. A. Onushchenko, Solid State Commun. 56, 921 (1985).

[2] L. Brus, IEEE J. Quantum Electron. QE-22, 1909 (1986).

[3] See, for example, Y. Masumoto, J. Lumin. 70, 386 (1996).

[4] S.-H. Wei, S. B. Zhang, and A. Zunger, Phys. Rev. Lett. 70, 1639 (1993).

[5] C. H. Park and D. J. Chadi, Phys. Rev. Lett. 76, 2314 (1996).

[6] D. V. Lang and R. A. Logan, Phys. Rev. Lett. 39, 635 (1977).

[7] A. Göbel, T. Ruf, M. Cardona, C. T. Lin, and J. C. Merle, Phys. Rev. Lett. 77, 2591 (1996); C. H. Park and D. J. Chadi, *ibid.* 77, 2592 (1996).

[8] Y. Masumoto, M. Yamazaki, and H. Sugawara, Appl. Phys. Lett. 53, 1527 (1988).

[9] T. Itoh, Y. Iwabuchi, and M. Kataoka, Phys. Status Solidi B 145, 567 (1988).

[10] Y. Masumoto, K. Kawabata, and T. Kawazoe, Phys. Rev. B 52, 7834 (1995).

[11] R. Jankowiak, R. Richert, and H. Bässler, J. Phys. Chem. 89, 4569 (1985).

[12] *Persistent Spectral Hole-Burning: Science and Applications*, edited by W. E. Moerner (Springer-Verlag, Berlin, 1988).

[13] W. Köhler, J. Meiler, and J. Friedrich, Phys. Rev. B 35, 4031 (1987).

[14] T. Kawazoe and Y. Masumoto, Phys. Rev. Lett. 77, 4942 (1996).

[15] M. Certier, C. Wecker, and S. Nikitine, J. Phys. Chem. Solids 30, 2135 (1969).

[16] S. A. Payne, L. L. Chase, and L. A. Boatner, J. Lumin. 35, 171 (1986).

[17] J. D. Barrie, B. Dunn, G. Hollingsworth, and J. I. Zink, J. Phys. Chem. 93, 3958 (1989).

[18] H. Kishishita, Phys. Status Solidi B 55, 399 (1973).

[19] V. Luaña and M. Flórez, J. Chem. Phys. 97, 6544 (1992); M. Flórez, M. A. Blanco, V. Luaña, and L. Pueyo, Phys. Rev. B 49, 69 (1994).

Persistent spectral-hole-burning spectroscopy of CuCl quantum cubes

Naru Sakakura* and Yasuaki Masumoto†
Institute of Physics and Center for TARA (Tsukuba Advanced Research Alliance), University of Tsukuba, Tsukuba, Ibaraki 305, Japan
(Received 26 March 1997)

A persistent spectral-hole-burning (PSHB) phenomenon was successfully applied to the precise site-selective spectroscopy of CuCl quantum dots embedded in NaCl crystals. In the PSHB spectra of CuCl quantum dots, a resonantly burned hole and lower-energy satellite holes were observed. These satellite holes are supposed to originate from hole burning of the ground states, which results from site-selective excitation of the corresponding excited states of excitons confined in CuCl quantum dots. Energy relation between the resonantly burned hole and each satellite hole is well explained by the simple concept of a particle in a quantum cube with an infinitely high potential barrier. However, actual quantum dots are considered to be a little deviated from cubes, resulting in the violation of the optical selection rule in quantum cubes. A cubic-shaped quantum-dot model is almost consistent with oscillatory fine structures observed in the Z_3 exciton absorption band. Its spectral decomposition into the ground state and the first excited state of excitons was made, and showed that the first excited state is in majority at the higher-energy region of the Z_3 exciton absorption band. This result was supported by the photoluminescence spectrum of the Z_3 exciton. [S0163-1829(97)07632-7]

In nanometer-size semiconductor crystallites, or zero-dimensional quantum dots, electronic and optical properties are dramatically different from those in three-dimensional bulk semiconductors. As a result, they have been attracting much interest not only from the viewpoint of fundamental physics but also from the expectation for their potential applications to various electronic and optical devices such as a quantum-dot laser. For application, it is very important to understand and control the physical properties of ordered quantum dots. Orders of quantum dots are classified as those in size, alignment, orientation, and shape. Ordering quantum dots in size is of major importance, because the size distribution of quantum dots is the primary source of inhomogeneous broadening that can completely cancel out the advantages of zero-dimensional density of states. Narrow distribution in dot size has been performed for self-organized $In_xGa_{1-x}As/GaAs$ quantum dots grown by molecular-beam epitaxy[1] and by metalorganic chemical vapor deposition (MOCVD),[2] and for colloidal CdSe quantum dots.[3] As for the order in alignment, an aligned array of $GaAs/Al_xGa_{1-x}As$ quantum dots was fabricated by using electron-beam lithography and plasma etching, although the size of each quantum dot is as large as 57 nm in diameter.[4] A self-alignment of the smaller self-organized $In_xGa_{1-x}As/GaAs$ quantum dots grown by MOCVD was recently achieved.[5,6] In the case of orientational order, the crystal axis of CuCl quantum dots and that of the NaCl matrix were found to be parallel to each other.[7] Order in dot shape, however, has been little studied. One of the purposes in this paper is to investigate the shape of CuCl quantum dots embedded in NaCl crystals by means of persistent spectral hole burning (PSHB) spectroscopy.

Recently, PSHB phenomenon in semiconductor quantum dots such as CuCl, CuBr, CuI, CdSe, CdTe, and CdS quantum dots embedded in glass, crystals, or polymers has been observed.[8–13] Ever since, the PSHB is considered to be applicable to the precise site-selective spectroscopy of quantum dots. When the spectrally narrow light excites the inhomogeneously broadened absorption band, a spectral hole is formed at the position of the excitation photon energy in the absorption band, and the spectral hole is preserved for a long time at low temperature. As a result of the PSHB, the electronic and excitonic quantum states, including the excited states, may be burned. This allows us to investigate the energies of quantum dots systematically. Because the energies of quantum dots depend on their shape, the precise study of the energies by means of PSHB spectroscopy is useful for the investigation of the shape of CuCl quantum dots. Another purpose of this paper is to investigate the correlation between the ground- and the excited-state excitons confined in CuCl quantum dots in NaCl crystals by means of PSHB spectroscopy.

Samples, CuCl quantum dots in NaCl, were made from the melted mixture of NaCl and CuCl, and grown by the transverse Bridgman method. The as-grown crystals were cleaved into several pieces and were annealed in Ar atmosphere for the control of the size distribution of CuCl quantum dots. The samples were directly immersed in superfluid helium at 2 K or mounted on a sample rod of a temperature variable cryostat. A spectrally narrow dye laser pumped by a Q-switched Nd^{3+}: YAG (yttrium aluminum garnet) laser was used as a pump source. The spectral width of the dye laser was 0.014 meV and the pulse duration was approximately 5 ns. The repetition rate of the laser system was 30 Hz. A halogen lamp was used as a probe source. The transmittance of the probe beam was detected by using a liquid-nitrogen-cooled charge-coupled-device optical multichannel analyzer in conjunction with a 75 cm monochromator. The spectral resolution of the experiment was 0.04 nm (0.35 meV). For the luminescence measurements, the third-harmonic light of the Nd^{3+}: YAG laser (355 nm, 3.49 eV) was used as a band-to-band excitation source.

It is known that photoexcited exciton in CuCl quantum dots is confined in the limited space and that its center-of-mass translational motion is quantized due to a small exciton Bohr radius of 0.68 nm.[14,15] Figure 1 shows absorption spec-

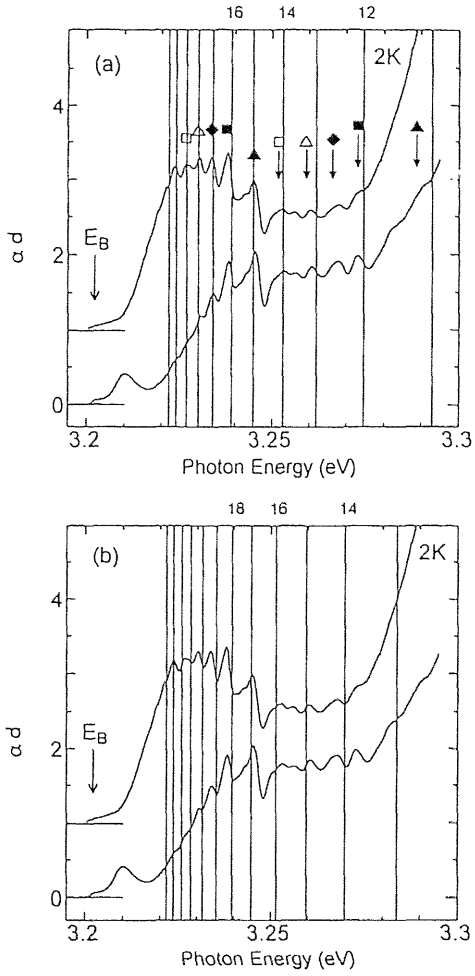

FIG. 1. Z_3 exciton absorption spectra of CuCl quantum dots in NaCl crystals at 2 K. Vertical solid lines in (a) and (b) indicate the calculated energies of the Z_3 exciton under the assumption of quantum cubes and spheres, respectively. E_B is the bulk Z_3 exciton energy.

tra of CuCl quantum dots in NaCl crystals at 2 K. Oscillatory fine structures are observed between 3.22 and 3.28 eV in the inhomogeneously broadened Z_3 exciton absorption band.[16] Origin of the inhomogeneous broadening has been explained partly by the size distribution of the quantum dots. Itoh *et al.* suggested that each oscillatory fine structure was explained by the size-quantized lowest energy of the Z_3 exciton confined in a quantum cube whose side changes stepwise in a unit of $a/2$, where a is a lattice constant of CuCl crystal.[17] If an infinitely tall potential barrier is assumed in a CuCl quantum cube with the side length of L, quantized exciton energy levels are easily derived from the simple concept of a particle in a quantum cube and are described by

$$E_{n_x,n_y,n_z}=E_B+\frac{\hbar^2\pi^2}{2M(L-a_B)^2}(n_x^2+n_y^2+n_z^2), \qquad (1)$$

where E_B is the bulk Z_3 exciton energy ($E_B=3.2022$ eV), M is the translational mass of exciton ($M=2.3m_0$), a_B is its Bohr radius ($a_B=0.68$ nm), quantum numbers n_x, n_y, and n_z, take values 1, 2, 3,..., and $(L-a_B)$ is used for the dead layer correction. Vertical solid lines in Fig. 1(a) indicate the expected energy of the ground state $E_{1,1,1}$ in cubes with the side length of each cube shown at the top in a unit of half the lattice constant a ($a=0.54$ nm).

On the other hand, if quantum dots are assumed to be a sphere with radius R and its diameter changes stepwise in a unit of $a/2$, quantized energy levels are calculated by

$$E_{n,l}=E_B+\frac{\hbar^2\pi^2}{2M(R-a_B/2)^2}\xi_{n,l}^2, \qquad (2)$$

where $\pi\xi_{n,l}$ is the nth root of the spherical Bessel function of the lth order and the principal quantum number n and the angular momentum quantum number l take values $n=1,2,3,\ldots$ and $l=0,1,2,\ldots$, respectively. $\xi_{n,l}$ takes values $\xi_{1,0}=1$, $\xi_{1,1}=1.4303$, $\xi_{1,2}=1.8346$, $\xi_{2,2}=2$, and so on. For the dead layer correction, $(R-a_B/2)$ is used. Vertical solid lines in Fig. 1(b) represent the calculated energy of the ground state $E_{1,0}$ with the diametric length of each sphere shown at the top in a unit of half the lattice constant a. The oscillatory fine structure below 3.25 eV is better fitted by $E_{1,1,1}$ rather than by $E_{1,0}$ and suggests that the shape of CuCl quantum dots is cubic rather than spherical. However, above 3.25 eV, the peak energies of the oscillatory fine structures do not coincide with the calculated energies for both quantum cubes and spheres. It also should be commented that the experimental peaks can be explained neither by the quantum sphere model nor the quantum cube model without the dead layer correction.

In order to explain peaks above 3.25 eV, the first excited state of excitons confined in CuCl quantum cubes was taken into account. They are well fitted by the first excited-state energy $E_{2,1,1}$ calculated on the basis of the energy relation $E_{2,1,1}-E_B=2(E_{1,1,1}-E_B)$ obtained from Eq. (1), as shown by downward arrows with ▲, ■, ◆, △, and □ in Fig. 1(a). Here, the first excited-state energy $E_{2,1,1}$ denoted by downward arrows with ▲, ■, ◆, △, and □ above 3.25 eV is calculated by the peak position of the ground-state energy $E_{1,1,1}$ denoted by ▲, ■, ◆, △, and □ below 3.25 eV, respectively. In this way, the observed peaks above 3.25 eV are energetically explained by the first excited states of excitons in CuCl quantum cubes. The optical selection rule, however, tells us that the first excited exciton state $E_{2,1,1}$ confined in a quantum cube does not contribute to the optical transitions because of the parity.[18,19] The exciton wave function for the center-of-mass motion is simply given by sine functions with quantum number n, which has even parity for the states of odd n and odd parity for those of even n. Integration of the wave functions over the cube gives the matrix element of the electric dipole transition between the ground and the nth state, and the matrix element is equal to zero for even quantum number n, according to the long-wavelength approximation. The reason why the optical selection rule is broken is discussed later.

Absorption and absorption change spectra of CuCl quantum dots at 2 K are shown in Figs. 2(a) and 2(b), respectively. The absorption change spectrum $-\Delta\alpha d$ is defined by the absorption spectrum of the sample exposed to the narrow-band dye laser minus that of the virgin sample. The sample was exposed to 72 000 shots of dye laser pulses with the photon energy of 3.2378 eV and excitation density of 46 nJ/cm^2. In addition to the spectral hole resonantly burned

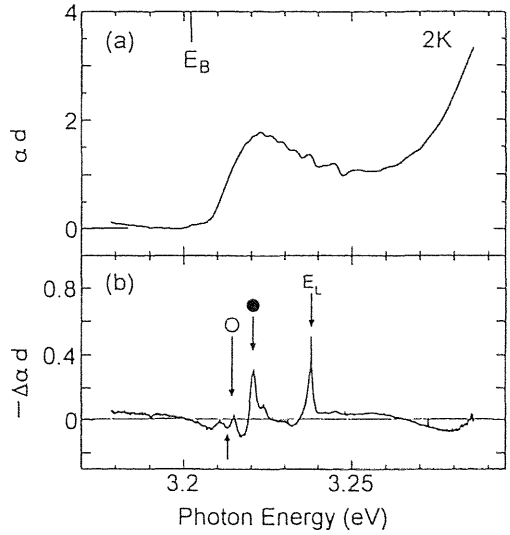

FIG. 2. Absorption (a) and absorption change (b) spectra in CuCl quantum dots in NaCl at 2 K. Excitation photon energy denoted by E_L is 3.2378 eV. Structures marked by a solid circle and an open circle show the spectral holes observed at $E=E_B+(E_L-E_B)/n$, where n takes values 2 and 3, respectively. An upward arrow indicates the position at $E=E_B+(E_L-E_B)/3.35$.

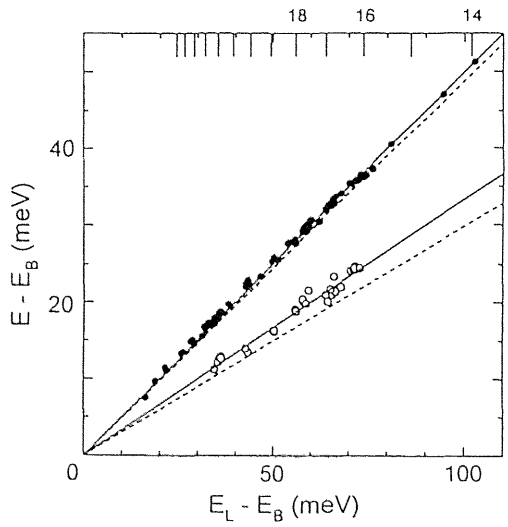

FIG. 3. Spectral hole positions E as a function of the excited photon energy E_L for CuCl quantum dots in NaCl. Solid circles and open circles are explained in the text. Calculated excited states for quantum cubes and for quantum spheres are shown by a solid line and a dashed line, respectively. The size of cubes in which the first excited states of excitons are confined is shown by the top long scale in a unit of half the lattice constant.

at the excitation photon energy denoted by E_L, lower-energy satellite holes were also burned at energy position E, where E satisfies $E_L-E_B=n(E-E_B)$ with $n=2$ or 3. Solid and open circles in Fig. 2(b) show the satellite holes for cases $n=2$ and 3, respectively. The appearance of these satellite holes can be explained as follows: if quantized exciton energy levels are described by Eq. (1), the ground state $E_{1,1,1}$ and the first and the second excited states $E_{2,1,1}$, $E_{2,2,1}$ satisfy the relations $E_{2,1,1}-E_B=2(E_{1,1,1}-E_B)$ and $E_{2,2,1}-E_B=3(E_{1,1,1}-E_B)$, respectively. Site-selective excitation of the excited states results in hole burning of the corresponding ground state, which is observed as the lower-energy satellite holes in Fig. 2(b). Although the state $E_{2,2,1}$ was excited, hole burning of the state $E_{2,1,1}$ relaxed from the $E_{2,2,1}$ state was not observed experimentally and only the ground state $E_{1,1,1}$ was burned. This suggests that the relaxation from the excited state to the ground state is considered to be much faster than the persistent spectral hole burning process and the recombination of the ground-state excitons. If quantum dots are assumed to be spheres, and if the second excited state is burned, the resultant satellite holes should appear in the energy positions marked by an upward arrow in Fig. 2(b). Absence of burned hole at the upward arrow indicates that the shape of CuCl quantum dots in NaCl matrix is cubic rather than spherical and that quantized exciton energy levels are described by Eq. (1). However, it should be noted that the optical transitions to both the first and second excited states are forbidden and the appearance of satellite holes cannot be explained by the excited states of excitons confined in ideal CuCl quantum cubes.

Figure 3 shows satellite hole positions E as a function of the excitation photon energy E_L. Several samples were used for this measurement. Solid circles and open circles correspond to the burned satellite holes of the ground states $E_{1,1,1}$, which result from the laser resonant excitation of the first excited states $E_{2,1,1}$ and the second excited states $E_{2,2,1}$, respectively. The corresponding calculated satellite hole positions based on Eqs. (1) and (2) are shown by solid and dashed lines, respectively. Although open circles are slightly scattered, agreement of experimental data and calculated results based on Eq. (1) is good. We should notice that satellite holes marked by solid circles move almost continuously, although the first excited exciton states $E_{2,1,1}$ confined in ideal quantum cubes shift discretely as shown by the long scale at the top horizontal axis. This feature can be understood under the following assumptions: Energies of the first excited-state excitons confined in quantum dots, whose shapes are a little deviated from an ideal cube, are expressed by $E_{2,1,1}-E_B=2(E_{1,1,1}-E_B)$ but the deviation is not so large to be a sphere. This possibility should be examined from the point of view of the selection rule. As mentioned before, if the shape of quantum dots is an ideal cube, the first excited state $E_{2,1,1}$ and the second excited state $E_{2,2,1}$ do not contribute to the optical transitions and solid and open circles in Fig. 3 should not appear. Our experimental results, that the excited states $E_{2,1,1}$ and $E_{2,2,1}$ are optically found, suggest that all of the dots are not ideal quantum cubes and that deviation from the cubic shape violates the selection rule.

One may consider strain between CuCl quantum dots and NaCl matrix or built-in electric field caused by trapped carriers is a possible origin of the violation of the selection rule. Hydrostatic pressure from the NaCl surrounding matrix may be applied to CuCl quantum dots, but the energy shift caused by the pressure was shown to be too small to explain the size-dependent energy shift of the exciton transition.[15] Moreover, isotropic hydrostatic pressure cannot be considered to give the violation of the selection rule. The selection rule in CuCl quantum cubes comes from the parity of the envelope function of exciton, which describes the exciton translational motion. It is different from the selection rule for dots in the strong confinement regime, where the selection rule comes

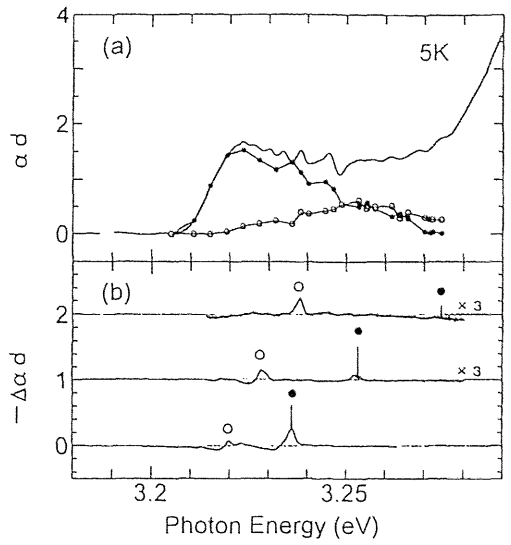

FIG. 4. An absorption spectrum (a) and absorption change spectra (b) of CuCl quantum dots in NaCl at 5 K. Solid and open circles in (a) represent the spectral profiles of the ground states and the first excited states in CuCl quantum dots, respectively.

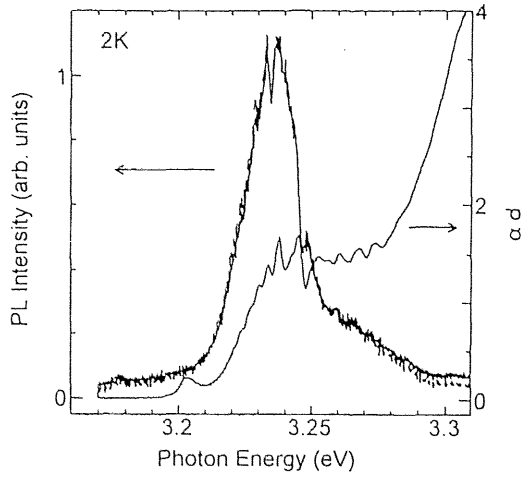

FIG. 5. An absorption and a photoluminescence spectra of CuCl quantum dots in NaCl at 2 K. Excitation photon energy is 3.49 eV for the luminescence spectrum. A dashed line indicates the luminescence spectrum made by the reabsorption correction.

from the parity of the envelope functions of the electrons and holes and is violated by the electric field.[20] Built-in electric field in the quantum dots can cause electron-hole separation in exciton and therefore change the internal motion of exciton, but cannot change the envelope function of exciton. This consideration excludes the electric field as an origin to violate the selection rule.

Figure 4 shows absorption (a) and absorption change (b) spectra with three excitation photon energies marked by solid circles. Excitation energies are 3.2745, 3.2531, and 3.2360 eV from top to bottom. Accumulated excitation energy density is 6 mJ/cm^2. It is apparent from Fig. 4(b) that the ratio of the satellite hole area (○) to the resonantly burned hole area (●) increases with the increase of the burning photon energy. This indicates that the contribution of the first excited states to the absorption band increases with the increase of the photon energy compared with that of the ground states. The resonantly burned hole is supposed to come from the ground states at the burning photon energy and not to contain the excited states as a result of the fast relaxation from the excited state to the ground state. Therefore, the ratio of the resonantly burned hole area (●) to the satellite hole area (○) gives the ratio of the ground state to the first excited state at the burning photon energy. Here, we evaluated the hole area including acoustic phonon wings. Solid and open circles in Fig. 4(a) show the contributions of the ground state and the first excited state of excitons confined in CuCl quantum dots to the absorption spectrum, respectively. To derive Fig. 4(a), we adopted following two assumptions. One is that actual quantum dots are deviated from cubes but preserve their high symmetry. Under this assumption, the ground state E_1 and the first excited state E_2 satisfy the equation $E_2 - E_B \simeq 2(E_1 - E_B)$. In fact, our simulated results showed that the three-directional side lengths of quantum boxes should not be different by twice $a/2$ from each other for reproduction of the oscillatory fine structures in the Z_3 exciton absorption band.[21] Another assumption is that only both the first excited state and the ground state contribute to the Z_3 exciton absorption band.

From the obtained spectral profiles in Fig. 4(a), we can estimate the oscillator strength of the ground state (f_1) and the first excited state (f_2). The oscillator strength of the first excited state is equal to zero if quantum dots are cubes. Simultaneously we can compare the obtained ratio f_2/f_1 with that expected for a quantum sphere.[22] Theoretical f_2/f_1 for a quantum sphere with radius R is 0.51 for $R/a_B = 5.8$ and 0.59 for $R/a_B = 4.4$, while from Fig. 4(b), the corresponding experimental f_2/f_1 is 0.28 and 0.23, respectively. The experimental oscillator strength ratio f_2/f_1 is about half the ratio for the quantum sphere and does not contradict with our model that the shape of CuCl quantum dots ranges from cubic to spherical while maintaining high symmetry. However, there are few studies concerning the problem how the oscillator strength depends on the shape of quantum dots. Further study is necessary to clarify this difficult problem.

In Fig. 5, absorption and photoluminescence spectra of CuCl quantum dots in NaCl are shown. The luminescence signal was accumulated while the sample was excited by 1800 shots of laser pulses with the very weak energy density of 3.1 μJ/cm^2 and the band-to-band excitation photon energy of 3.49 eV. The luminescence spectrum has the same oscillatory structure as the absorption spectrum and shows small Stokes shift (~0.6 meV), which suggests that the luminescence spectrum comes from recombination of free excitons confined in CuCl quantum dots. The luminescence spectrum drawn by a dashed line is corrected by taking account of the reabsorption effect and is normalized at the peak energy. We note that the luminescence signal is smaller above 3.25 eV, though the exciton absorption intensity does not decrease so much in this energy region. This fact does not contradict with our idea that the excited states are in the majority at the higher-energy region of the Z_3 exciton absorption band.

In summary, we have observed the excited-state excitons in CuCl quantum cubes by means of the PSHB spectroscopy. Energy positions of satellite holes in the PSHB spectrum show that the shape of quantum dots in NaCl matrix is not

spherical but rather cubic. However, actual quantum dots are considered to be deviated from ideal cubes and have almost continuously distributed shapes without breaking high symmetry. We have determined the spectral profiles of the ground state and the first excited state in CuCl quantum dots. The Z_3 exciton luminescence spectrum showed that the excited state excitons are in majority at the higher-energy region of the Z_3 exciton absorption band.

We are indebted to Dr. T. Kawazoe and Dr. T. Okuno for their valuable experimental advice and to Dr. S. Nair and Dr. N. Matsuura for valuable discussions.

*Present address: Atsugi Base, Ayase, Kanagawa 252, Japan.
†Author to whom correspondence should be addressed.

[1] D. Leonard, M. Krishnamurthy, C. M. Reaves, S. P. Denbaars, and P. M. Petroff, Appl. Phys. Lett. **63**, 3203 (1993).
[2] J. Oshinowo, M. Nishioka, S. Ishida, and Y. Arakawa, Jpn. J. Appl. Phys. Part 2, **33**, L1634 (1994).
[3] C. B. Murray, D. J. Norris, and M. G. Bawendi, J. Am. Chem. Soc. **115**, 8706 (1993).
[4] T. D. Bestwick, M. D. Dawson, A. H. Kean, and G. Duggan, Appl. Phys. Lett. **66**, 1382 (1995).
[5] F. Heinrichsdorff, A. Krost, M. Grundmann, D. Bimberg, A. Kosogov, and P. Werner, Appl. Phys. Lett. **68**, 3284 (1996).
[6] M. Kitamura, M. Nishioka, J. Oshinowo, and Y. Arakawa, Appl. Phys. Lett. **66**, 3663 (1995).
[7] D. Fröhlich, M. Haselhoff, K. Reimann, and T. Itoh, Solid State Commun. **94**, 189 (1995).
[8] K. Naoe, L. G. Zimin, and Y. Masumoto, Phys. Rev. B **50**, 18 200 (1994).
[9] Y. Masumoto, S. Okamoto, T. Yamamoto, and T. Kawazoe, Phys. Status Solidi B **188**, 209 (1995).
[10] Y. Masumoto, T. Kawazoe, and T. Yamamoto, Phys. Rev. B **52**, 4688 (1995).
[11] Y. Masumoto, K. Kawabata, and T. Kawazoe, Phys. Rev. B **52**, 7834 (1995).
[12] J. Qi and Y. Masumoto, Solid State Commun. **99**, 467 (1996).
[13] Y. Masumoto, K. Sonobe, and N. Sakakura, *Proceedings of the 23rd International Conference on the Physics of Semiconductors*, edited by M. Scheffler and R. Zimmermann, (Springer-Verlag, Berlin, 1996), p. 1481.
[14] A. I. Ekimov, Al. L. Eflos, and A. A. Onushchenko, Solid State Commun. **56**, 921 (1985).
[15] T. Itoh, Y. Iwabuchi, and M. Kataoka, Phys. Status Solidi B **145**, 567 (1988).
[16] M. Ueta, M. Ikezawa, and S. Nagasaka, J. Phys. Soc. Jpn. **20**, 1724 (1965).
[17] T. Itoh, S. Yano, N. Katagiri, Y. Iwabuchi, C. Gourdon, and A. I. Ekimov, J. Lumin. **60&61**, 396 (1994).
[18] Z. K. Tang, A. Yanase, T. Yasui, Y. Segawa, and K. Cho, Phys. Rev. Lett. **71**, 1431 (1993).
[19] Z. K. Tang, A. Yanase, Y. Segawa, N. Matsuura, and K. Cho, Phys. Rev. B **52**, 2640 (1995).
[20] A. Sacra, D. J. Norris, C. B. Murray, and M. G. Bawendi, J. Chem. Phys. **103**, 5236 (1995).
[21] N. Sakakura and Y. Masumoto, Jpn. J. Appl. Phys. (to be published).
[22] Y. Kayanuma, Phys. Rev. B **38**, 9797 (1988).

Size-dependent energy levels of CdTe quantum dots

Yasuaki Masumoto and Koji Sonobe*
Institute of Physics and Venture Business Laboratory, University of Tsukuba, Tsukuba 305, Japan
(Received 17 April 1997)

Successful observation of persistent spectral hole burning in CdTe quantum dots embedded in the glass enabled us to investigate their size-dependent electronic energy levels. Luminescence excitation spectroscopy was utilized to confirm them. The observed size-dependent electronic transitions show a monotonic increase with decrease of the radius from 4.3 to 2.5 nm and valence level crossing was not observed up to the sixth transition. These experimental results are discussed with reference to the calculated results on the multi-valence-band envelope formalism. [S0163-1829(97)02739-2]

Quantum size effect of semiconductor nanometer size crystals (nanocrystals) has been one of the targets of extensive research of the optical spectroscopy of semiconductors. Single nanocrystals are ideal for the study of their quantum size effect. Another alternative approach is the site-selective laser spectroscopy of size-dispersed quantum dots. In fact, hole burning and fluorescence line-narrowing spectroscopy are effective to extract the optical properties of single quantum dots from the inhomogeneously broadened optical spectra of the assembly of size-dispersed quantum dots.[1,2]

Recently, persistent spectral hole burning (PSHB) phenomena were observed in many semiconductor quantum dots, such as CdS, CdSe, CuCl, CuBr, and CuI quantum dots embedded in glass, crystals, or polymers.[3] These phenomena enable us to investigate precisely the size-dependent energy levels in "laser-marked" quantum dots by observing the site-selectively burned energies in the inhomogeneously broadened absorption spectra. As a result of the persistent spectral hole burning, the electronic and excitonic quantum states including the excited states are burned. This allows us to investigate the quantized energies of quantum dots systematically.

Although the single-band effective-mass model including Coulomb interaction between an electron and a hole gives a successful description of the lowest quantized levels in many semiconductor quantum dots,[4,5] it does not always apply to the excited quantized levels. Especially, valence-band degeneracy complicates the excited quantized levels in many zinc-blende semiconductors.[6–8] In zinc-blende CdTe, the conduction band is made of the s orbital of Cd and its valence band is made of the p orbital of Te as the first approximation. Orbital angular momentum is mixed with spin angular momentum, and the valence band is split into the topmost $J=\frac{3}{2}$ band and the split-off $J=\frac{1}{2}$ band. Quantum confinement of holes gives an additional angular momentum L for the envelope function, so that the L-J coupling is considered to make complicated energy levels for the hole band. However, CdTe has the largest spin-orbit splitting of 0.927 eV and the smallest band-gap energy, $E_g=1.606$ eV, among CdS, CdSe, and CdTe.[9] As a result, the split-off band is expected to mix weakly with the topmost valence band. Additionally, the valence band of zinc-blende CdTe is less complicated than that of wurtzite CdS and CdSe.

In this paper, PSHB is reported for CdTe quantum dots in the strong confinement regime and its spectroscopic application to the observation of the excited electronic quantum states is carried out.[10] This spectroscopic tool is compared with luminescence excitation spectroscopy and its utility is evaluated. Size-dependent quantized electronic levels are observed to shift monotonously without any crossing or anticrossing, reflecting the rather simple valence-band structure of CdTe.

Samples studied in this work were CdTe nanocrystals embedded in GeO_2:Na_2O glass. Molar concentration of 1.5–4.5% CdTe mixed with GeO_2:Na_2O glass was sealed in a quartz ample, melted in a rotating electric furnace at 1200 °C, and quenched. Then, glass pieces were heated for the growth of CdTe nanocrystals. The size of the nanocrystals was controlled by the CdTe doping concentration and the annealing time and was evaluated by means of the small-angle x-ray scattering. It ranges from 2.5 to 5.1 nm.

Samples were directly immersed in superfluid helium at 2 K for the optical measurement. The excitation light source for the persistent spectral hole burning was a narrow-band dye laser pumped by the second harmonic of the output of a 10 Hz Q-switched Nd^{3+}:YAG (yttrium aluminum garnet) laser. The spectral linewidth of the dye laser light was 0.014 meV. The absorption spectra of samples were measured by means of a diode-array optical multichannel analyzer or a liquid-nitrogen-cooled charge-coupled-device optical multichannel analyzer equipped with a 25-cm monochromator. The spectral resolution was set to be 1.2 nm. The probe light source was a halogen lamp. Before and after the samples were exposed to the dye laser light pulses, the absorption spectra were measured and the absorption change spectra were derived by subtracting the absorption spectrum taken after the dye laser exposure from that taken before the dye laser exposure.

The luminescence excitation spectra of samples were measured by monitoring the luminescence intensity at the high-energy part of the luminescence band for the better resolution of the excited states. The excitation light source was the 25-cm monochromator output of a 500-W Xe arc lamp. Its bandwidth was set to be 3 nm.The luminescence was measured by means of a 50-cm monochromator and a photomultiplier. The overall spectral resolution of the excitation spectra was 4.2 nm.

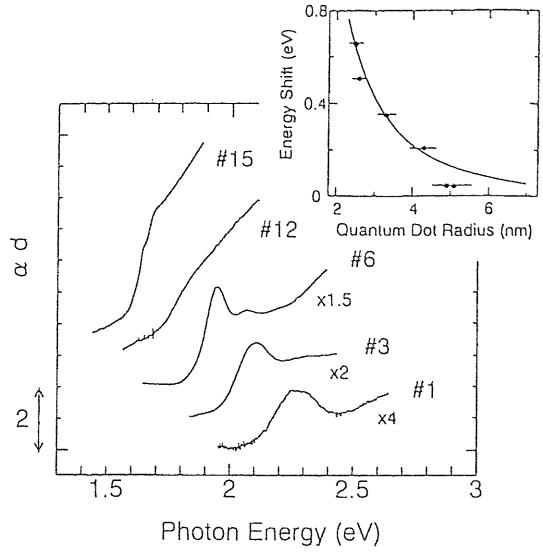

FIG. 1. Optical absorption spectra of five samples, CdTe quantum dots embedded in GeO_2 glass, at 2 K. The average radii of dots in samples 1, 3, 6, 12, and 15 are 2.5, 2.6, 3.3, 4.3, and 5.1 nm, respectively. In the inset, blueshift of the lowest structures in the absorption spectra from the lowest exciton energy in bulk CdTe, 1.596 eV, is shown as a function of the mean radius estimated by the small-angle x-ray scattering measurements together with the calculation in the strong confinement regime.

Absorption spectra of five typical samples are shown in Fig. 1. With the decrease of the size, the absorption peak shows blueshift due to the quantum size effect. In the top inset, the blueshift is plotted as a function of the average radius evaluated by means of the small-angle x-ray scattering. The observed blueshift agrees with the calculated one based on the strong confinement model of a spherical quantum dot except the largest size data. The calculation is made by the formula[11]

$$\Delta E = E - E_g + \mathcal{R} = \frac{\hbar^2 \pi^2}{2\mu R^2} - \frac{1.786 e^2}{\varepsilon R} + 0.752\,\mathcal{R},$$

where $E_g = 1.606$ eV is the band-gap energy, R is the radius of the dot, $\mu = 0.0774 m_0$ is the reduced mass of an electron mass $m_e^* = 0.096 m_0$ and a hole mass $m_h^* = 0.4 m_0$, $\varepsilon = 7.1$ is the dielectric constant and $\mathcal{R} = 10$ meV is the exciton Rydberg energy.[9,12] Here m_0 is the electron bare mass. The good agreement between the experimental data and the calculated curve shows that the simple strong confinement model of a spherical quantum dot is enough to explain the blueshift of the lowest quantized level of CdTe quantum dots. Because the largest size is still smaller than twice the exciton Bohr radius, $2a_B = 15$ nm,[13] the onset of the intermediate confinement regime,[11] the disagreement at the largest size regime is not explained by the collapse of the strong confinement model, but probably by the crystal structure transformation to wurtzite structure as discussed later.

Figure 2 shows the inhomogeneously broadened absorption spectra (the upper column) and the absorption spectrum change (the lower column) of the samples, CdTe quantum dots embedded in GeO_2 glass. The absorption spectra show a remarkable blueshift with the decrease in the dot size. After the samples are exposed to narrow-band dye laser pulses

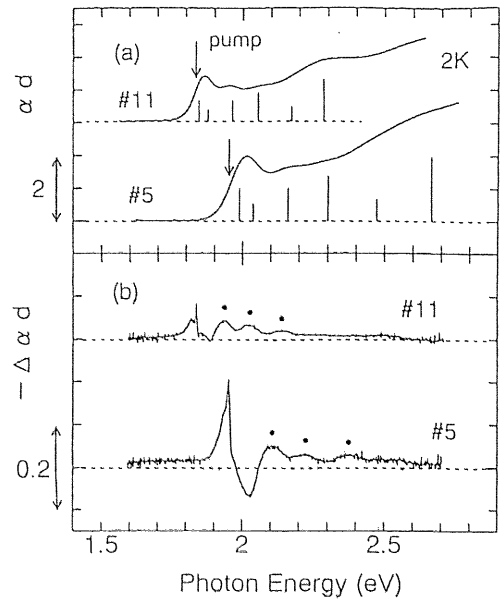

FIG. 2. Optical absorption spectra (upper column) and the absorption change spectra (lower column) of CdTe quantum dots embedded in GeO_2 glass at 2 K. The average radii of dots in samples 11 and 5 are 3.7 and 2.9 nm, respectively. Vertical arrows show the burning photon energies of 1.8336 and 1.9526 eV, respectively. The absorption change spectra were measured, after the samples were exposed to 1800 shots of dye laser pulses with the excitation energy of 640 μJ/cm^2. Positions of vertical bars in (a) represent the energy positions of the transition deduced from the straight lines in Fig. 4 and their lengths represent the oscillator strength obtained from Ref. 8, except the $3SDD_{3/2} \rightarrow 1S_e$ transition.

whose photon energy corresponds to the lowest absorption band and after the dye laser exposure was stopped, we started taking the absorption spectrum change at 1.5 min. They showed the hole burning and the burned hole persists for more than 1 h in contrast with the previous report on the microsecond hole burning of CdTe.[13] Clear persistent hole burning structures together with the higher-energy satellite structures move with the change of the burning photon energy. The higher-energy satellite structures are considered to be excited states of the burned quantum dots.

It is known that luminescence excitation spectra are useful for the observation of the excited states in quantum dots.[14,15] Luminescence excitation spectra and PSHB spectra were compared and the validity of the PSHB as a spectroscopic tool was examined. Figure 3 shows the PSHB spectrum and the luminescence excitation spectrum. The higher-energy satellite structures in the absorption spectrum change almost coincide with the structures in the luminescence excitation spectrum. Good coincidence between the PSHB spectrum and the luminescence excitation spectrum indicates the reliability of the peak positions determined by both methods. Although a clear shoulder due to the lowest excited state is observed in the luminescence excitation spectrum, it is not observed at the higher-energy side of the resonantly burned hole in the absorption change spectrum except the absorption increase structure. The absorption increase structure at the higher-energy side of the resonantly burned hole has been often observed in the PSHB spectrum of quantum dots. It seems to mask the excited states around its spectral position

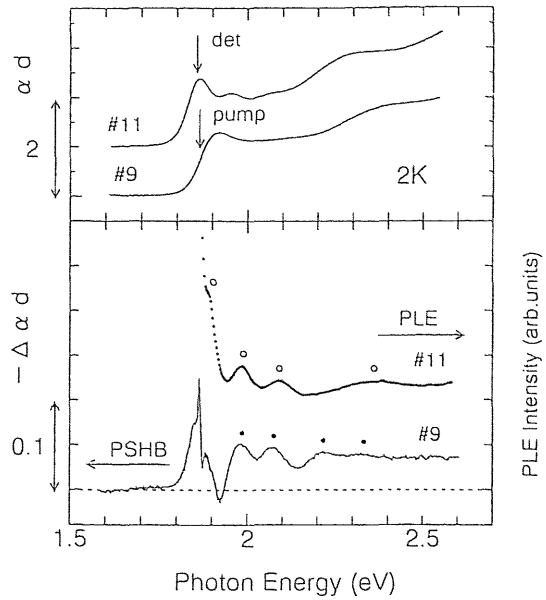

FIG. 3. Comparison of the persistent hole burning spectrum and the luminescence excitation spectrum of CdTe quantum dots embedded in GeO_2 glass at 2 K. The average radii of dots in samples 11 and 9 are 3.7 and 3.5 nm, respectively. Downward arrows show the burning photon energy, 1.8678 eV, and luminescence detection photon energy, 1.853 eV, respectively.

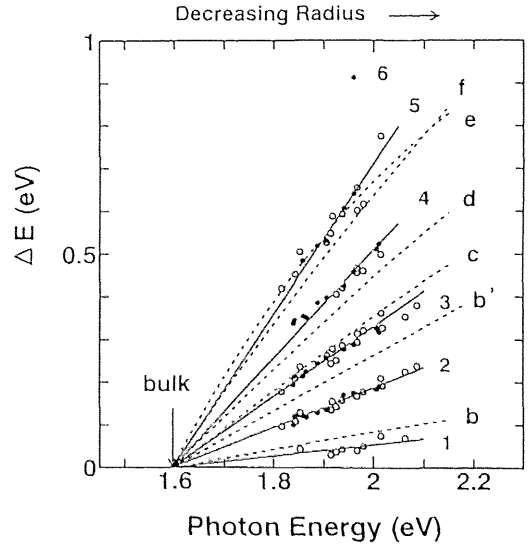

FIG. 4. Excited-state spacings measured relative to the lowest burned structure (center of gravity) shown by solid circles and those measured relative to the luminescence detection energy shown by open circles. Dashed lines labeled by b, c, d, e, and f correspond to the transitions $2SDD_{3/2}\rightarrow 1S_e$, $1PFP_{3/2}\rightarrow 1P_e$, $1PFF_{5/2}\rightarrow 1P_e$, $1PP_{1/2}\rightarrow 1P_e$, and $2PFF_{5/2}\rightarrow 1P_e$ calculated by using the result of Ref. 8, assuming that the lowest burned structure corresponds to the transition $1SDD_{3/2}\rightarrow 1S_e$. A dashed line labeled by b' corresponding to $3SDD_{3/2}\rightarrow 1S_e$ is also calculated by using the result of Ref. 8. Straight lines go through experimental data and a converging point at the lowest exciton transition energy of bulk CdTe, 1.596 eV.

and may give a limitation to the PSHB spectroscopy to investigate the low-energy excited states of quantum dots.

Plotting these transition energies as a function of the excitation photon energy in Fig. 4, we can find straight lines, 1, 2, and 3, converging on the bulk-energy fit the experimental data. However, slopes of straight lines 4 and 5 are a little different from those of experimental data. Nevertheless, rather good straight-line fitting meets the two-valence-band theory for CdTe quantum dots where the mixing of the split-off band is not taken into account. Confinement energies of quantized hole states in CdTe dots were calculated by a multiband effective-mass approximation. By using the calculated results, we can obtain the size-dependent transition energies between quantized hole states and electron states. Therefore, in comparison with the experimental data, we replotted the calculation in which intermixing between three valence bands are considered.[8] The energy difference between transitions, $2SDD_{3/2}\rightarrow 1S_e$, $1PFP_{3/2}\rightarrow 1P_e$, $1PFF_{5/2}\rightarrow 1P_e$, $1PP_{1/2}\rightarrow 1P_e$, and $2PFF_{5/2}\rightarrow 1P_e$, and the transition of $1SDD_{3/2}\rightarrow 1S_e$ is plotted by b, c, d, e, and f, respectively. The comparison shows that the experimental data sets 1, 3, and 4 are identified as transitions $2SDD_{3/2}\rightarrow 1S_e$, $1PFP_{3/2}\rightarrow 1P_e$, and $1PFF_{5/2}\rightarrow 1P_e$, respectively. Data set 5 is identified as overlapped transitions, $1PP_{1/2}\rightarrow 1P_e$ and $2PFF_{5/2}\rightarrow 1P_e$. Although experimental data set 2 was not predicted by the theory, they are assigned to be the transition $3SDD_{3/2}\rightarrow 1S_e$. The energy difference between the transition of $3SDD_{3/2}\rightarrow 1S_e$ and the transition of $1SDD_{3/2}\rightarrow 1S_e$ is calculated as is shown by b' in Fig. 4 on the basis of the calculated confinement energy of the quantized hole states, $3SDD_{3/2}$ and $1SDD_{3/2}$.[8] The calculated energy difference ΔE between $3SDD_{3/2}$ and $1SDD_{3/2}$ is 3.3 times that between $2SDD_{3/2}$ and $1SDD_{3/2}$. On the other hand, the experimental ΔE of data set 2 is 3.5 times ΔE of data set 1. If data set 1 is identified as the transition $2SDD_{3/2}\rightarrow 1S_e$, data set 2 is reasonably identified as the transition $3SDD_{3/2}\rightarrow 1S_e$.

The Luttinger parameters γ_1 and γ_2 so far reported or used are scattered,[16] so that the calculated relative energy positions of the excited states may change crucially depending on the parameter set. Following the previous evaluation of the hole quantized energy of a dot whose radius is 2 nm, the quantized energies of $1SDD_{3/2}$ and $1PFP_{3/2}$ states vary at most by 0.1 eV depending on three sets of Luttinger parameters but the energy separation between $1SDD_{3/2}$ and $1PFP_{3/2}$ changes at most by 6.4 meV. This trial calculation shows that the relative energy between quantized hole states whose principal quantum number for the envelope function is 1 varies little with the change of Luttinger parameters. On the other hand, the energy difference between $1SDD_{3/2}$ and $2SDD_{3/2}$ or $3SDD_{3/2}$ changes by more than 0.1 eV. The experimental data are within the estimation uncertainty. Energy splitting of $J=\frac{3}{2}$ hole states depending on the orientation of the crystal can be evaluated by the known k-linear term.[17] The evaluated splitting by the expression $\sqrt{6}K_l(\pi/R)$ is 15 meV for $R=2.5$ nm, where K_l is the coefficient of the k-linear term. The value is comparable to data scattering and does not change the relative energy between quantized hole states. It is also noted that the size-dependent Coulomb energy is not taken into account in the calculation. On the other hand, the energy separation between $1SDD_{3/2}$ and $1PFP_{3/2}$ changes considerably, when the effective mass of the electron, m_e^*, varies. It changes from 0.995 to 1.063 eV or 0.957 eV for a CdTe dot whose radius is 2 nm, when a set of

parameters, γ_1, γ_2, and m_e^*, changes from $\gamma_1 = 5.29$, $\gamma_2 = 1.89$, and $m_e^* = 0.096 m_0$ to $\gamma_1 = 5.29$, $\gamma_2 = 1.89$, and $m_e^* = 0.090 m_0$, or $\gamma_1 = 4.7$, $\gamma_2 = 1.45$, and $m_e^* = 0.099 m_0$. The experimental data are within the estimation uncertainty. Therefore, agreement between experimental data and calculation can be improved by the good choice of the parameters.

We also compared our data with that of the previous work on CdTe quantum dots based on the luminescence excitation spectroscopy.[18] Two data sets of the previous work are very close to lines 1 and 4 in Fig. 4 and a data set lies between lines 2 and 3. We consider that the second and third excited states are merged and are not resolved well in the previous work.

When the radius of CdTe dots exceeds 4 nm, the absorption spectrum become obscure and almost structureless. Simultaneously, PSHB was not observed. Luminescence excitation spectrum was structureless, too. These observations reflect the missing data region in Fig. 4. The reason why the optical spectra are structureless may be explained by assuming that the samples contain a mixture of CdTe quantum dots of zinc-blende structure and wurtzite structure.[19] The absorption spectrum of sample 15 whose radius is 5.1 nm shows two shoulders at 1.6397 and 1.6837 eV as is shown in Fig. 1. Crystal-field splitting is generally observed in wurtzite CdSe and CdS large quantum dots. Energy separation between the two shoulders is 0.044 eV, which agrees well with the crystal-field splitting, 0.0465 eV, observed in wurtzite bulk-like CdTe. The PSHB phenomena should depend strongly on the size of nanocrystals, and should disappear with the increase of the size. This may also explain the presence of the missing data region at the low photon energy regime. Further experimental effort is necessary for the measurement of the size-dependent quantum energy in this large-size region.

In summary, we have successfully observed the PSHB in CdTe quantum dots embedded in GeO_2:Na_2O glass. The PSHB was utilized to reveal the size-dependent electronic energy levels in CdTe quantum dots as a new site-selective laser spectroscopy. The luminescence excitation spectroscopy was also utilized to investigate them. Good coincidence of the structures revealed by the PSHB and the luminescence excitation spectroscopy show that the PSHB is a reliable spectroscopic tool to investigate the size-dependent electronic energy levels in size-dispersed quantum dots. The observed size-dependent electronic transitions show a monotonic increase with the decrease of the size and valence-band mixing was not present up to the sixth transition. These experimental results are discussed with reference to the calculated results.

The authors wish to thank Dr. S. Nair for valuable discussions and a critical reading of this paper. Small-angle x-ray scattering experiments were done at the Photon Factory (PF) of the National Laboratory for High-Energy Physics by the approval of the PF Advisory Committee (Proposals 95G343). This work was partially supported by a Grand-in-Aid for Scientific Research No.8454075 from the Ministry of Education, Science, Sports and Culture of Japan.

*Present address: Hino Laboratory, Fuji Electric Corporate Research and Development, Ltd., Asahigaoka, Hino 191, Japan

[1] T. Wamura and Y. Masumoto, Appl. Phys. Lett. **59**, 1758 (1991).

[2] T. Itoh and M. Furumiya, J. Lumin. **48&49**, 704 (1991).

[3] For review see Y. Masumoto, J. Lumin. **70**, 386 (1996).

[4] A. I. Ekimov, Al. L. Effros, and A. A. Onuschenko, Solid State Commun. **56**, 921 (1985).

[5] A. D. Yoffe, Adv. Phys. **42**, 173 (1993).

[6] J-B. Xia, Phys. Rev. B **40**, 8500 (1989).

[7] A. I. Ekimov, F. Hache, M. C. Schanne-Klein, D. Ricard, and C. Flytzanis, J. Opt. Soc. Am. B **10**, 100 (1993).

[8] T. Richard, P. Lefebvre, H. Mathieu, and J. Allègre, Phys. Rev. B **53**, 7287 (1996).

[9] *Numerical Data and Functional Relationships in Science and Technology, Physics of II-VI and I-VII Compounds, Semimagnetic Semiconductors*, edited by O. Madelung, Landolt-Börnstein, New Series, Group III, Vol. 17, Pt. b (Springer-Verlag, Berlin, 1982).

[10] Y. Masumoto, K. Sonobe, and N. Sakakura, in *Proceedings of the 23rd International Conference on the Physics of Semiconductors*, Berlin, 1996, edited by M. Scheffler and R. Zimmermann (World Scientific, Singapore, 1996), p. 1481.

[11] Y. Kayanuma, Solid State Commun. **59**, 405 (1986); Phys. Rev. B **38**, 9797 (1988).

[12] *Physics and Chemistry of II-VI Compounds*, edited by M. Aven and J. S. Prener (North-Holland, Amsterdam, 1967), Chap. 7.

[13] V. Esch, B. Fluegel, G. Khitrova, H. M. Gibbs, Xu. Jiajin, K. Kang, S. W. Koch, L. C. Liu, S. H. Risbud, and N. Peyghambarian, Phys. Rev. B **42**, 7450 (1990).

[14] D. J. Norris, A. Sacra, C. B. Murray, and M. G. Bawendi, Phys. Rev. Lett. **72**, 2612 (1994).

[15] D. J. Norris and M. G. Bawendi, Phys. Rev. B **53**, 16 338 (1996).

[16] P. Lefebvre, T. Richard, H. Mathieu, and J. Allègre, Solid State Commun. **98**, 303 (1996).

[17] W. Dreybrodt, K. Cho, S. Suga, F. Willmann, and Y. Niji, Phys. Rev. B **21**, 4692 (1980).

[18] C. R. M. de Oliveira, A. M. de Paula, F. O. Plentz Filho, J. Medeiros Neto, L. C. Barbosa, O. L. Alves, E. A. Menezes, J. M. M. Rios, H. L. Fragnito, C. H. Brito Cruz, and C. L. Cesar, Appl. Phys. Lett. **66**, 439 (1995).

[19] P. Lefebvre, T. Richard, J. Allègre, H. Mathieu, A. Combette-Roos, and W. Granier, Phys. Rev. B **53**, 15 440 (1996).

Biexciton and Triexciton States in Quantum Dots in the Weak Confinement Regime

Michio Ikezawa,[1] Yasuaki Masumoto,[1,3] Toshihide Takagahara,[2] and Selvakumar V. Nair[3]
[1]*Institute of Physics, University of Tsukuba, Tsukuba 305, Japan*
[2]*NTT Basic Research Laboratories, 3-1 Morinosato Wakamiya, Atsugi 243, Japan*
[3]*ERATO Single Quantum Dot Project, JST, 5-9-9 Tokodai, Tsukuba 300-26, Japan*
(Received 28 May 1997)

Biexciton and triexciton states in CuCl quantum dots were studied by means of time-resolved size-selective pump-and-probe technique. A clear induced absorption band is observed on the high-energy side of the excitation photon energy. The new induced absorption is assigned to the transition from the exciton ground state to one of the weakly correlated exciton pair states which were theoretically predicted to exist and to play an important role in nonlinear optical processes. Its pump energy dependence and temporal evolution strongly support this assignment. Under high-density or two-color excitation condition, a triexciton state in quantum dots is observed for the first time. [S0031-9007(97)04397-4]

PACS numbers: 78.66.Li, 71.35.Gg, 78.47.+p

Semiconductor nanocrystals dispersed in a large-bandgap matrix can be treated as quantum dots. Three-dimensional quantum confinement of electrons, holes, and excitons makes it possible to observe quantum size effect in quantum dots [1–3]. We can classify the quantum confinement effects into two main categories according to the ratio of the quantum dot radius R to the exciton Bohr radius a_B. One is the *strong confinement* ($R < a_B$) where electrons and holes are quantized individually, and the other is the *weak confinement* ($R > a_B$) where the translational motion of excitons is quantized. A CuCl quantum dot is known as a prototypical system in the weak-confinement regime because of its small exciton Bohr radius and has often been used to investigate excitons and biexcitons.

The study of the quantum confinement effect on many-exciton states, e.g., biexciton and triexciton, is still in the elementary stage. There are many experimental reports showing unique nonlinear optical properties of quantum dots, for example, enhancement of the biexciton binding energy [4], a nonmonotonic size dependence of the optical nonlinearity [5], and biexciton lasing [6]. Through these studies, the importance of weakly correlated exciton pair states has been pointed out [7]. The weakly correlated exciton pair state is one of the excited biexciton states. Roughly speaking, that state is an antibonding state of two excitons and has a higher energy and a larger spatial extent than the biexciton ground state, leading to a larger oscillator strength of transition from the exciton state. This state is of general character and is expected to be present as well in other low-dimensional structures, e.g., quantum wells and quantum wires. However, the actual observation was successful for the first time in the quantum dot as reported here, because the continuum states overlapping the weakly correlated exciton pair state inhibit clear observation of this state in other structures. So far, the experimental study of the excited biexciton states has been limited to the strong-confinement regime where the excited biexciton state is blurred by the size inhomogeneity and the ground state biexciton is masked by the broad exciton bleaching [8,9]. Therefore, it is important and interesting to study the excited biexciton states in the weak-confinement regime, making use of the advantageous situation that the exciton and biexciton binding energies are quite large. In this Letter, the excited biexciton states are identified unambiguously in CuCl quantum dots from comparison between theory and experiments. Furthermore, a triexciton state in quantum dots is observed for the first time. Along this line of approach, we can study the many-exciton states in a quantum dot successively. From details of the exciton addition spectrum, we can clarify the exciton correlation with renewed interest and investigate, for example, the ionization threshold of excitons and biexcitons which has been discussed so far only in the mean-field approximation. Thus, the present study holds a great promise of revealing new aspects in many-body physics.

We used the time-resolved size-selective pump-and-probe method. The sample was CuCl quantum dots embedded in a NaCl crystal. The absorption band of the sample was inhomogeneously broadened because of the size inhomogeneity of the quantum dots. The laser source was a self-mode-locked titanium sapphire laser and a titanium sapphire regenerative amplifier. After amplification, the output pulse has a pulse duration of 300 fs at a repetition rate of 1 kHz, and a pulse energy of 200 μJ/pulse. The amplified laser pulses were converted to their second harmonic. The second harmonic pulses were spectrally filtered by means of a spectral filter stage made of a grating and were used as pump pulses for the size-selective excitation. Their typical spectral width was 1.7 meV. A part of the amplified laser pulse was focused in pure water to produce a white continuum which was used as a probe beam. The transient absorption spectra were recorded by a spectrometer and a liquid-nitrogen cooled charge-coupled device multichannel detector.

 0031-9007/97/79(18)/3522(4)$10.00

A solid line in the upper part of Fig. 1 shows the absorption spectrum of the sample at 77 K. The Z_3 exciton and $Z_{1,2}$ exciton absorption structures are observed. These exciton absorption energies are shifted to the higher energy side compared to those of the bulk material due to the quantum confinement effect. The Z_3 exciton energy of bulk CuCl is shown by a downward arrow. The spectrum of the spectrally filtered pump pulse is shown in the inset by a solid line together with that of the unfiltered pulse shown by a broken line. According to the well-known relation between the quantum confined exciton energy and the quantum dot radius [10], the pump pulse energy of 3.259 eV excites quantum dots of 2.3 nm radius. The dashed line shows the absorption spectrum at 10 ps after the excitation. The solid line in the lower part of Fig. 1 shows the difference between two spectra in the upper part. The spectrum consists of a spectral hole at the pump photon energy and two induced absorption structures at both sides (3.180 eV, 3.296 eV) of the spectral hole. Persistent hole burning was much smaller than the transient hole burning at 77 K [11]. Bleaching around 3.335 eV is related to the $Z_{1,2}$ exciton.

Differential absorption spectra are shown at the lower part of Fig. 1 for four different pump photon energies. Two prominent induced absorption bands shift with the change of the excitation photon energy. The energies of the spectral hole and the induced absorption bands are plotted in Fig. 2 as a function of the excitation photon energy. The solid circles show spectral hole energies, and they are on a line of slope 1.0, since their energy coincides with the excitation photon energy. Open (solid) triangles exhibit the energies of the induced absorption located at the higher (lower) energy side. Open circles show the energies of induced absorption measured previously by nanosecond pump-and-probe method [4] which was identified as the transition from the exciton to the biexciton ground state. The coincidence between open circles and solid triangles confirms the proper present measurement.

The solid line through the open triangles is a fitted line by the least squares method. The slope of this line is 2.0. This line crosses the line of slope 1.0 near the Z_3 exciton energy of bulk CuCl. Furthermore, the spectral hole and the induced absorption on the higher energy side exhibit almost the same temporal evolution. They show an exponential decay with a time constant of 480 ps which almost coincides with the luminescence decay time of excitons in CuCl quantum dots [12]. This fact indicates that the induced absorption on the higher energy side arises from the excitons preexcited in the quantum dots. These features agree well with those of the theoretically predicted [7] strong induced absorption transition from the exciton state to excited biexciton states.

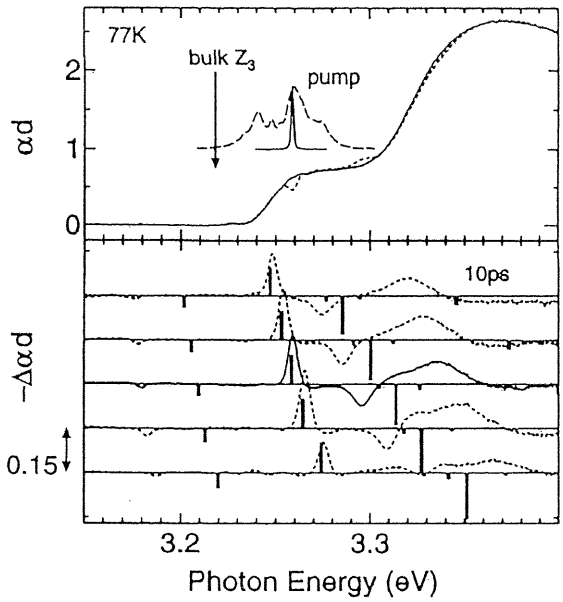

FIG. 1. Upper panel: The solid line shows absorption spectrum of CuCl quantum dots embedded in a NaCl crystal at 77 K, while a dashed line represents that at 10 ps after photoexcitation. Lower panel: The solid line shows differential absorption spectrum corresponding to the upper figure, while dashed lines are those for different excitation photon energies. The radii of quantum dots which were excited are 2.65, 2.46, 2.32, 2.19, and 2.03 nm from top to bottom, respectively. Thick solid bars are theoretical results normalized at the spectral hole. In the inset, filtered and unfiltered pump spectra are shown by a solid line and a dashed line, respectively.

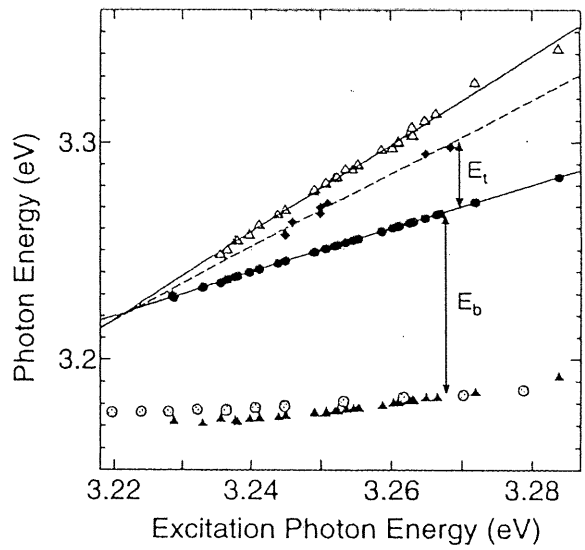

FIG. 2. Excitation energy dependence of the structures appearing in the differential absorption spectrum. The solid circles represent spectral hole energies, and they are on a line of slope 1.0. Open (solid) triangles show the energy of the induced absorption located at the higher (lower) energy side of the spectral hole. Open circles indicate the energy of the induced absorption measured by nanosecond pump-and-probe method in Ref. [4]. Solid diamonds correspond to additional induced absorption under high-density excitation. E_b denotes the biexciton binding energy defined by $2E_X - E_{XX}$ and E_t shows $E_{XXX} - E_{XX} - E_X$. Then the triexciton binding energy defined by $3E_X - E_{XXX}$ is given by $E_b - E_t$.

In CuCl where both the uppermost valence band and the lowermost conduction band are doubly degenerate, the angular momentum of the Bloch part exciton wave function is either 0 or 1. Then the angular momentum of the biexciton can be either of 0, 1, and 2. The explicit biexciton wave function for $J = 0$ and 2 can be written as $\Psi_{XX0} = \sqrt{3}/2\Phi_{XX}^{++}\chi_{00}^{00} - 1/2\Phi_{XX}^{--}\chi_{00}^{11}$, $\Psi_{XX2} = \Phi_{XX}^{--}\chi_{2M}^{11}$, where $\chi_{JM}^{j_e j_h}$ denotes the Bloch part wave function which has the total angular momentum (J, M) and is composed of two-electron wave function of angular momentum j_e and two-hole wave function of angular momentum j_h. In the limit of weak confinement, it has been shown that the weakly correlated exciton pair states may be approximated by product states of two independent excitons [7], namely,

$$\Phi_{XX}^{\pm\pm} = \frac{1}{\sqrt{2}}[\phi_X^g(r_{e1}, r_{h1})\phi_X^g(r_{e2}, r_{h2}) \pm \phi_X^g(r_{e1}, r_{h2})\phi_X^g(r_{e2}, r_{h1})], \quad (1)$$

where ϕ_X^g is the envelope function of the exciton ground state and r_{e1} and r_{e2} (r_{h1} and r_{h2}) denote the electron (hole) coordinates. The oscillator strengths of transitions from the ground state exciton X to these excited biexciton states are calculated as $f(X \rightarrow XX0) = 2/3f_0, f(X \rightarrow XX2) = 4/3f_0$, where f_0 is the oscillator strength of the excitonic transition.

The theoretical induced absorption spectrum from the exciton ground state is shown by thick solid bars in Fig. 1. The energy shifts of strong bands show good correspondence with experiments. Furthermore, the relative strengths of the induced absorption lines and the spectral hole are reproduced quite well by the theory, although there is a discrepancy in the energy positions of the induced absorption lines. Hence the strong peak above the pump energy can be assigned to the induced absorption transition to $XX2$ states.

Next we discuss experimental observation of triexciton states in CuCl quantum dots. At the upper part of Fig. 3(A), we exhibit the excitation density dependence of the differential absorption spectrum at 10 ps after photoexcitation. Under low density excitation, spectra in Fig. 3(A) are similar to those in Fig. 1, and the biexciton luminescence cannot be observed. Under high density excitation condition, we observed an additional induced absorption band which is shown by an arrow. Simultaneously the biexciton luminescence became observable.

In Fig. 3(B), the time evolution of the additional induced absorption is shown. Together with it, the temporal evolution of the spectral hole and the higher energy induced absorption band are also presented in the figure, although the excitation density was slightly low. Two solid curves through the solid circles and open triangles show an exponential decay with a time constant of 480 ps. On the other hand, the decay time constant of the additional induced

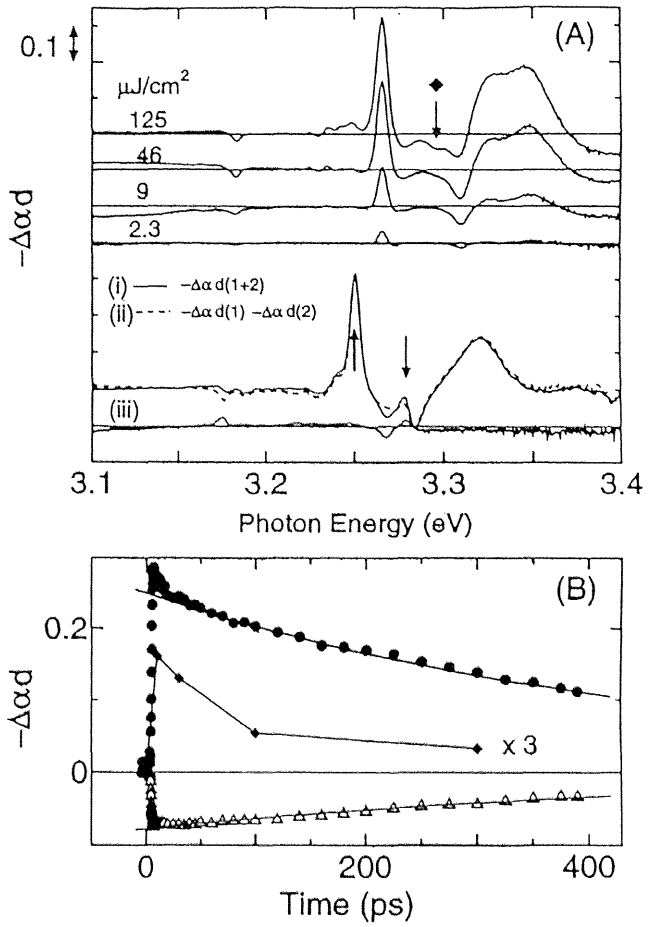

FIG. 3. (A) Upper panel: Excitation density dependence of the differential absorption spectrum at 10 ps after photoexcitation with the excitation photon energy fixed at 3.265 eV. Additional induced absorption shown by an arrow appears with the increase of the excitation. Lower panel: Experimental results of the two-color pump-and-probe measurement. The photon energy of the first (second) pump pulse is indicated by an upward (a downward) arrow. (i) Shows the differential absorption spectrum induced by both the first and second pulses. (ii) Exhibits the sum of differential absorption spectra induced by the first pump pulse and by the second one alone. (iii) = (i) − (ii). (B) Time evolution of the additional induced absorption under high-density excitation together with the spectral hole and the higher energy induced absorption. Symbols are the same as in Fig. 2.

absorption is less than 100 ps and corresponds to the luminescence lifetime of biexciton which is known to be 70 ps for CuCl nanocrystals [13]. If a triexciton state consists of a biexciton and an exciton, the intensity of the induced absorption transition from a biexciton to a triexciton should be proportional to the number of biexcitons. Therefore the time evolution and the excitation density dependence suggest strongly that the additional induced absorption can be assigned to transition from the biexciton ground state to a triexciton state.

We examined this assignment by the two-color pump-and-probe method. The energy of the second pump pulse is tuned to the induced absorption caused by the

first pump pulse. This combination produces biexciton effectively only in quantum dots of particular size and enables us to observe the induced absorption to triexciton states. At the lower part of Fig. 3(A), results of the experiment are shown. Photon energy of the first or second pump pulse is represented by an upward or a downward arrow, respectively. Time delay between two pump pulses was 5 ps, and the probe pulse delay to the second pump pulse was also 5 ps. The solid line (i) shows the differential absorption spectrum induced by two successive pump pulses, while the dotted line (ii) exhibits the sum of differential spectra induced by the first pump pulse and by the second one alone. Spectrum (iii) shows the difference between two spectra. If the second pump pulse increases (decreases) the absorption of the quantum dots excited selectively by the first pulse, we would observe negative (positive) signal in spectrum (iii). In fact, we observed an increased absorption region between the spectral hole and the induced absorption in spectrum (iii). The relative peak position is similar to that of the additional induced absorption in the upper part of Fig. 3(A). Hence both structures should be of the same origin. Excitation energy dependence of this induced absorption is shown in Fig. 2 by solid diamonds. The fitted line has a slope of 1.7, and this line also crosses the other two lines near the bulk Z_3 exciton energy.

In addition to an increased absorption region, we observed two decreased absorption regions in spectrum (iii). The lower or higher energy one indicates the decrease of the transition from the exciton state to the biexciton ground state or excited biexciton state, respectively. This can be explained by noticing that the biexcitons are produced size-selectively by the second pump pulse.

The linear proportionality of the induced absorption energy to the exciton confinement energy suggests that the exciton addition energy is primarily determined by the increase in the kinetic energy proportional to the inverse square of the quantum dot radius. As proposed previously [7], since the weakly correlated exciton pair state ($XX2$) is an antibonding state of two excitons, its kinetic energy can be assumed to be equal to that of two excitons independently confined in a region of half the volume of the quantum dot. Then its energy is written as $E_{XX2} = 2E_{bk} + 2\sqrt[3]{4}(E_X - E_{bk})$, where $E_X(E_{bk})$ is the exciton energy in a quantum dot (bulk material) and the slope in Fig. 2 is estimated as $2\sqrt[3]{4} - 1 \cong 2.2$ in good agreement with the experiment. The observed triexciton state has an energy greater than that of an independent biexciton-exciton pair but smaller than that of three excitons. Thus, while this state is a bound state, it may be regarded as an antibonding combination of a biexciton and an exciton. Therefore the above argument may be extended to the case of exciton addition to the biexciton ground state assuming the added exciton to occupy half the volume of the quantum dot without affecting the biexciton ground state. Then we have $E_{XXX} - E_{XX_g} = \sqrt[3]{4}(E_X - E_{bk}) + E_{bk}$ with $E_{XXX(XX_g)}$ being the energy of the triexciton (biexciton ground) state, and this gives the slope in Fig. 2 as $\sqrt[3]{4} \cong 1.6$, again in good agreement with the experiment. These qualitative arguments provide a strong support to the identification of the newly observed induced absorption as the transition from the biexciton to a triexciton state.

In conclusion, we studied biexciton and triexciton states in quantum dots in the weak-confinement regime by using the time-resolved size-selective pump-and-probe technique. One of the observed induced absorption bands was unambiguously identified as the transition from the exciton state to the weakly correlated exciton pair state whose presence was theoretically predicted. We observed a triexciton state in quantum dots for the first time by two independent methods employing high-density excitation and two-color excitation scheme. These experiments open a new direction of research and hold a great promise of revealing new aspects of many-exciton states in confined systems.

[1] A. I. Ekimov, A. L. Efros, and A. A. Onushchenko, Solid State Commun. **56**, 921 (1985).
[2] A. D. Yoffe, Adv. Phys. **42**, 173 (1993).
[3] L. Bányai and S. W. Koch, *Semiconductor Quantum Dot* (World Scientific, Singapore, 1993).
[4] Y. Masumoto, S. Okamoto, and S. Katayanagi, Phys. Rev. B **50**, 18 658 (1994).
[5] T. Kataoka, T. Tokizaki, and A. Nakamura, Phys. Rev. B **48**, 2815 (1993).
[6] Y. Masumoto, T. Kawamura, and K. Era, Appl. Phys. Lett. **62**, 225 (1993).
[7] S. V. Nair and T. Takagahara, Phys. Rev. B **53**, R10516 (1996); **55**, 5153 (1997).
[8] Y. Z. Hu, S. W. Koch, M. Lindberg, N. Peyghambarian, E. L. Pollock, and F. F. Abraham, Phys. Rev. Lett. **64**, 1805 (1990).
[9] Y. Z. Hu, M. Lindberg, and S. W. Koch, Phys. Rev. B **42**, 1713 (1990).
[10] T. Itoh, Y. Iwabuchi, and M. Kataoka, Phys. Status Solidi B **145**, 567 (1988).
[11] Y. Masumoto, J. Lumin. **70**, 386 (1996).
[12] T. Itoh, M. Furumiya, T. Ikehara, and C. Gourdon, Solid State Commun. **73**, 271 (1990).
[13] Y. Masumoto, S. Katayanagi, and T. Mishina, Phys. Rev. B **49**, 10782 (1994).